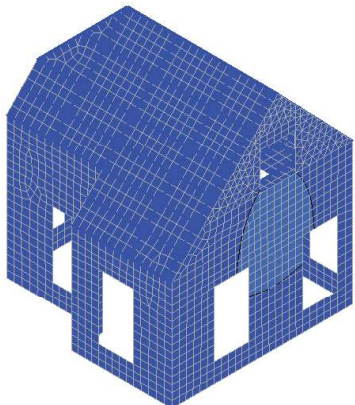
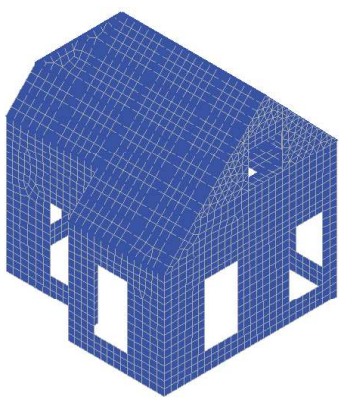
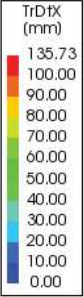
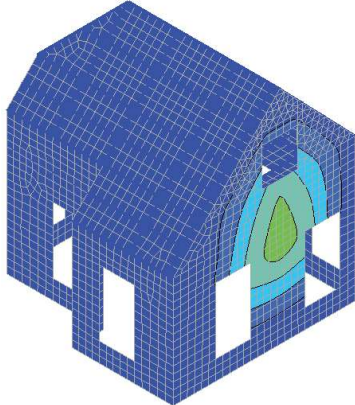
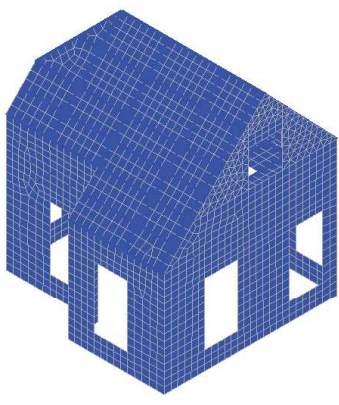
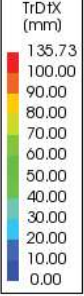
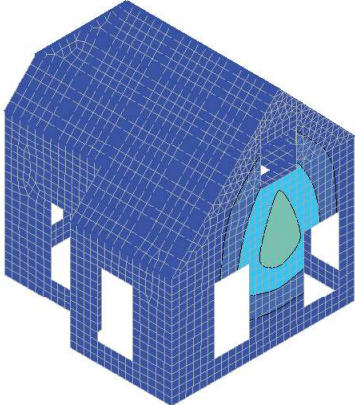
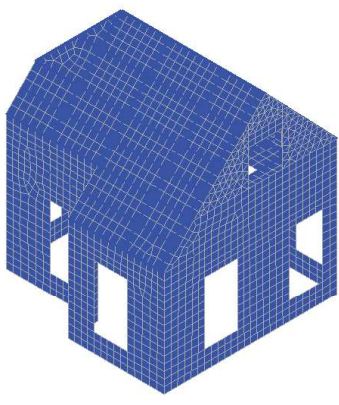
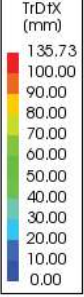


Appendix

The appendix reports a comparison between the maximum absolute deflections measured during the seven NLTH analyses performed for both Model A and Model B.

Table 1. Maximum absolute displacements measured during the NLTH analyses. South-West view.

	Model A	Model B	Scale
M5			
M6			
M7			

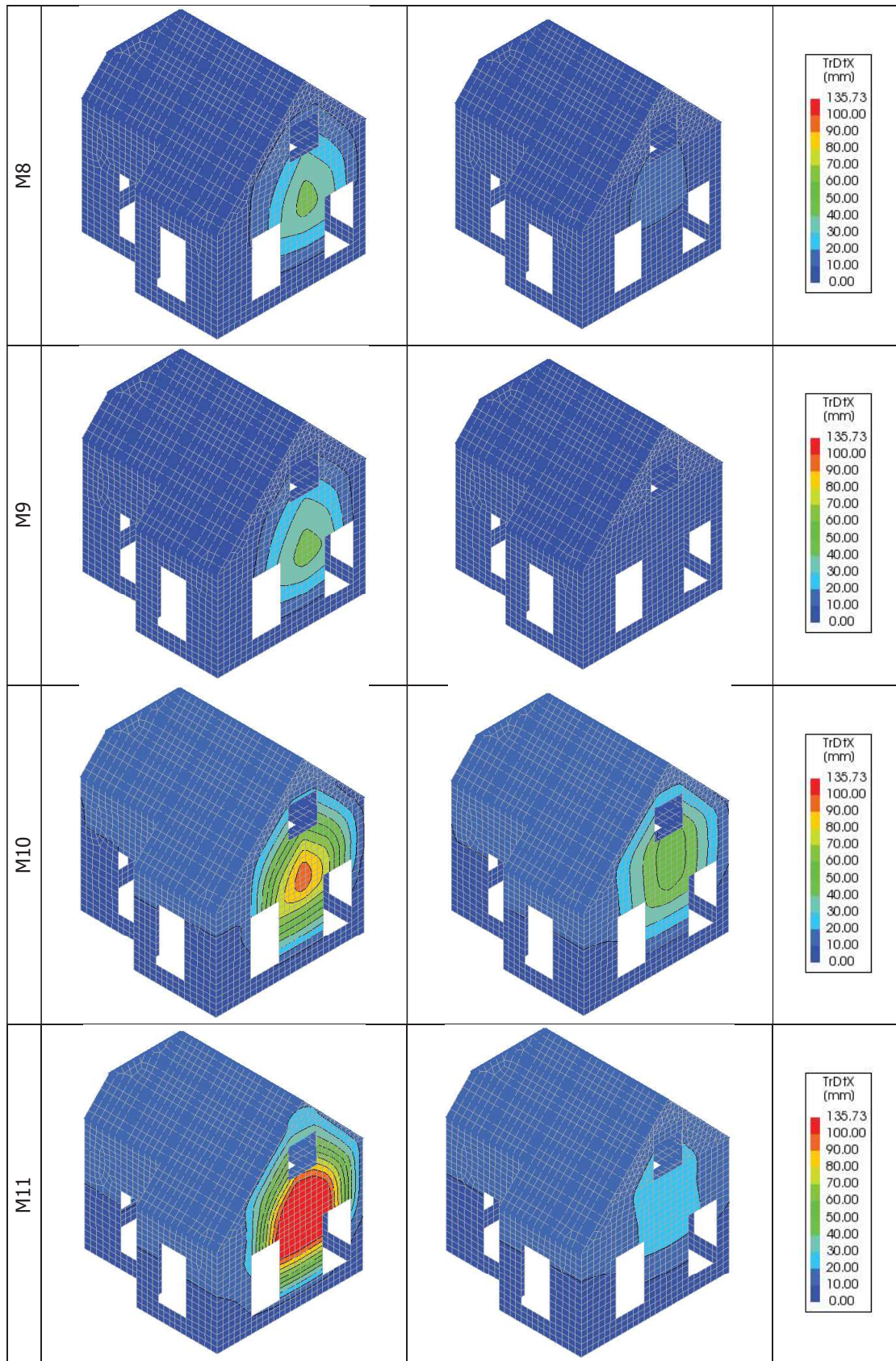
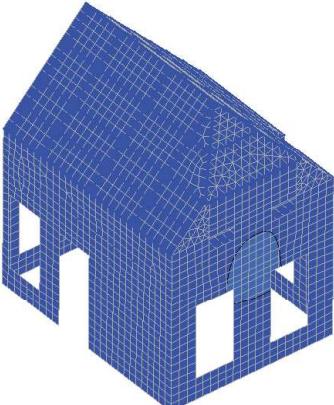
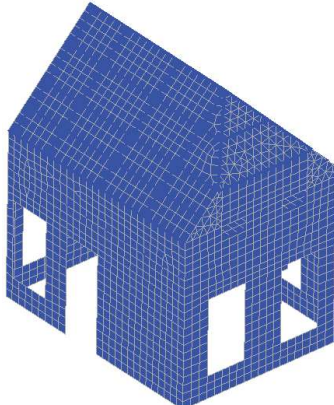
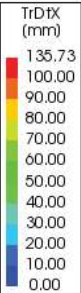
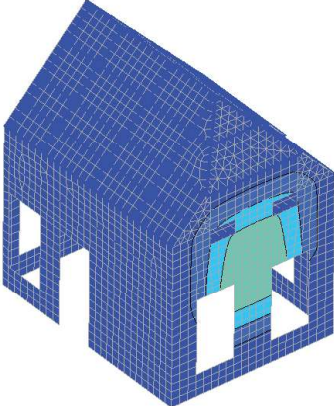
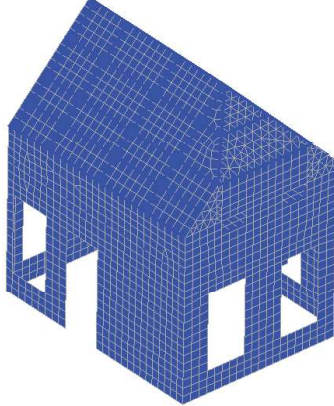
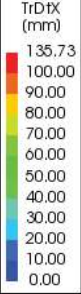
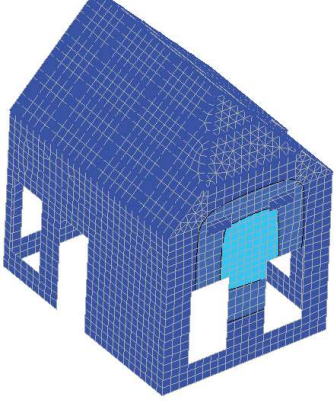
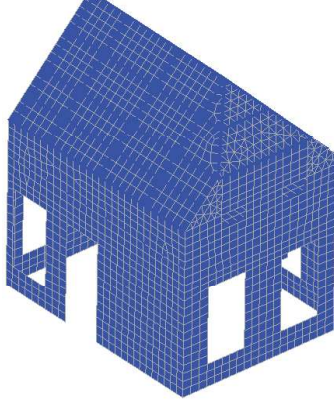
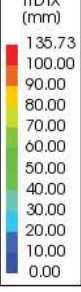
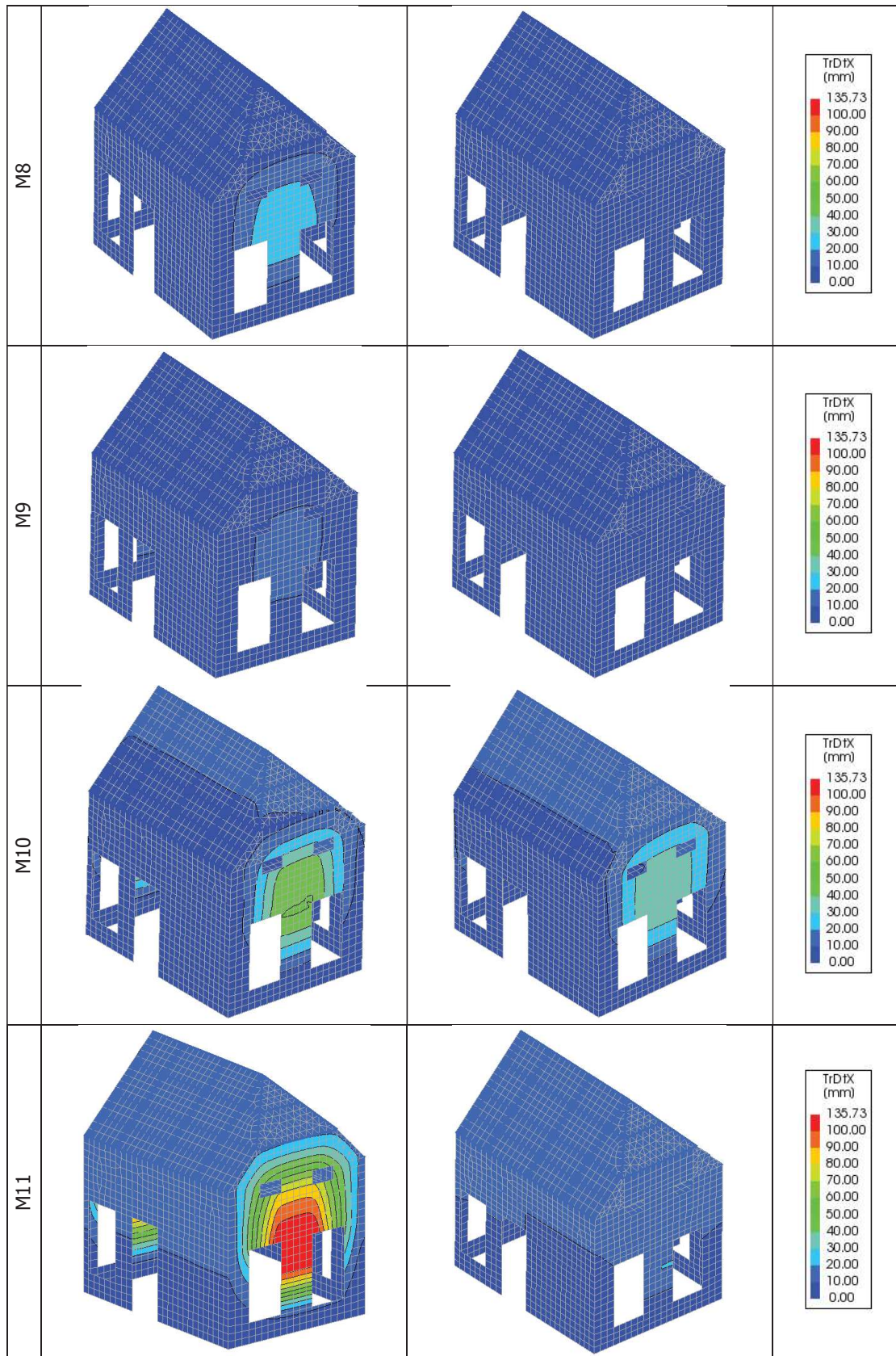


Table 2. Maximum absolute displacements measured during the NLTH analyses. North-East view.

	Model A	Model B	Scale
M5			 <p>TrDtX (mm)</p> <p>135.73 100.00 90.00 80.00 70.00 60.00 50.00 40.00 30.00 20.00 10.00 0.00</p>
M6			 <p>TrDtX (mm)</p> <p>135.73 100.00 90.00 80.00 70.00 60.00 50.00 40.00 30.00 20.00 10.00 0.00</p>
M7			 <p>TrDtX (mm)</p> <p>135.73 100.00 90.00 80.00 70.00 60.00 50.00 40.00 30.00 20.00 10.00 0.00</p>



## E Effect van materiaal verdiepingsvloer

Singla, A., Messali, F., Influence of the floor type at first storey level on the seismic behaviour of a detached house, TU Delft Memorandum, 25 juni 2020

## **Influence of the floor type at first storey level on the seismic behaviour of a detached house**

### **Introduction**

For the 'Typology based assessment' of the building stock in Groningen, the self-standing (also called 'detached') houses with a gutter line at the height of the first storey level are grouped into the typology Metselwerk C. This typology is further divided in three sub-typologies: Metselwerk 5-6-7, depending on the characteristics of walls and floors. Namely, Metselwerk 6 is characterized by cavity perimeteral walls and concrete floors, whereas Metselwerk 7 by cavity walls and timber floors. The study presented in this memorandum aims at investigating the influence of two different floor types (a timber floor and a reinforced concrete slab) on the seismic response of a detached house. In other words, the memorandum studies the seismic performance of two similar buildings, one belonging to the sub-typology Metselwerk 6 and one to Metselwerk 7. To achieve this scope, the current document presents a comparison between the outcomes of Nonlinear Time History (NLTH) analyses performed on two buildings that differ only for the floor type.

The detached house considered in this study is the one used also to investigate the seismic behaviour of buildings belonging to typology Metselwerk 7 [1]. This building is based on the specimen EUC-BUILD-2 tested on a shake table test at the laboratory of EUCENTRE (Pavia, Italy) in 2016 [1]. The specimen was designed to resemble a typical one-storey detached house with a pitched roof (Figure 1). The house is composed of a first-floor timber diaphragm and of a pitched timber roof finished with clay tiles. The timber floor and the roof framing members are supported by double-wythe solid clay URM walls. A gable is present on the front (North) and back (South) façade, as shown in Figure 2. More details regarding the specimen EUC-BUILD-2 are provided in the testing report [2]. With respect to EUC-BUILD-2, cavity walls made by solid clay bricks are considered in place of the original double-wythe walls. This structure, already considered in [1], is hereinafter called "model A". In this variation study, a new building is introduced, where the timber floor is replaced by a reinforced concrete (RC) slab with the same characteristics of that used in EUC-BUILD-6 [3]. The alternative building, named "model B", belongs to typology Metselwerk 6.

NLTH analyses are performed for the two cases (models A and B) by applying seven ground motions of increasing intensity at the base of the structure. The ground motions are part of those used for the

Hazard and Risk study [4], and especially for the NLTHA performed by ARUP [5]. Only the stronger motions (M05 to M11) have been considered to have more information on the behaviour of the building at collapse. Each ground motion consists of three orthogonal components: two horizontal components (one parallel to the East-West façades and one to North-South façades) and one vertical component. Additional information about the ground motions can be found in Appendix A of [1].

The obtained results are compared in terms of normalized base shear force-floor displacement curves, of backbone curves and of maximum out-of-plane (OOP) deformations of the walls.



**Figure 1: Buildings with construction details similar to those adopted for the shake-table test specimen (from [2]), and actual specimen tested at the laboratory of Eucentre (from [6]).**

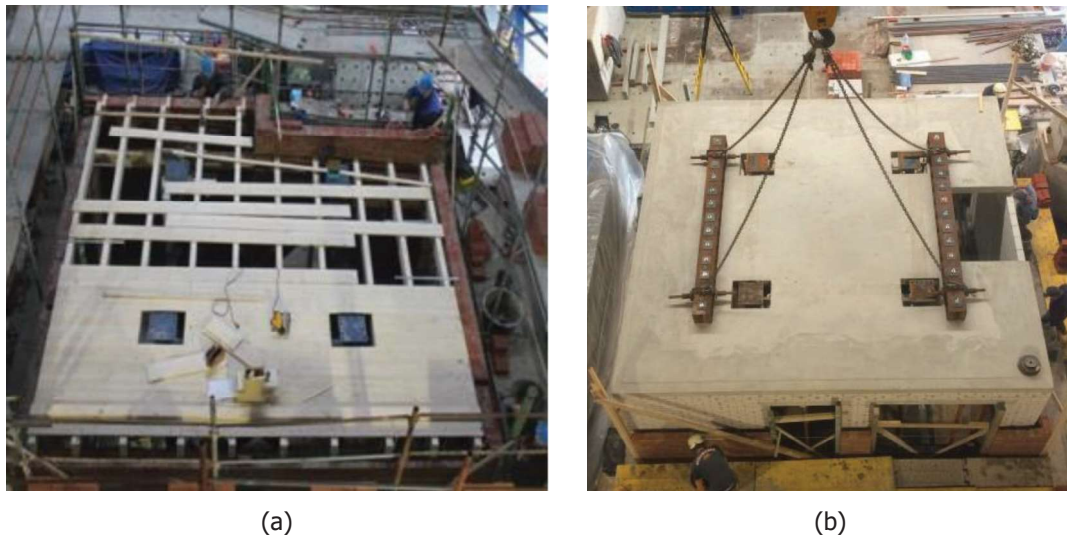


**Figure 2. Timber floor (a) of specimen EUC-BUILD-2 (from [2]) and RC slab (b) of specimen EUC-BUILD-6 (from [3]), used for models A and B, respectively.**

## Methodology

The same methodology described in section 3 of report [1] (on the numerical investigation of building typology 'Metselwerk 7') is followed. Also the definitions of the displacement at near collapse and of the backbone curve are the same as presented in [1].

## Comparison between the outcomes of the NLTH analyses

The results of the NLTH analyses performed for models A and B are shown in Figure 3 for all the seven ground motions, in terms of normalised base shear force vs. average attic displacement curves. The figure shows also the points (represented as dark grey circles) derived for each motion to define the backbone curves of the two models, shown in Figure 4. The values of the displacements and of the normalized forces of the two backbone curves are listed in Table 1. The largest out-of-plane (OOP) displacements of the walls, measured in the longitudinal (North-South) x-direction during ground motion 11, are shown in Figure 5. The maximum deflections obtained for each ground motion are shown in the Appendix.

The response of both the buildings is characterised by large OOP displacements of the walls for the ground motions of larger intensity. However, significant differences between the response of the two buildings are observed, since the presence of the concrete floor determines a more global response of the building. The South façade of Model B shows much smaller OOP displacements than that of Model A, whereas the central pier of the North façade undergoes large OOP displacements, although not exceeding 100 mm (the threshold value set for the OOP collapse). Besides, also the consequence of the possible OOP collapse of the walls is different: if the OOP collapse of the two facades would almost certainly determine the global collapse of the building, the collapse of the central pier of the North wall may result in a local collapse, since the load originating from the portion of masonry above could be redistributed to the two piers at the sides, also thanks to the presence of the concrete floor. It should be noted also that the maximum OOP displacements of Model B are consistently smaller than those of Model A for every ground motion (as shown in the Appendix).

The differences highlighted above are consistently reflected by the hysteretic curves and the backbone curves of the two buildings. In fact, although Model B reaches at peak slightly lower normalized base shear forces (-12%), the post-peak behaviour is characterized by a stable plateau up to large displacements, and no collapse is observed until the end of the analyses. For this reason, the backbone curve of Model B does not show a softening branch, which could be computed only by performing additional NLTH analyses and applying ground motions of increased intensity. It should be noted that these additional analyses may also increase the value of the peak normalized base shear force. Finally, Model B is also much stiffer ( $K_{in,B}$  is approximately five times  $K_{in,A}$ ), as expected for a building with a stiff diaphragm when compared to the corresponding building with a timber floor.

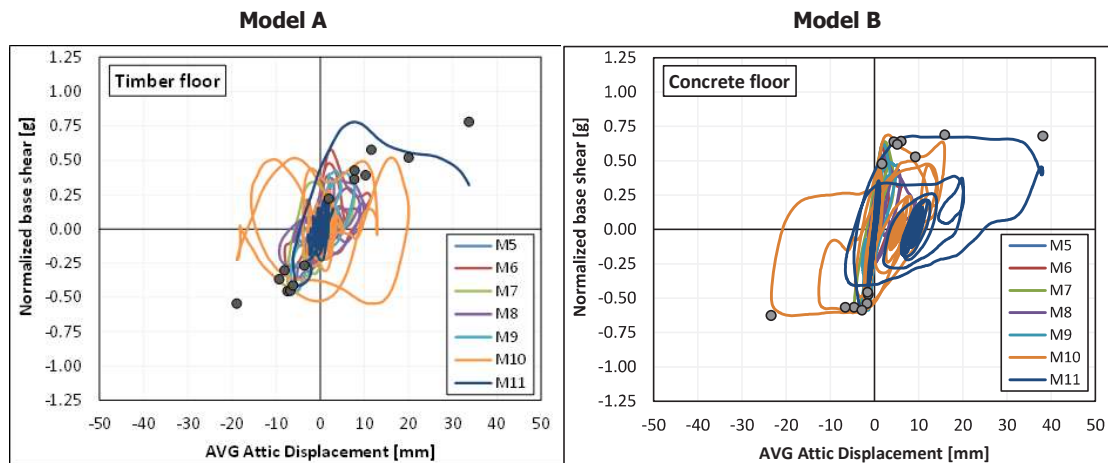


Figure 3. Normalized base shear – displacement curves for the NLTH analyses performed for models A and B

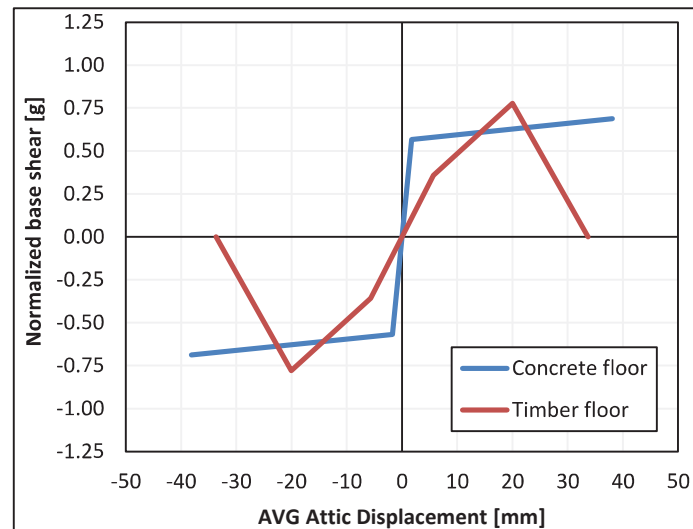


Figure 4. Backbone curves defined for the NLTH analyses performed for models A and B

Table 1. Displacements and normalized base shear of the backbone curves for models A and B

	Model A		Model B			
	d (mm)	$\nu$ (g)	d (mm)		$\nu$ (g)	
Yielding	5.66	0.36	1.72	(-70%)	0.57	(+58%)
Peak	20.0	0.78	38.1	(+90%)	0.69	(-12%)
Collapse	33.7	0	-	-	-	-

d = average attic displacement

$\nu$  = normalized base shear

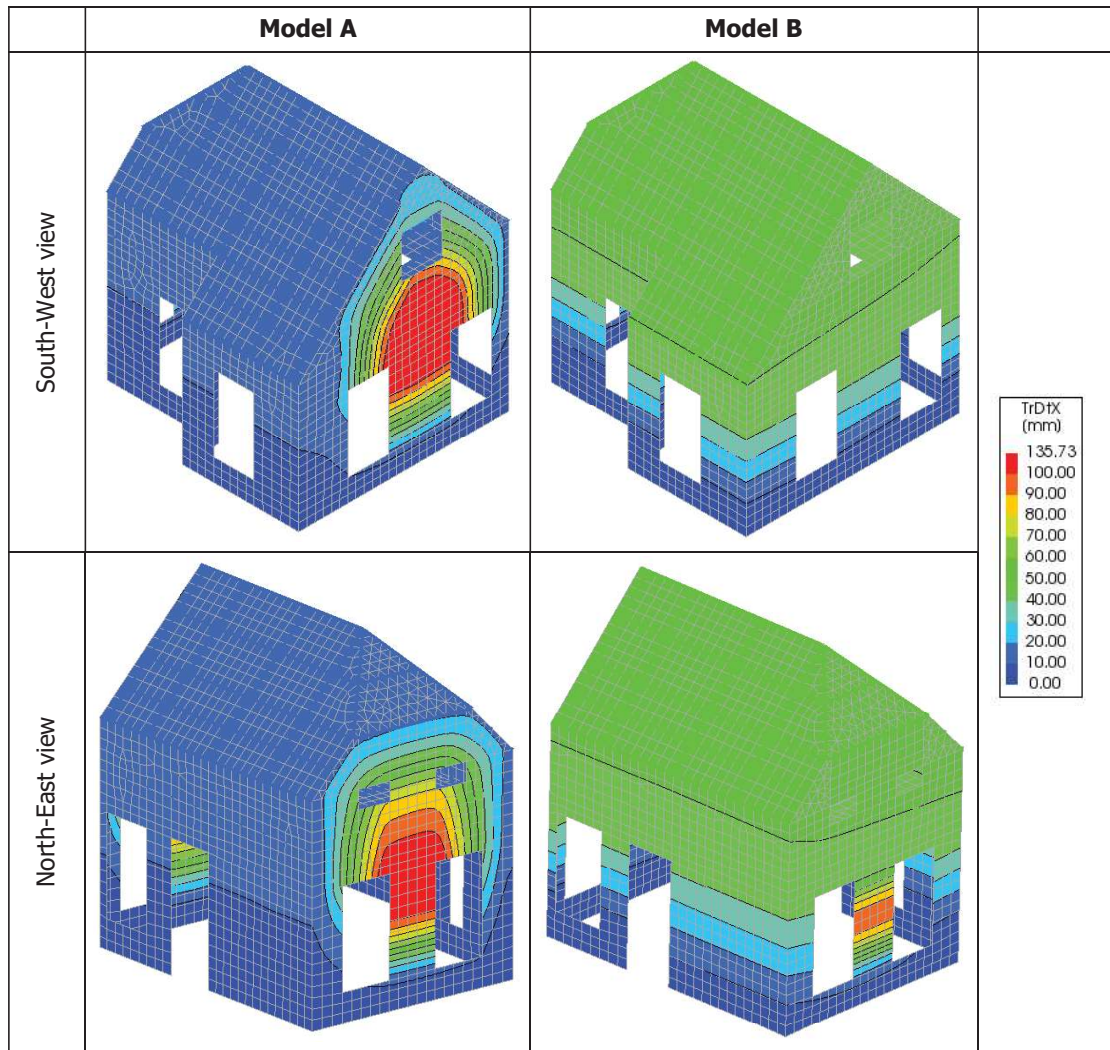


Figure 5. Maximum longitudinal (x-direction) displacements measured during ground motion 11 for both models A and B, from two different perspectives

## Conclusive remarks

This study aims at investigating the influence of two different floor types (a timber floor and a reinforced concrete slab) on the seismic response of a detached house. To achieve this scope, the terraced house used to investigate the seismic behaviour of buildings belonging to the typology Metselwerk 7 is considered also in this study. This building is a variation of specimen EUC-BUILD-2, where the original double-wythe solid walls have been replaced by cavity walls. The building is further varied in this study by replacing the timber floor at attic level (Model A) with a RC slab (Model B). The seismic behaviour of the two models is investigated by comparing the outcomes of seven Nonlinear Time History (NLTH) analyses, which show several differences between the structural response of the two buildings to the applied ground motions.

In detail, although both models are characterised by large out-of-plane (OOP) displacements, these displacements determine the OOP collapse of the wall only for Model A. Besides, the OOP failure mechanism involves the whole North and South facades of Model A, but it regards only the central pier in the North façade of Model B: if the OOP collapse of the two facades would almost certainly cause the global collapse of the building, the failure of the central pier in the North wall would likely result in a local collapse, since the loads deriving from the portion of structure above the pier could be redistributed to the two piers at the side, also thanks to the presence of the concrete floor. The absence of collapse for Model B is reflected also in its hysteretic and backbone curve, which does not have a final softening branch (unlike that of Model A). The point of collapse for Model B may be computed only by performing additional NLTH analyses with ground motions of increased intensity. Finally, Model B is also largely stiffer than Model A.

The remarks reported above suggest that the modelled detached house with a RC slab floor (Model B) is less vulnerable than the corresponding one with a timber floor (Model A) when subjected to the same set of ground motions.

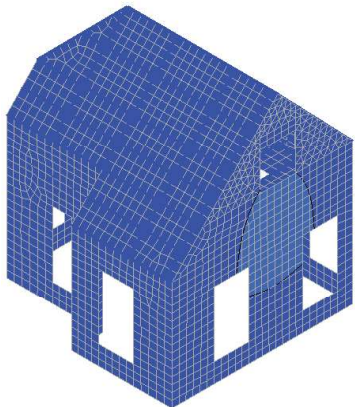
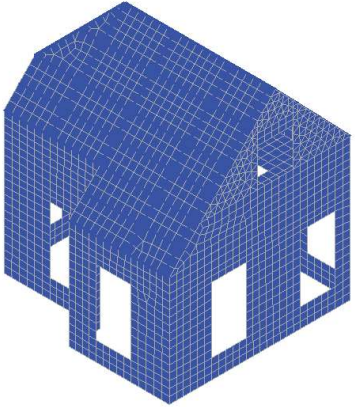
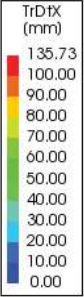
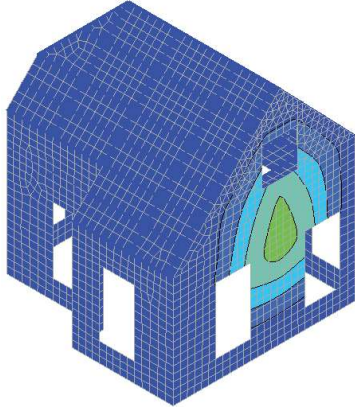
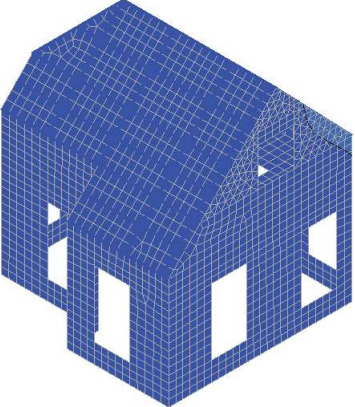
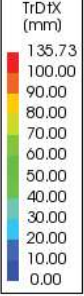
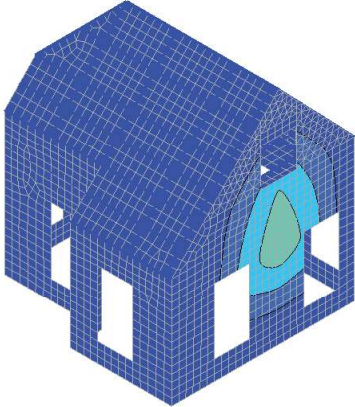
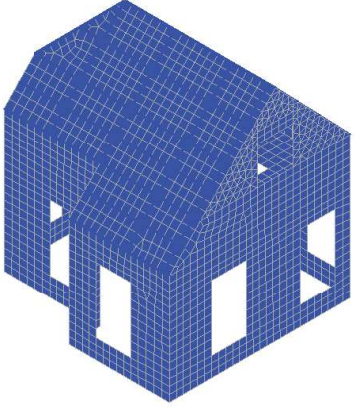
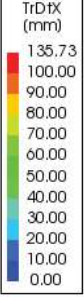
## References

- [1] Messali, F., Longo, M. (2020). A numerical investigation of building typology 'Metselwerk 7'. Delft University of Technology. Report number 03, Version 01, 19 June 2020
- [2] Graziotti, F., Tomassetti, U., Rossi, A., Marchesi, B., Kallioras, S., Mandirola, M, Fragomeli, A., Mellia, E., Peloso, S., Cuppari, F., Guerrini, G., Penna, A., Magenes, G. (2016). Shaking table tests on a fullscale clay-brick masonry house representative of the Groningen building stock and related characterization tests. Report EUC128/2016U, EUCENTRE, Pavia, IT
- [3] Miglietta, M., Mazzella, L., Grottoli, L., Guerrini, G., Graziotti, F. (2019). Full-scale shaking table test on a Dutch URM cavity-wall terraced-house end unit – EUC-BUILD-6. EUCENTRE report EUC160/2018U. Version 2.0, 07 March 2019
- [4] Crowley, H., Pinho, R. (2020). Report on the Fragility and Consequence Models for the Groningen Field (Version 7). NAM report, March 2020
- [5] Merczel, D., Abeysekera, I., McVitty, W., Grant, D., Kluwer, R., (2017). Typology Modelling: Analysis Results in Support of Fragility Functions – 2017 Batch Results. NAM report, October 2017
- [6] Kallioras, S., Guerrini, G., Tomassetti, U., Peloso, S., & Graziotti, F. (2018). Dataset from the dynamic shake-table test of a full-scale unreinforced clay-masonry building with flexible timber diaphragms. Data in brief, 18, 629-640

Appendix

The appendix reports a comparison between the maximum absolute deflections measured during the seven NLTH analyses performed for both Model A and Model B.

Table 2. Maximum absolute displacements measured during the NLTH analyses. South-West view.

	Model A	Model B	Scale
M5			
M6			
M7			

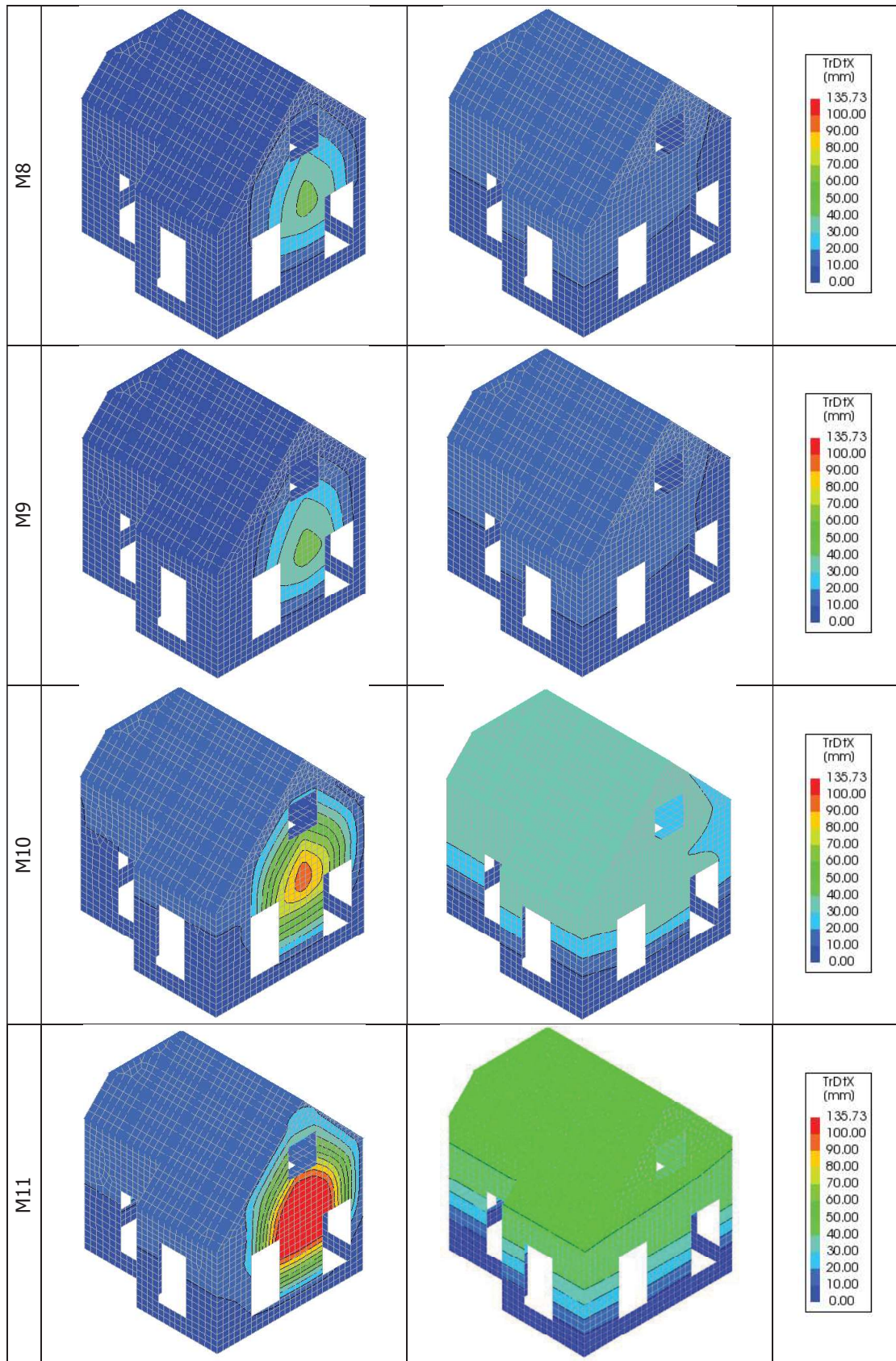
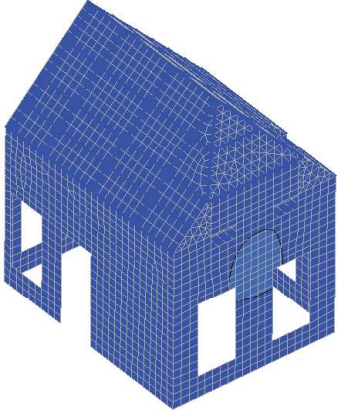
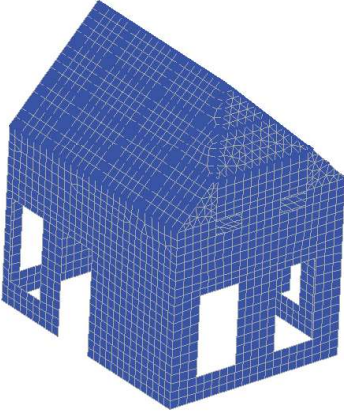
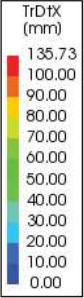
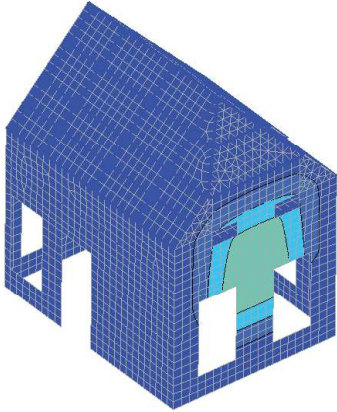
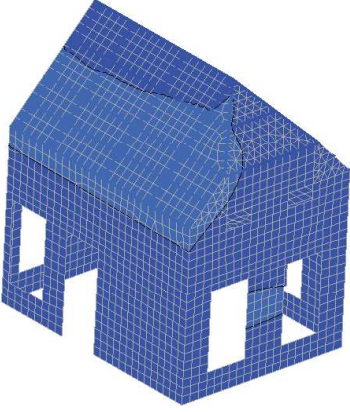
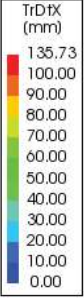
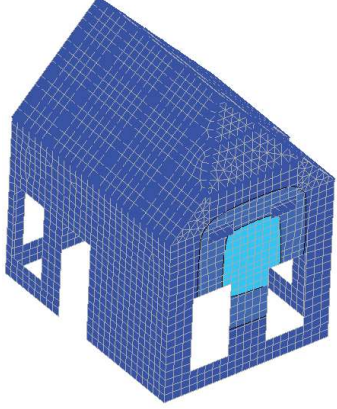
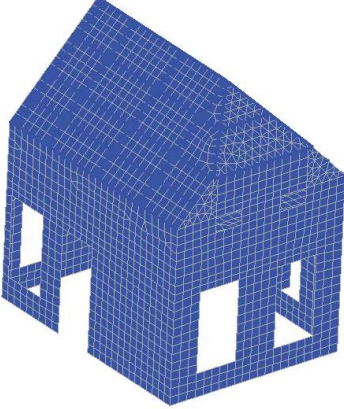
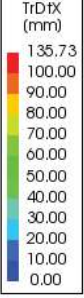
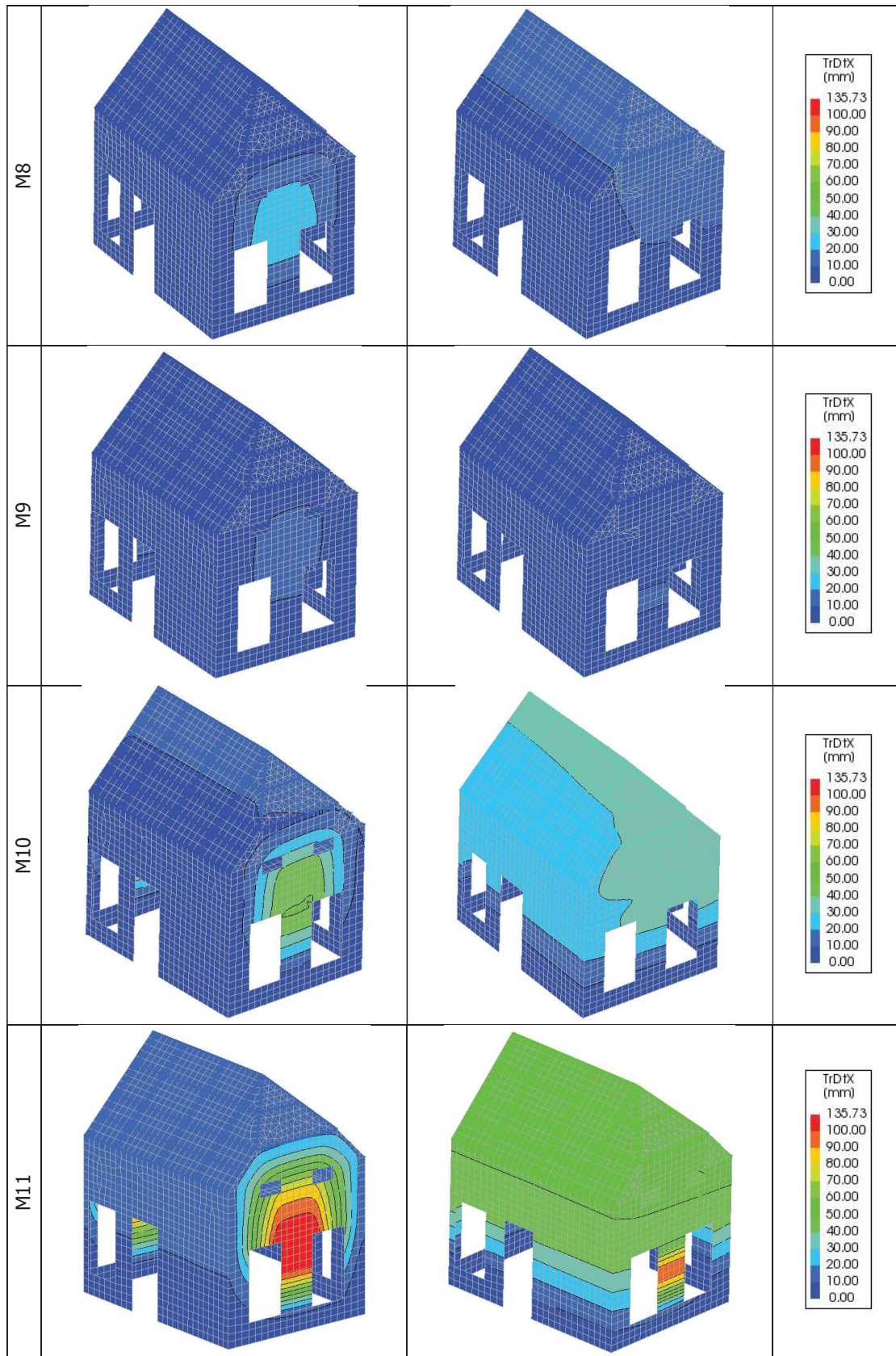


Table 3. Maximum absolute displacements measured during the NLTH analyses. North-East view.

	Model A	Model B	Scale
M5			 <p>TrDtX (mm)</p> <p>135.73 100.00 90.00 80.00 70.00 60.00 50.00 40.00 30.00 20.00 10.00 0.00</p>
M6			 <p>TrDtX (mm)</p> <p>135.73 100.00 90.00 80.00 70.00 60.00 50.00 40.00 30.00 20.00 10.00 0.00</p>
M7			 <p>TrDtX (mm)</p> <p>135.73 100.00 90.00 80.00 70.00 60.00 50.00 40.00 30.00 20.00 10.00 0.00</p>



## F      Numeriek modelleren van uit het vlak falen van steens muren

Singla A., Messali, F., Analytical prediction of the out-of-plane capacity of a solid wall (typology Metselwerk 5), TU Delft Memo, 4 april 2020

## Analytical prediction of the out-of-plane capacity of a solid wall (sub-typology Metselwerk 5)

### Introduction

For the 'Typology based assessment' of the building stock in Groningen, the self-standing (also called 'detached') houses with a gutter line at the height of the first storey level are grouped into the typology Metselwerk C. This typology is further divided in three sub-typologies: Metselwerk 5-6-7, depending on the characteristics of walls and floors. Namely, Metselwerk 5 is characterized by solid perimetral walls and timber floors. This sub-typology corresponds to the typology URM6L as defined in the Hazard and Risk (HRA) study. The HRA study identifies one or more index buildings per typology, whose seismic response (expressed in terms of force-displacement backbone curves and description of the failure mechanisms at different collapse states) has been used by Eucentre as starting point to define the fragility curve of the typology. The seismic response of such buildings was investigated by ARUP via Non-Linear Time History (NLTH) numerical analyses. Since the work performed in support to the HRA represents useful material to be used for the Typology based assessment, it is important for TNO and TU Delft to discuss critically the choices made by Eucentre and ARUP. In this specific case, the current memorandum discusses critically the selection of specimen LNEC-BUILD-3 (tested on a shake table at LNEC, Lisbon, in 2018) as index building for the HRA typology URM6.

In detail, the contents of this memorandum are based on the following premises:

1. The backbone curve of typology URM6L is defined in the HRA study:
  - in version 5 of HRA [1] via the nonlinear time history (NLTH) analyses performed by ARUP of building "Nieuwstraat 8 (Loppersum)" (Figure 1);
  - in version 6 of HRA [2] by the shake table test performed at LNEC on specimen "LNEC-BUILD-3" (Figure 1).
2. LNEC-BUILD-3 was designed to be representative of buildings belonging to typology URM6L (such as Nieuwstraat 8). However, due to the limited size of the shake table, the length of the East and West façades in LNEC-BUILD-3 had to be shorter by approximately 20-30% of a typical URM6L building, reducing the effects on the OOP vulnerability of the walls [3]. As a way to counterbalance the favourable effects of shortening the length of the East façade, it was decided to build it as a single-wythe wall (unlike the double-wythe wall in Nieuwstraat 8).

3. The NLTH analyses of Nieuwstraat 8 show failure between the girders and the walls [4], mainly caused by the out-of-plane deformation of the walls, with consequent collapse of the floor. The shake table test does not show the failure of this connection [3], although the girder is supported on a wall with half of the thickness.

This short memorandum aims to assess whether the reduction of the thickness of the East wall in LNEC-BUILD-3 (from double- to single-wythe) is a conservative solution to compensate for the shorter length of the wall with respect to the corresponding façade in Nieuwstraat 8.

## **Methodology and assumptions**

In principle, to achieve the scope mentioned in the introduction, the displacement of the point of the wall that supports the girder (the centre of the East wall, at the attic level) should be computed in dynamic conditions with a significant ground motion applied at the base of the structure for both the investigated buildings. This requires sophisticated and time consuming analyses. Alternatively, in this work the out-of-plane capacity of the East wall is computed according to two simple analytical procedures, described in the Australian standards AS3700 [5] and in the Commentary on Annex H of NPR 9998 (2018) [6], this latter procedure largely refers to the method described by Willis in his doctoral thesis [7]). It is then assumed that a larger capacity of the wall corresponds to smaller deformations and hence to a smaller displacement of the point where the girder is supported.

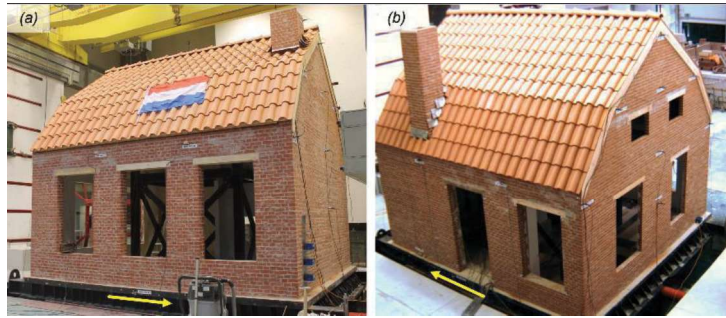
It is also assumed that the presence of the openings on the East wall can be neglected, since they may trigger the activation of one-way bending failure mechanisms, which are less sensitive to the length of the walls than two-way mechanisms. A wall with no openings and subjected to a two-way bending failure mode is a case that enhances the effects of the change in length of the wall.

The geometry of the East walls of the two buildings is considered for the comparison. The North and South facades are assumed to provide lateral supports to the East wall, whereas no support is given by the floor on the top. The wall is then assumed to be supported on three sides (bottom and lateral sides: "U"-type restraints).

The axial overburden on top of the wall is not known, because it can vary during a seismic motion. For this reason, two values representative of a small overburden (0.05 MPa) and of a medium-large overburden (0.2 MPa) are considered.



Nieuwstraat 8 (Loppersum)



LNEC-BUILD-3

Figure 1. The building at Nieuwstraat 8 (Loppersum) and LNEC-BUILD-3 (from [3])

## Results of the analysis

The out-of-plane capacity of single- and double-wythe walls is computed in terms of lateral pressure (Figure 2). This parameter does not depend on the dimensions of the wall, and it allows to compare walls of different length. The specific cases of Nieuwstraat 8 and LNEC-BUILD-3 are highlighted.

For all the four considered cases, the capacity computed for the East wall of the LNEC-BUILD-3 is smaller than the one of the corresponding wall in Nieuwstraat 8. It should also be noted that the difference is larger when the method proposed in [6] is used.

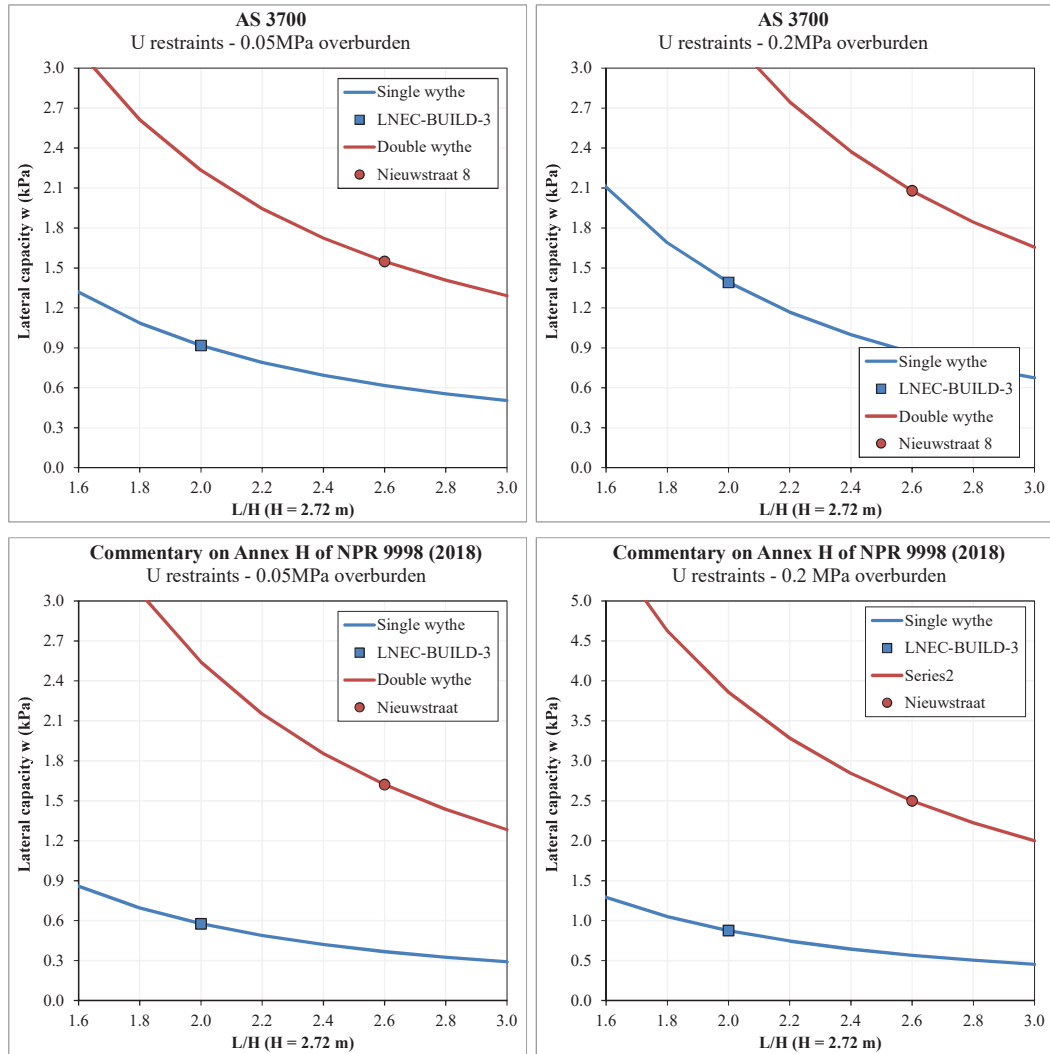


Figure 2. Out of plane capacity of single- and double-wythe walls computed according to the formulations provided in the Australian standard AS3700 [5] and in the Commentary on Annex H of NPR 9998:2018 [6] for different values of the axial overburden.

## Conclusive remarks

Based on the results shown in the previous section, the reduction in thickness of the East wall of LNEC-BUILD-3 is a conservative solution to compensate for the reduction in length of the wall, when compared to the corresponding wall in Nieuwstraat 8.

## References

- [1] Crowley, H., Pinho, R. (2017). Report on the v5 Fragility and Consequence Models for the Groningen Field. NAM report, November 2017
- [2] Crowley, H., Pinho, R., Cavalieri, F. (2018). Report on the v6 Fragility and Consequence Models for the Groningen Field. NAM report, March 2019
- [3] Kallioras S, Correia AA, Marques AI, Bernardo V, Candeias PX, Graziotti F. LNEC-BUILD-3: An incremental shake-table test on a Dutch URM detached house with chimneys. EUCENTRE Technical Report EUC203/2018U, EUCENTRE, Pavia, Italy; 2018. Available at [www.eucentre.it/nam-project](http://www.eucentre.it/nam-project)
- [4] Merczel, D., Abeysekera, I., McVitty, W., Grant, D., Kluwer, R. (2017). Typology Modelling: Analysis Results in Support of Fragility Functions – 2017 Batch Results. NAM Report, October 2017
- [5] Standard Association of Australia (2018). AS 3700-2018: Masonry Structures. Sydney, Australia
- [6] Sharma, S., Tomassetti, U., Graziotti, F. (2019). Commentary Eucentre on Annex H of NPR 9998 (2018). Eucentre report, 21 February 2018, v1.0
- [7] Willis, C.R. (2004). Design of unreinforced masonry walls for out-of-plane loading (Doctoral dissertation)

## G Beschouwing op basis van controleberekeningen

This Annex summarizes the findings of the numerical simulations performed by TU Delft on two selected buildings of typology METSELWERK7 and compares the findings against the building currently implemented in the Typology Approach. Non-linear time history (NLTH) analyses are performed using a set of 11 ground motions with different intensities. These calculations are reported in Annex H.

The analysed buildings are Damsterweg 37 and Wirdumerweg 4 both being a detached house with unreinforced masonry cavity walls:

- Wirdumerweg 4, which is a two-storey detached house made of unreinforced masonry (URM) cavity walls with gutter height at first floor. The 1<sup>st</sup> floor and attic floor are made of timber beams spanning in the short direction. This building can be assigned to METSELWERK 7 typology for which the index building is *Badweg12*.
- Damsterweg 37, which is a two-storey detached house made of unreinforced masonry (URM) cavity walls and partially made of single leaf (half brick width) clay walls, with gutter height at first floor. The 1<sup>st</sup> floor and attic floor are made of timber beams. These characteristics place the building in the METSELWERK 7 typology for which the index building is *Badweg12*.

### Wirdumerweg 4

Wirdumerweg 4, is a two-storey (plus attic) detached house made of unreinforced masonry (URM) cavity walls with gutter height at first floor, built in 1909. The 1<sup>st</sup> floor and attic floor are made of timber beams spanning in the short direction. The figure of the building and the corresponding FEM model are shown in Figure G.1. A complete description of the model and the simulations can be found in Annex H.

Non-linear elements are used to model masonry walls. The pocket connections between the timber beams of the attic floor and between the purlins and the masonry gables are assessed according to a force-based criterion. Namely, the failure of the connections is defined when the force capacity is exceeded for more than 0.1 s. This is assumed to provoke as consequence the failure of the connected masonry walls too. Timber elements are modelled with a linear elastic material.

Due to the implicit solver of the time history calculations performed with Diana, it should be noticed that explicit (and progressive) collapse cannot be modelled using an implicit calculation. Due to this, a set of “stop criteria” are implemented in order to cap the capacity and the ultimate displacement of the analyses.

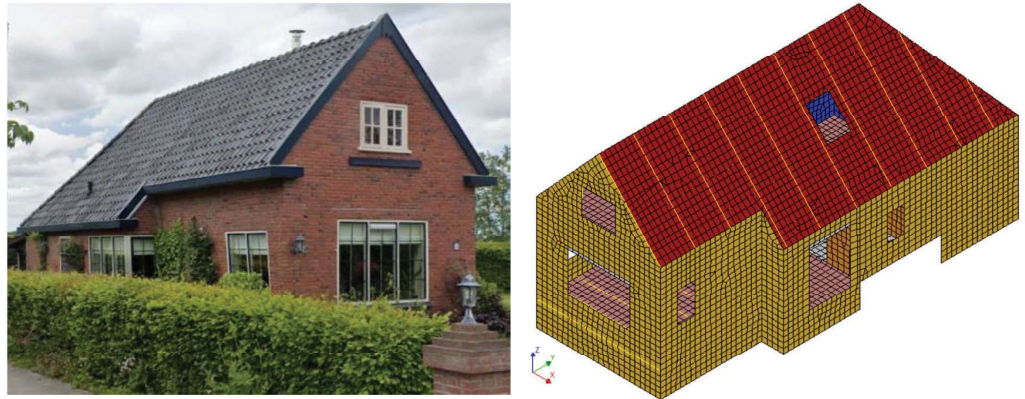


Figure G.1: Wirddumerweg 4 detached house: side view of the building (left) and the 3D model created with DIANA FEA (right). taken from Annex H.

The failure mechanisms considered are:

- In-Plane failure is reached when the masonry piers experience a drift of 1.5% (ductile mechanism) and 0.6% (shear type).
- Out-of-Plane (OOP) failure is reached when the OOP displacement of a load-bearing wall exceeds 100mm.
- Connection failure, computed based on a frictional force criterion derived from experimental tests performed by TU Delft.

The results of the NLTHA are elaborated to produce backbone curves. The curves describe the relation between the base shear and attic displacement along the main building axes. Those curves are typically normalized against the dynamic weight obtained as the product between the effective mass (participating in the motion) and the gravity acceleration. For this particular building, high foundations were present and an upper and lower bound of the dynamic mass were adopted for the normalization of the backbone curves: Mass A (46 ton, 49% of the total mass) and Mass B (81.4 ton, 86% of the total mass), shown in Figure G.2. It should be noted that the larger the mass, the more conservative is the resulting backbone curve.

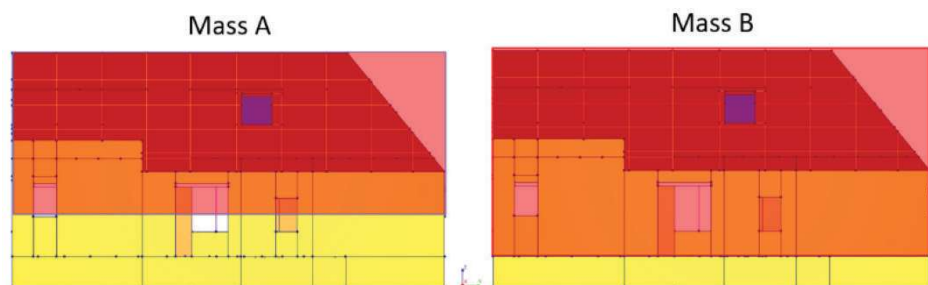


Figure G.2 Considered effective masses (portion of the house highlighted in red) for Wirddumerweg 4: Mass A (46 ton, left) and Mass B (81.4 ton, right). Adapted from Annex H.

In Figure G.3, the resulting backbone curves are compared with the backbone curve of Badweg 12 (index building used to define the median of METSELWERK7 typology).

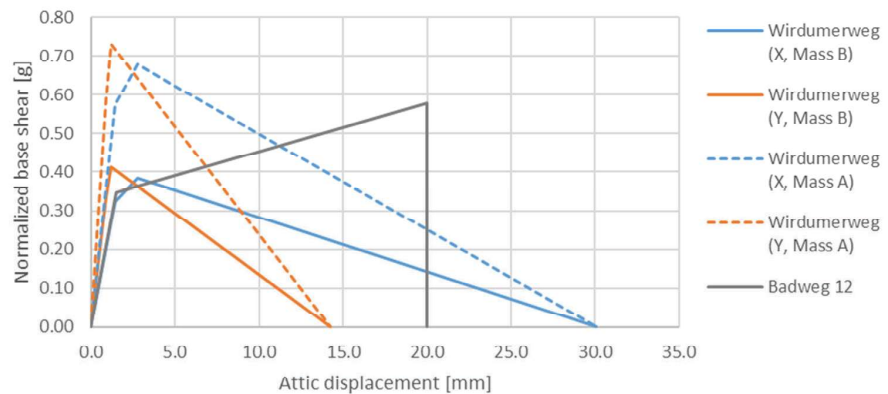


Figure G.3 Backbone curves of the Wirdumerweg 4 building (X and Y directions) for 100mm OOP displacement limit for Mass A (dashed lines) and Mass B (solid lines) and backbone curves of the Badweg12 index building adopted for METSELWERK7 typology (in grey).

Figure G.3 shows that the collapse displacement of Badweg12 is between the one of Wirdumerweg 4 in X and Y direction. The peak acceleration is also in good agreement with the one observed for Wirdumerweg 4, and it's in between Mass A and Mass B variations for both direction, being closer to Mass A. This is also in good agreement since the effective mass for Badweg12 was 44 ton, and 42% of the total mass. Due to this, the backbone curves related to Mass A are the ones adopted for the comparison with Badweg 12, as discussed in Annex H.

The collapse mechanisms observed in Annex H involve mostly an out-of-plane failure of the bearing walls in both X and Y direction. Figure G.4 shows the walls for which the out-of-plane displacement exceeded 100mm.

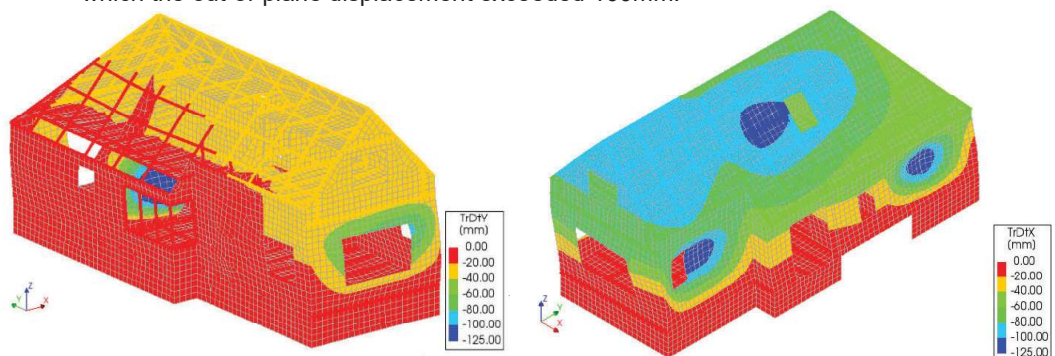
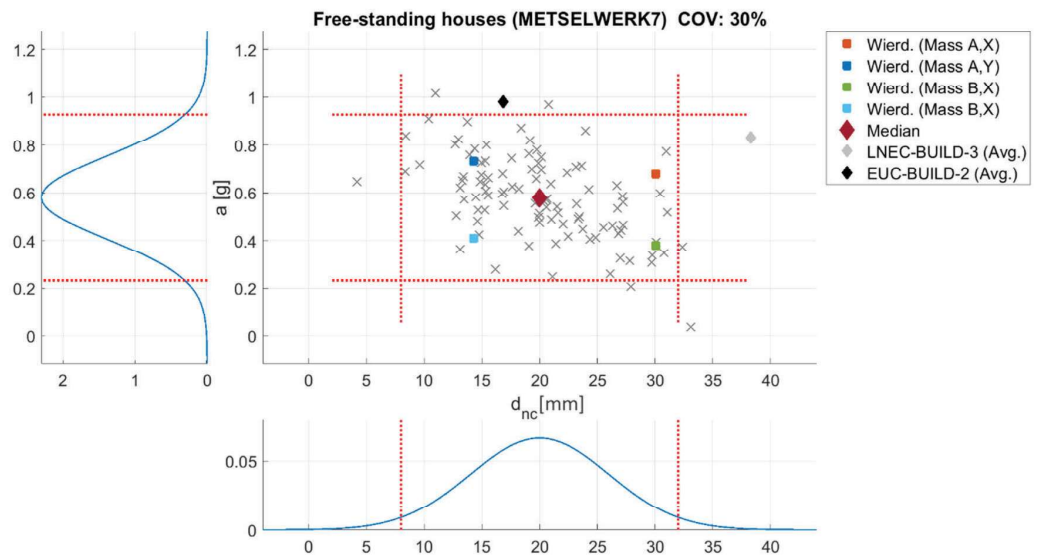


Figure G.4 OOP failures mechanisms observed for Wirdumerweg 4 building: in the Y direction (left) the internal wall and façade fail OOP while in X direction (right) the failure of perimetral walls is governing. Adapted from Annex H.

In particular, the collapse of the building in Y-direction is governed mainly by OOP collapse of the internal load-bearing wall and the façade while in the X direction is governed by the OOP collapse of the perimetral walls. The collapsed internal wall didn't carry beams (that are spanning in the direction parallel to the wall), therefore progressive collapse is not expected. However, the out-of-plane collapse of the façade was also close to 80mm, so the global collapse capacity is expected to be larger but not much. The failure mechanisms observed for Badweg12 involved the out-of-plane collapse of the gable walls and part of the longitudinal walls.

To check how the backbone curves relate to the buildings within the typology, 100 samples were produced in terms of near-collapse displacement and peak normalized base shear by means of a Latin hypercube sampling (LHS). Figure G.5 shows the 100 samples obtained from a coefficient of variation (COV) of 30% and adopting Badweg12 as the median of the distributions. Figure G.5 shows that both the variations (Mass A and B) fall within the confidence intervals.



**Figure G.5** Normalized base shear and collapse displacement of the backbone curves of: Badweg 12 index building (referred as median), the 100 variations obtained with LHS (grey crosses), Wirdumerweg 4, Mass A and B (squares) and the median building obtained by the variation study on free-standing houses of TU-Delft (Diamonds). The confidence interval from the distributions is plotted as dashed red lines.

Conclusions will be drawn after discussing the results of the Damsterweg 37 model.

### Damsterweg 37

Damsterweg 37 is a two-storey (plus attic) detached house made of unreinforced masonry (URM) cavity walls with gutter height at first floor, built in 1936. The 1<sup>st</sup> floor and attic floor are made of timber beams spanning in the short direction.

The figure of the building and the plan view are shown in Figure G.6 while the corresponding FEM model is shown in Figure G.7. A complete description of the model and the simulations can be found in Annex H.



Figure G.6 Damsterweg 37 detached house: North-west façade (left) and plan view (right). Adapted from Annex H.

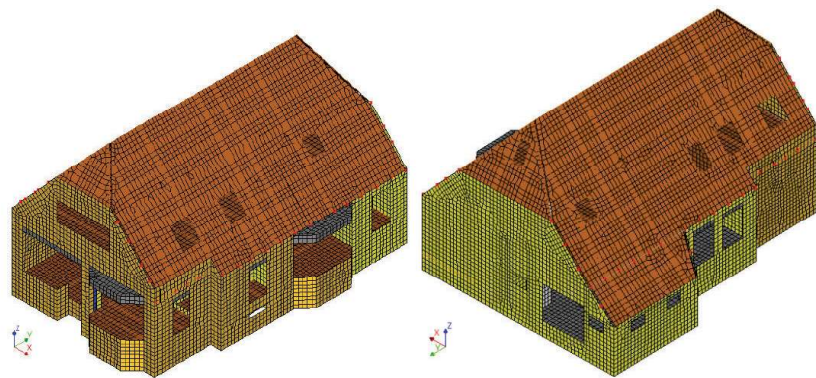


Figure G.7 Damsterweg 37 detached house: 3D model in DIANA FEA. Adapted from Annex H.

Non-linear elements are used to model masonry walls. Non-linear point interfaces are used to model the pocket connections between the beams of the attic floor and the masonry walls, and between the purlins and the masonry gables. A coulomb-friction model is employed for the interfaces. Timber elements are modelled with a linear elastic material.

Due to the implicit solver of the time history calculations performed with Diana, it should be noticed that explicit (and progressive) collapse cannot be modelled using an implicit calculation. Due to this, a set of “stop criteria” are implemented in order to cap the capacity and the ultimate displacement of the analyses. The failure mechanisms considered are:

- In-Plane failure is reached when the masonry piers experience a drift of 1.5% (ductile mechanism) and 0.6% (shear type).

- *Out-of-Plane (OOP) failure is reached when the OOP displacement of a load-bearing wall exceeds 60 mm. This was done because the maximum displacement of one of the wall bearing the floor/roof structure was found to be approximately 70mm; larger values could not be observed due to numerical instability of the analyses. Thus backbone curves for 100mm OOP displacement limit are not available for Damsterweg 37.*
- *Connection failure, computed according to the displacement capacity of the connections, assumed equal to 60 mm.*

The results of the NLTHA are elaborated to produce backbone curves. As it was done for Wirdumerweg 4, the backbone curves are normalized against the dynamic weight. For this particular building, high foundations were present and an upper and lower bound of the dynamic mass was adopted for the normalization of the backbone curves: Mass A (53.3 ton, 45% of the total mass) and Mass B (99.1 ton, 83% of the total mass), shown in Figure G.8.



*Figure G.8 Considered effective masses (portion of the house highlighted in red) for Damsterweg 37: Mass A (53.3 ton, left) and Mass B (99.1 ton, right). Adapted from Annex H.*

Since the collapse of the building is governed by the failure of the elements in Y-direction (long spanning direction), only the backbone curves for the Y direction are considered. In the X-direction (short spanning) the stop criteria were not reached.

Figure G.9 presents the resulting backbone curves and compares them against the backbone curve of Badweg12 (index building of METSELWERK7 typology). The backbone curves obtained for Damsterweg 37 appears to be a stronger and less ductile building when compared to the index building Badweg12. In particular, both the backbone curves present a larger normalized base shear but a smaller collapse displacement.

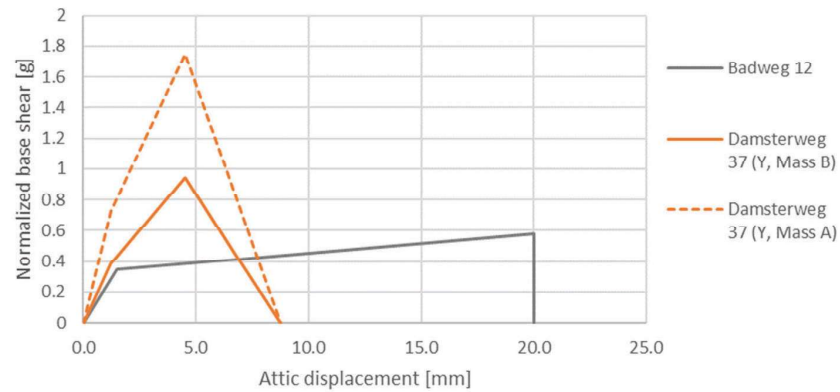


Figure G.9 Backbone curves of the Damsterweg 37 building (Y direction) for 60mm OOP displacement limit for Mass A (dashed line) and Mass B (solid lines) and backbone curve of the Badweg12 index building adopted for METSELWERK7 typology (in grey).

Figure G.10 shows that the full collapse of Damsterweg 37 is governed mainly by the OOP collapse of an internal wall, located at the West side of the building, while the local failure of the West gable is also observed. However this local collapse is estimated not to lead to the global collapse of the building since the rafters (which support both the roof and the attic floor) are supported on the North and South walls, and only the purlins are connected to the West façade. The maximum displacements reached in the simulations and the position of the collapsed walls are also shown.

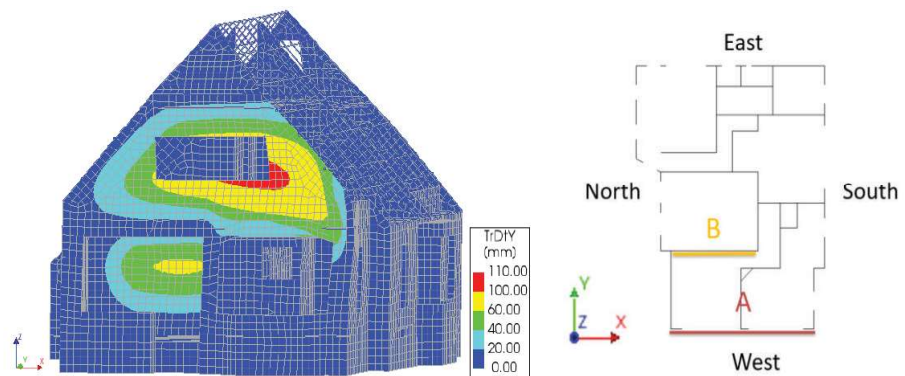


Figure G.10 Main failure mechanism observed for Damsterweg 37 building (left) and location of the collapsed walls (right): OOP failure of an internal wall (wall B) and the gable wall of the west façade (wall A). Adapted from Annex H.

These failure mechanisms are in line with the ones observed for Badweg12 which involved the first the out-of-plane collapse of the gable walls followed by the collapse of the longitudinal walls.

## Influence of different assumptions on the fragility function

To understand how the backbone curves of the freestanding houses Wirdumerweg 4 (Mass A) and Damsterweg 37, relates to the Badweg 12 index building a variation study is performed. In particular, backbone curves are sampled from Badweg 12 in terms of near-collapse displacement and peak normalized base shear by means of a Latin hypercube sampling (LHS). The median values for the sampling process are taken from Badweg12 while the coefficient of variation (COV) and the correlation between the 2 variables are adopted from the variation study of [Messali et al. 2020a] on terraced houses, assuming for this study the same variability for the free-standing house as was found for the terraced houses. A COV of 30% is adopted for both the variables and the correlation matrix is provided in Table G.1.

Table G.2: Correlation coefficients for sample generation with the LHS.

$\rho$	$a$	$d_{NC}$
$a$	1	-0.54
$d_{NC}$	-0.54	1

A total number of 100 samples are generated in terms of normalized acceleration and near collapse displacement. Figure G.11 shows the relationship between the peak normalized acceleration and near collapse displacement. In the figures, the median backbone curves obtained from the variation study of TUDelft in Annex H on the LNEC-BUILD-3 and EUC-BUILD-2 are also included.

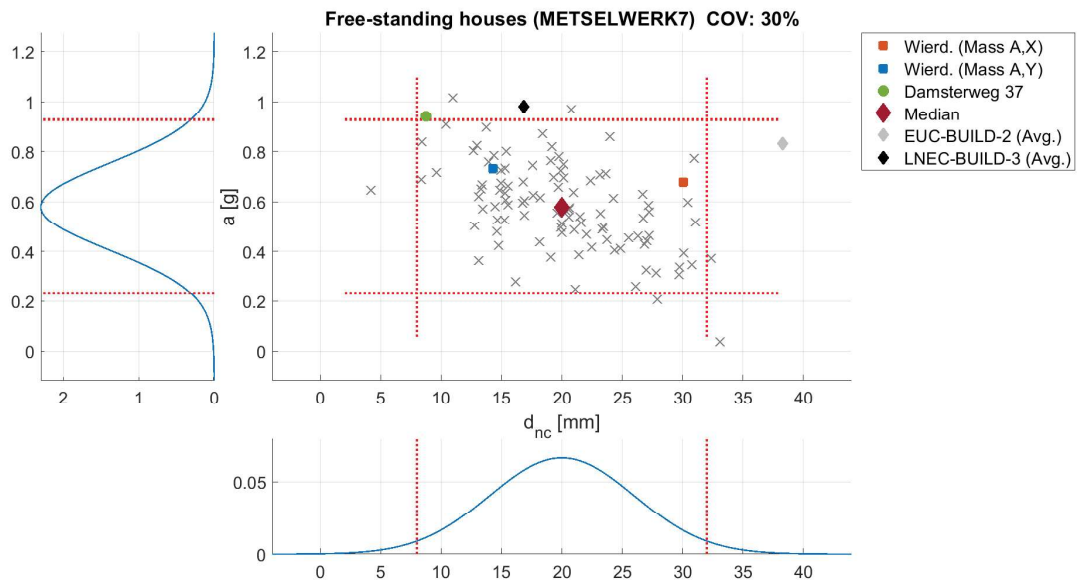


Figure G.11 Normalized base shear and collapse displacement of the backbone curves of: Badweg12 index building(referred as median), the 100 variations obtained with LHS (grey crosses), Damsterweg 37 (green dot), Wirdumerweg 4, the representative Mass A of Wirdumerweg 4, (squares) and the median building obtained by the variation study on free-studing houses of TU-Delft (Diamonds). The confidence interval from the distributions is plotted as dashed red lines.

Figure G.11 shows that all the backbone curves obtained from the NLTHA of TU Delft present a larger normalized base shear capacity than the one adopted for the median building. However, Damsterweg 37 appears to be a less ductile building, characterized by a smaller collapse displacement and a higher collapse normalized base shear. To assess whether this drop in displacement capacity is compensated by the increase in base shear capacity, a variation study on Badweg 12 was performed by modifying the collapse displacement and peak normalized base shear of the original Badweg12 backbone curve.

In particular, 4 variations of base shear and collapse displacement combinations were performed for which the values of collapse displacement and peak base shear are summarized in Table G.3.

Table G.3 Collapse displacement and peak normalized base shear adopted for Badweg12 and the variations of the latter.

<b>Model</b>	<b>Collapse displacement [mm]</b>	<b>Peak norm. base shear [g]</b>
Badweg12	20	0.579
VAR1	17	0.708
VAR2	15	0.708
VAR3	10	0.708
VAR4	5	0.708

Fragility functions are computed for each of the four backbone variations from Badweg12 and compared to the original Badweg 12 fragility. The fragility functions are shown in Figure G.12 and Figure G.13 using respectively a linear and logarithmic scale for the probability of full collapse. The values of the median and dispersion are also provided in Table G.4.

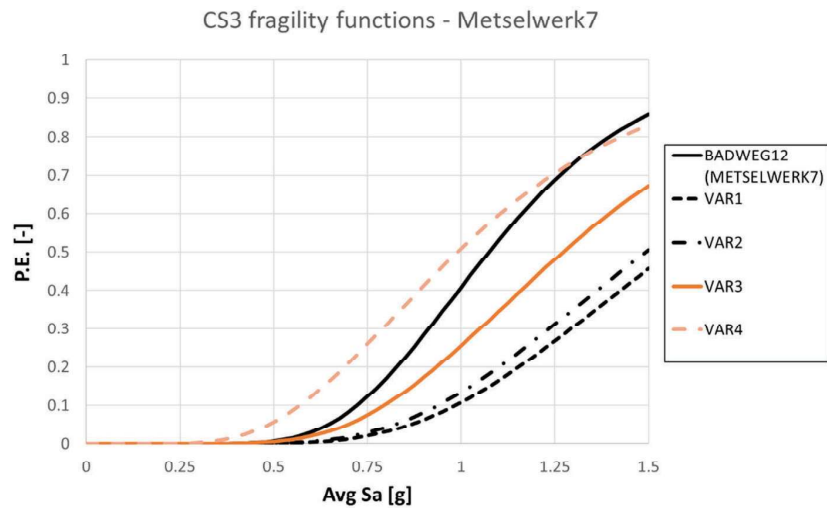


Figure G.12 Fragility functions computed from the backbone curves adopted for the variation study in linear scale.

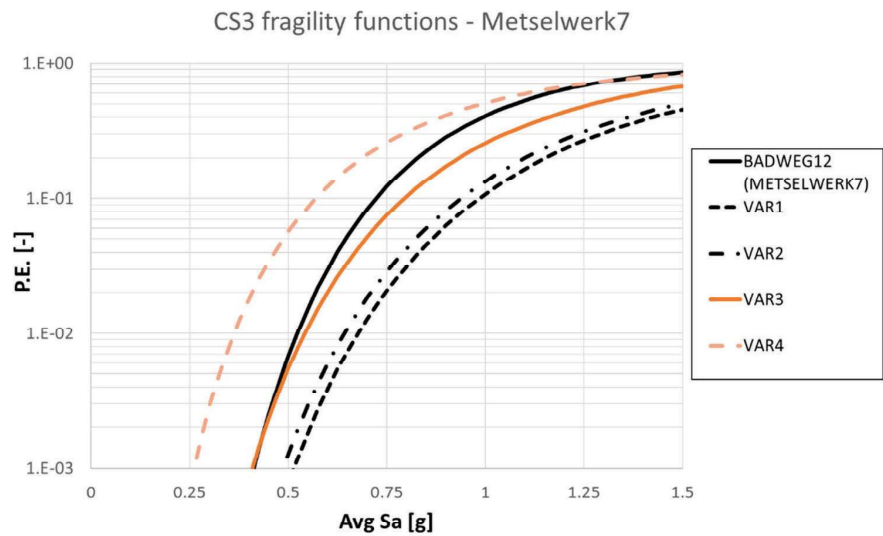


Figure G.13 Fragility functions computed from the backbone curves adopted for the variation study with the probability of full collapse in logarithmic scale.

Table G.4 Median and dispersion of the fragility functions computed in the variation study.

<b>Model</b>	<b>Median [g]</b>	<b>Dispersion [-]</b>
Badweg12	1.07	0.31
VAR1	1.56	0.36
VAR2	1.49	0.36
VAR3	1.27	0.37
VAR4	0.99	0.43

From Table G.4 and Figures G.11-G.13 the following is observed

- When reducing the collapse displacement, the record-to-record variability increases.
- The reduction of collapse displacement is fairly compensated by the increase in base shear capacity.
- VAR 4 is more unfavorable than Badweg 12, but also more unfavorable than Damsterweg 37 and Wirdumerweg 4.

This means that Badweg12 is the most fragile building if compared to Damsterweg 37 and Wirdumerweg 4. This confirms that Badweg 12 is a safe choice for the median fragility for the typology METSELWERK7.

## H NLTH berekeningen controlegebouwen

TU Delft rapporten:

2021.07.12 - NLTHA Wirdumerweg 4\_V03

2021.04.12 - NLTHA Damsterweg37\_V01

Project	Typology based assessment
Report number	06
Internal Reference	B2B-R06
Date	July 12, 2021
Version	03
Status	Final


# **SEISMIC PERFORMANCE OF A DETACHED HOUSE: CASE STUDY WIRDUMERWEG 4, WIRDUM**

*A quick, safe and validated typology based seismic assessment of  
buildings*

Client: Ministerie van Economische Zaken en Klimaat (EZK)

Authors  
Francesco Messali  
F.Messali@tudelft.nl  
Michele Longo  
M.Longo@tudelft.nl

Address  
Delft University of Technology  
Faculty of Civil Engineering and Geosciences  
Stevinweg 1, 2628 CN, Delft

 <p>Faculty of Civil Engineering and Geosciences Stevinweg 1 2628 CN Delft PO 5048 2600 GA Delft <a href="http://www.citg.tudelft.nl">www.citg.tudelft.nl</a></p>	<b>Report</b>	
	<i>Title:</i> Seismic performance of a detached house: case study Wirdumerweg 4, Wirdum	
	<i>Author(s):</i> Michele Longo Francesco Messali	
	<i>Date:</i> 12/07/2021	
<i>Client(s):</i> Ministerie van Economische Zaken en Klimaat (EZK)	<i>Version:</i> 03	<i>Status:</i> Final
<i>Project number:</i> TBA-20/21	<i>Project name:</i> A quick, safe and validated typology based seismic assessment of buildings	<i>File reference:</i> B2B-R06
<i>Cite as:</i> Messali, F., Longo, M. (2021). Seismic performance of a detached house: case study Wirdumerweg 4, Wirdum. Delft University of Technology. Report number 06, Version 03 (Final), 12 July 2021.		

### Copyright statement

All rights reserved. No part of this publication may be reproduced, stored in a retrieval system of any nature, or transmitted, in any form or by any means, electronic, mechanical, photocopying, recording or otherwise, without the prior written permission of TU Delft.

### Liability statement

TU Delft and those who have contributed to this publication did exercise the greatest care in putting together this publication. However, the possibility should not be excluded that it contains errors and imperfections. Any use of this publication and data from it is entirely on the own responsibility of the user. For everybody who has contributed to this publication, TU Delft disclaims any liability for damage that could result from the use of this publication and data from it, unless the damage results from malice or gross negligence on the part of TU Delft and/or those who have contributed to this publication.

## Table of Contents

1	Introduction .....	4
2	Building and model description.....	5
3	Results .....	10
3.1	Failure (stop) criteria .....	10
3.2	Analyses Results.....	11
3.3	Backbone curves .....	17
4	Conclusions.....	20
	References.....	22
	Appendix A: Material properties.....	23
	Appendix B: original motions (stronger X-direction) .....	25
	Appendix C: original motions (stronger Y-direction) .....	27
	Appendix D: scaled motions (stronger X-direction) .....	29
	Appendix E: scaled motions (stronger Y-direction).....	31
	Appendix E: consistency of the definition of the effective mass with 'Badweg 12' .....	33

## 1 Introduction

This report summarizes the results of the numerical simulations of the detached house located in Wirdumerweg 4, 9917 PE in Wirdum. Non-linear time history (NLTH) analyses are carried out. A set of 11 ground motions having different intensity is used.

Backbone curves representative of the global behavior of the building in the two main building directions are built from the entire set of analyses results. Both local and global failure mechanisms are considered to define the base shear capacity and the ultimate displacement of the building. The capacity is also limited by the failure of the timber beam-masonry connection.

The analyses are conducted employing the Finite Element software DIANA FEA version 10.4 [1].

## 2 Building and model description

The Wirdumerweg building is a two-storey (plus attic) detached house with the gutter line at the level of the first floor, built in 1909. The building is made of unreinforced masonry (URM) cavity walls. A picture and a plan section of the building is shown in Figure 1. The building is made with a cavity wall system with clay bricks for both outer leaf and inner load bearing leaf. It has a height of 6.1 m measured at the ridge beam. The ground floor is built with two different materials. The West side is made of pre-cast concrete and the rest is made of timber beams and chipboard panels. At the 1<sup>st</sup> floor and at the attic floor, timber beams spanning in the X direction (North-South) are connected with chipboard panels. The roof is composed by timber purlins and rafters, connected with chipboard panels.



**Figure 1. Wirdumerweg building detached house. South-East façade view (left) and plan view (right).**

The detached house is numerically modelled in 3D by means of the software Diana 10.4. A representation of the model is shown in Figure 2.

The cavity wall system is implemented by explicitly modelling the inner leaf and considering the outer leaf as dynamic mass acting in the direction perpendicular to the wall. The assumption in this case is that the wall ties are unable to transfer any shear force. The overview of the modelled inner leaf is depicted in Figure 3. Lintels above the openings are modelled as linear elastic steel elements. The internal partition walls at the ground floor are made of clay masonry and they are bearing the first floor. They are directly connected to the timber beams of the floor, but they are disconnected from the floor planks. Partition walls at the first floor are made of timber, modelled as linear elastic and they are not load bearing. An overview of the walls is shown in Figure 4. Both internal and external walls are modelled using the Engineering Masonry Model [2]. The timber frame of the large window opening at the South façade is explicitly modelled with linear elastic beam elements (Figure 5).

The precast concrete ground floor and the timber at the first floor and attic are modelled as linear elements (Figure 6). The timber beams part which are part of the floor sheets, are shown in Figure 7. They are also modelled as linear elastic material.

The roof purlins, struts, rafter, wall plates and ridge beam are modelled with beam elements using a linear elastic isotropic material (Figure 8). The timber boards, representing the floor diaphragms and the roof structure are modelled as shell elements using linear elastic orthotropic material (Figure 9).

A full list of the material properties used in the model is provided in Appendix A.

The total dynamic mass (the one acting during the motion) of the model is equal to 96.8 tons. Three variations of the effective mass are proposed and implemented in the computation of the normalized force. Mass A considers the participation of the building above half of the ground storey height, consistently to the criterion

adopted for the analyses performed in support of the Typology based assessment. However, unlike the buildings studied for Metselwerk 7 [3], the current building presents high foundations, so that it is expected that the mass of the ground floor is activated by the ground motions. For this reason, a second effective mass, Mass B, is computed taking into account the mass of the entire ground storey (including the floor mass). An overview of the selected effective mass is depicted in Figure 10 and listed in Table 1.

The effective height is considered at the location of the first floor height, equal to 2.94 m from the ground floor.

Quadratic 8-noded curved shell elements (CQ40S and CT30S) are used to model the walls, floors and lintels of the 3D building. The timber beams at the second floor and at the roof level are modelled with Class-III beam element (CL18B). The model is assumed to be fixed-base (no soil-structure interaction is considered), so that it is fully restrained at the bottom from translations and rotations. The elements are meshed with an average size of 200x200 mm (Figure 2).

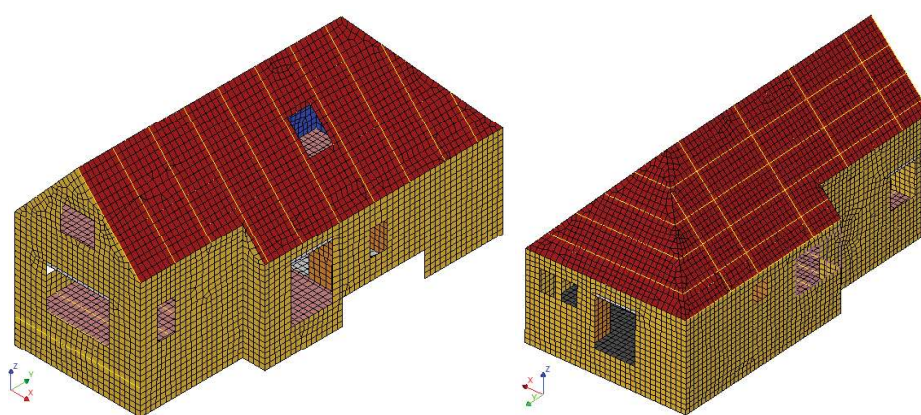


**Figure 2. Diana model of Wirdumerweg. North-East view (left) and South-West view (right).**

Non Linear Time History (NLTH) analyses are performed. The model is first subjected to gravity loads, applied in ten equal steps. Afterwards, live loads at floor levels, and additional roof masses are applied in ten steps. Then, the different acceleration motions are applied in the longitudinal, transversal and vertical direction at the base nodes, using a time step of 2.5 milliseconds. A Rayleigh damping of 2% is accounted in the calculation. The Secant BFGS (Quasi-Newton) method is employed as iterative method. Energy norm must be satisfied during the iterative procedure with a tolerance of 0.01%. The Parallel Direct Sparse method is employed to solve the system of equations. The second order effects are accounted via the Total Lagrange geometrical nonlinearity.

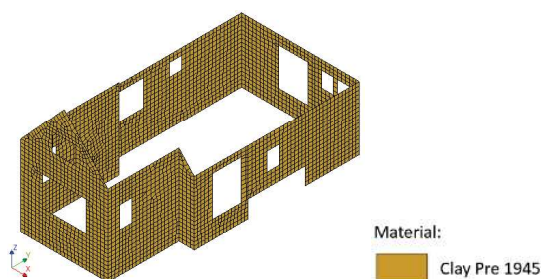


**Figure 3. External walls material.**

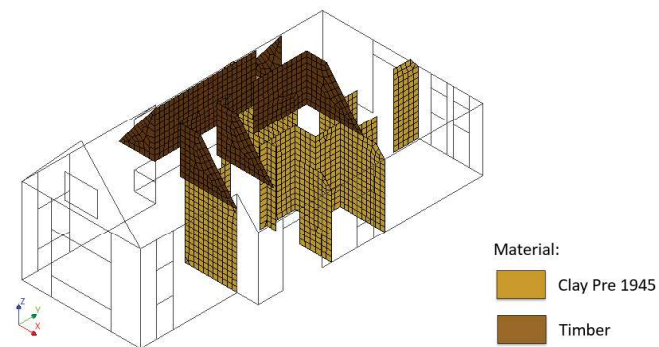


**Figure 4. Internal walls material.**

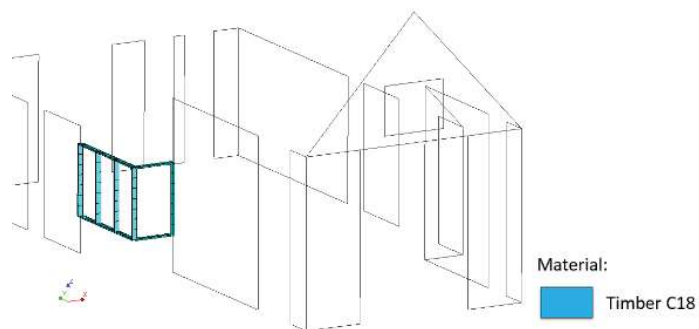


**Figure 5. Window timber frame ground floor.**

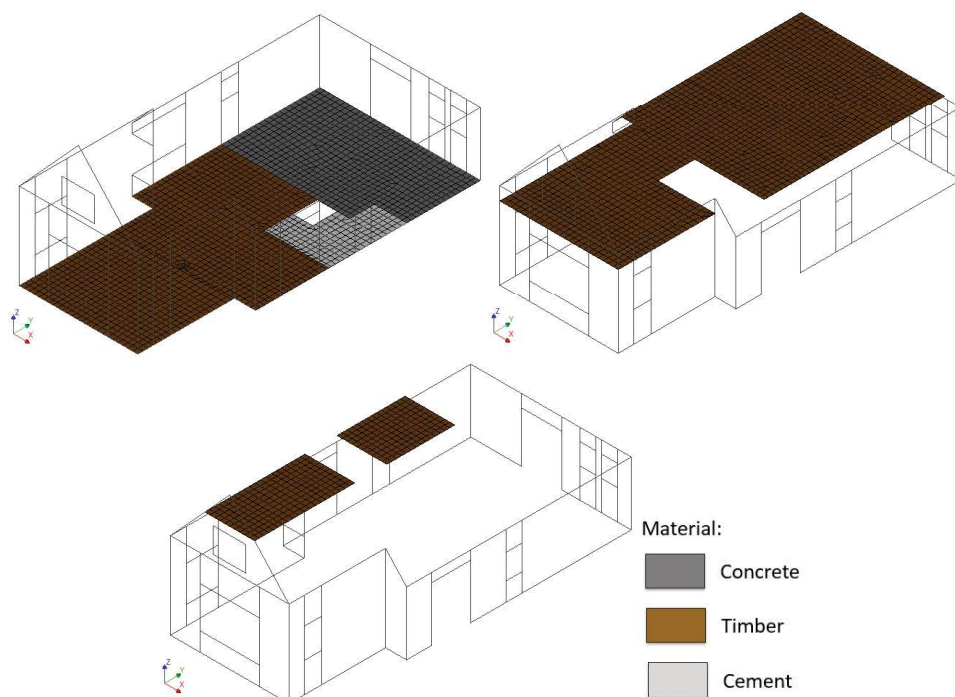


**Figure 6. Floor material. Ground floor (top left), first floor (top right) and attic floor (bottom).**

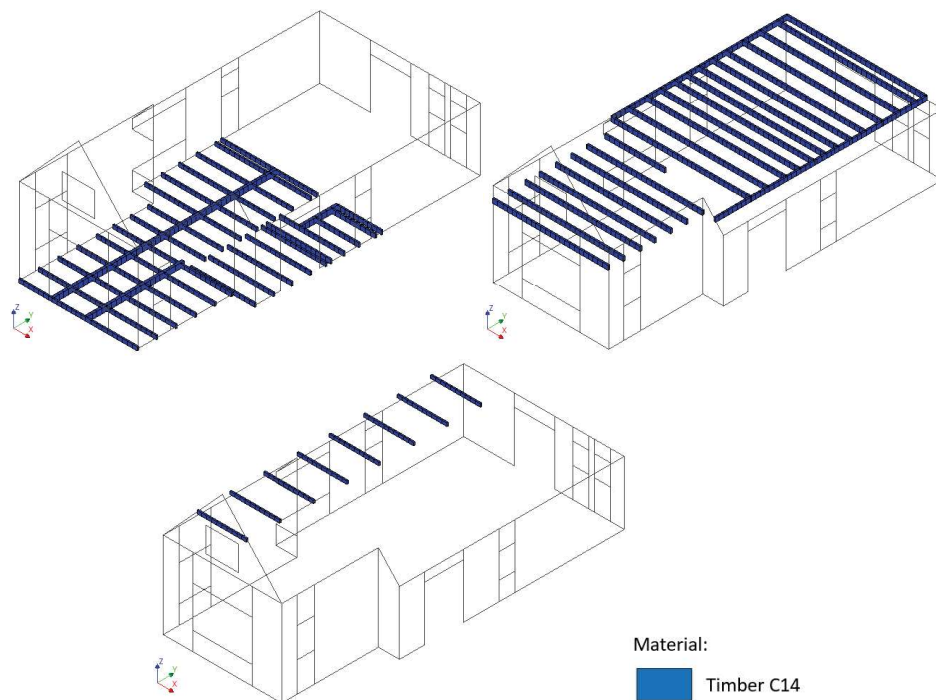


Figure 7. Floor timber beams. Ground floor (top left), first floor (top right) and attic floor (bottom)..

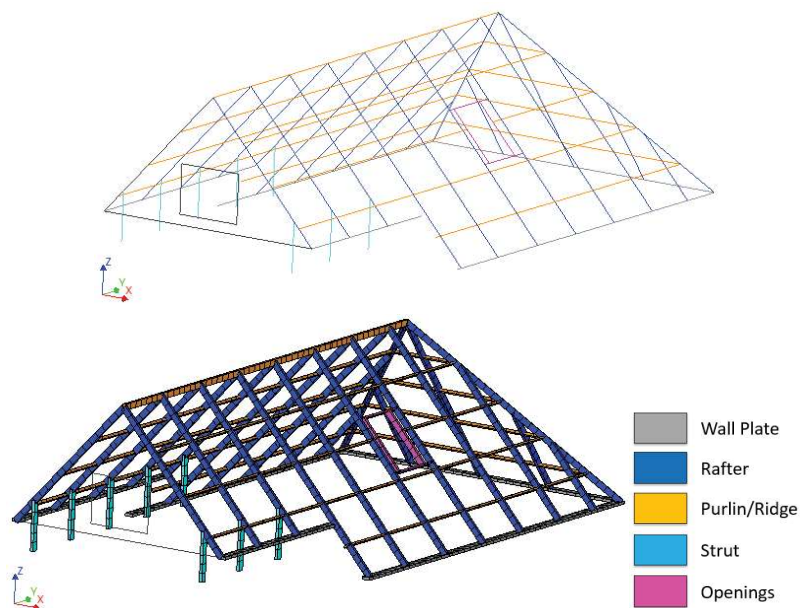


Figure 8. Roof beam structure.

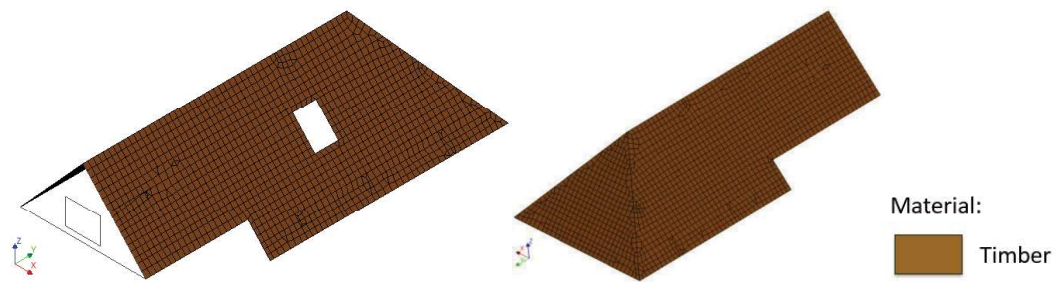


Figure 9. Roof boards. North-East view (left) and South-West view (right).

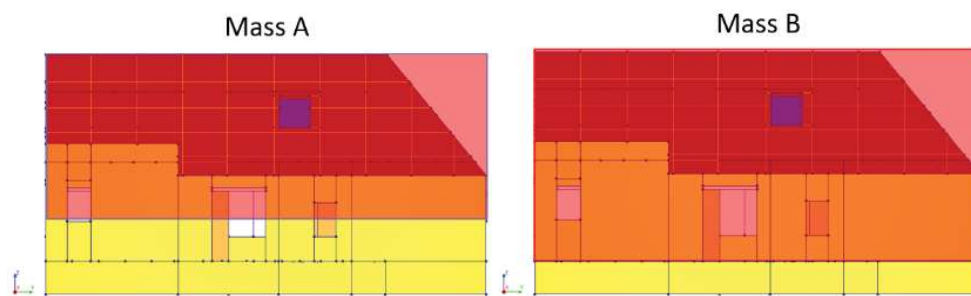


Figure 10. Considered effective masses (highlighted in red).

Table 1. Values of the three considered effective masses.

	Mass A	Mass B	Total mass
Effective Mass	46.0 ton	81.4 ton	96.8 ton

The seismic input is described by 11 different ground motions applied in the three directions. The strongest horizontal motion (indicated as "weak direction" motion) is applied in a first run of analyses in the global Y direction and in another series, in the global X direction. Table 2 lists the PGAs for different earthquakes in different directions. Since the original series of ground motions did not allowed to determine the ultimate displacement capacity of the building, a second series of motions was considered, with the original PGAs scaled up by a factor two for all three motion direction. The complete ground motions used for the simulations are reported in [3].

Table 2. PGAs of the 11 selected ground motion.

	M1	M2	M3	M4	M5	M6	M7	M8	M9	M10	M11
PGA strong dir [g]	0.061	0.317	0.215	0.136	0.191	0.416	0.505	1.021	0.403	0.422	0.710
PGA weak dir [g]	<b>0.090</b>	<b>0.192</b>	<b>0.237</b>	<b>0.245</b>	<b>0.257</b>	<b>0.948</b>	<b>0.542</b>	<b>0.780</b>	<b>0.535</b>	<b>0.843</b>	<b>1.302</b>
PGA vertical dir [g]	0.034	0.099	0.080	0.182	0.168	0.315	0.196	0.401	0.461	0.503	0.386

## 3 Results

### 3.1 Failure (stop) criteria

Due to the implicit nature of the time history calculations performed with Diana, a set of “stop criteria” are implemented in order to cap the capacity and the ultimate displacement of the analyses. Different criteria are selected:

- **In-Plane failure:** the maximum allowable drift limit for the masonry piers in the in-plane direction is set to 1.5% for ductile mechanism and to 0.6% for a brittle (shear type) failure. In terms of displacements, this is equal to 38.25 mm and 44.10 mm respectively to part 1 (West side) and part 2 (East side) of the building for ductile failure (Figure 11). For the shear type failure the displacement limit are 15.30 mm and 17.64 mm for part 1 and 2. The criteria is applied to all load-bearing masonry walls. These values are applied conservatively, since they are selected based on the recommendations of NPR 9998, although the standard refers to the characteristic and not the mean capacity of the building. A correction factor similar to that used in [6] and [7] for the SLAMA analyses may be applied to this limit too, but this would have a limited impact to the definition of the backbone curve, since the collapse is usually governed by the out-of-plane of the walls. For this reason, such factor is omitted.
- **Out-Of-Plane failure:** the maximum permitted OOP displacement for all load-bearing-walls is set to 100 mm. A variation study is made, by considering a limit of 60 mm.
- **Connection failure:** the connections between masonry and timber beam at roof and first floor level (Figure 12) are checked during the entire dynamic motion for the most severe ground motions, which are namely M9, M10, and M11, for both the cases when the strong motion is applied either in the X- or in the Y-direction. The axial pulling force of the timber beam generated at the connection with the masonry are assessed according to a frictional criterion, for which the maximum resistance is equal to 0.3 kN plus 0.7 times the vertical shear force acting at the connection. The values are based on experimental tests performed at TU Delft [4][5]. Since the temporary exceedance of the force capacity of one of the beam-wall connections does not determine immediately the collapse of the wall, the connection failure is defined when the axial force exceeds the limit in any of the timber beams for 0.1 seconds or longer (as shown in Figure 14). In that situation the overall failure of the building is considered due to the failure of the connections. According to the moment of failure, the maximum normalized force at connection failure (averaged over the entire set of analyses), is used to cap the capacity of the backbone curves.

Displacement at different floors and roof level are computed at the location represented in Figure 13 and then averaged to a single value. It must be noted that the floor node at the first floor at the East side coincide with the node of the masonry East façade.

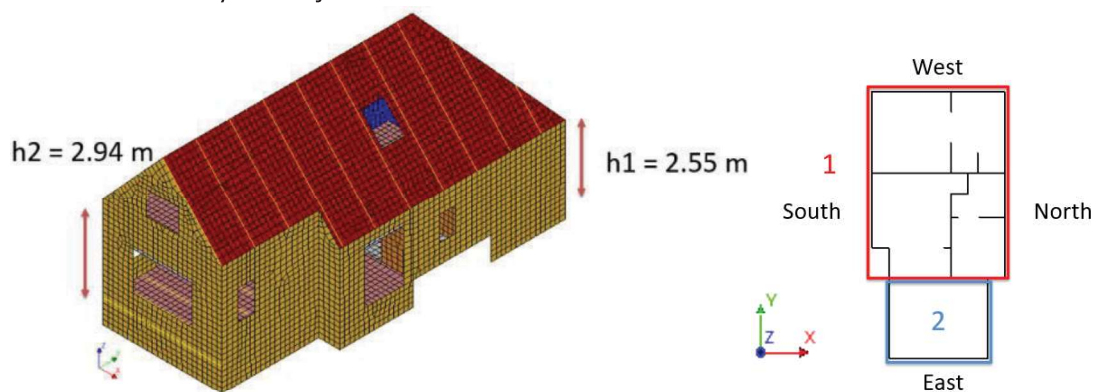
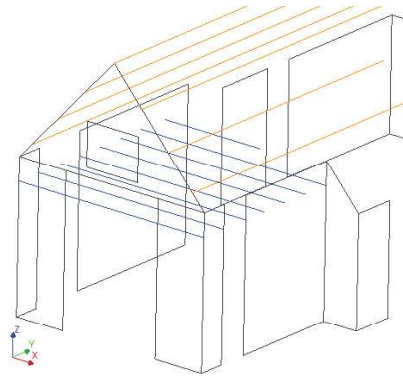
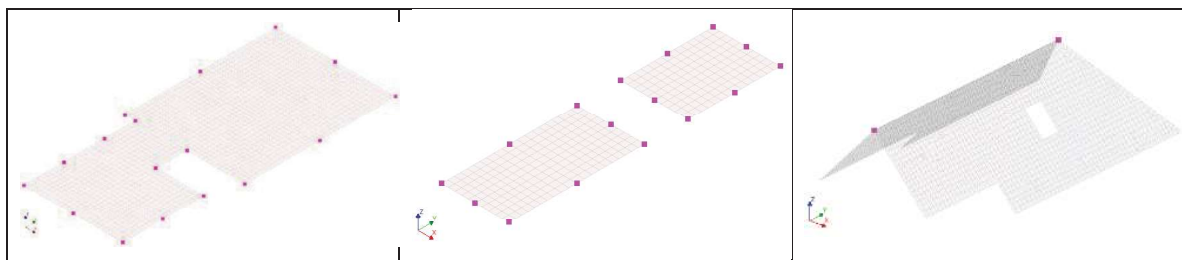


Figure 11. Inter-storey height of the different building part.



**Figure 12.** Timber beams at first floor (in blue) and at roof (in orange) level connected to masonry, considered to check the force in the timber-masonry connections.



**Figure 13.** Output location for Wirdumerweg building. First floor/effective height (left), attic floor (middle) and roof (right).

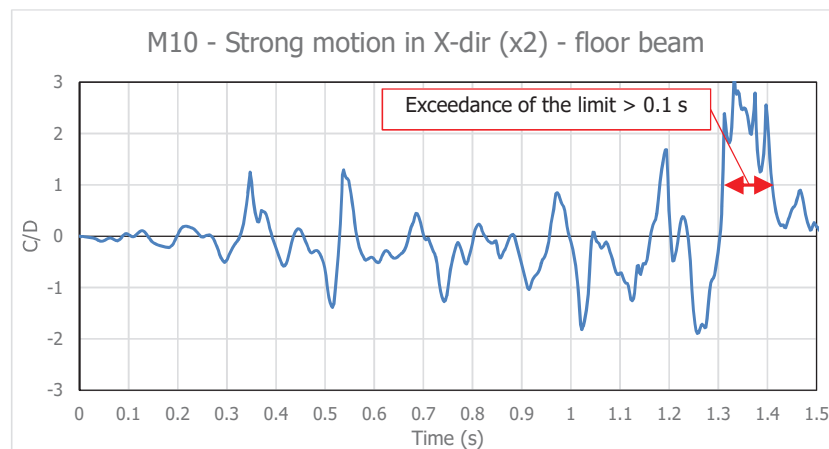


**Figure 14.** Capacity over demand ratio of the first beam for which the frictional criterion is exceeded for more than 0.1 s.

### 3.2 Analyses Results

Before running the NLTH calculation, an analysis of the eigen mode is performed. The global displacement contours and the overview of the main frequencies are shown in Figure 15. The selected modes, which are the ones with highest participation mass, are also used to compute the Rayleigh damping coefficients.

Hysteresis plots of the four different motion series, namely original PGA with the strongest motion in X and Y and scaled PGA (by a factor 2) with the strongest motion applied in X and Y direction, are depicted from Figure 16 to Figure 19. The normalized force refers to the effective mass B. Such plots are showing the entire time history and they are not capped at the above mentioned displacement limits nor by the limit related to the failure of the connections. In fact, the capping according to the criteria is applied directly to the computation

of the backbone curves. All the hysteretic curves are shown in Appendix B-C-D and E. The maximum displacement reached in the X-direction for the original motion applied in the X-direction is around 20 mm with a maximum normalized force of 0.8 g. As regards the y direction for the same set of motions, the force values is also around 0.8 g with a maximum displacement of 3.5 mm. When the stronger input motion is applied in the y direction, similar displacements are obtained, while the force capacity increases up to 1.0 g. The displacements in the x direction drop to a maximum of 10 mm. None of the stop criteria is reached when the building are subjected to original motions. When the motions are doubled, the capacity reaches acceleration of about 1.25 g when the strongest motion is applied in the X direction and about 1.5g when applied to the Y direction. The stop criteria are exceeded for some of the motions of the two series.

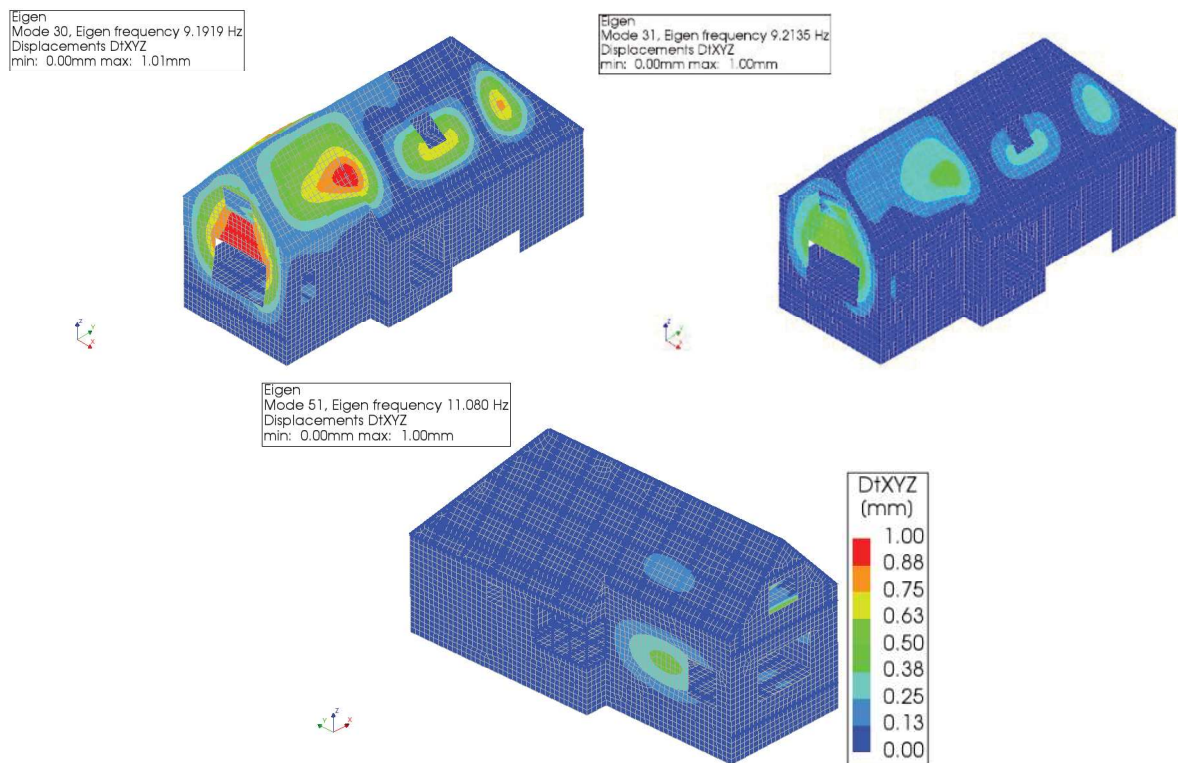


**Figure 15. Eigen modes for Wirdumerweg building. Mode 30 (top-left), mode 31 (top-right) and mode 51 (bottom).**

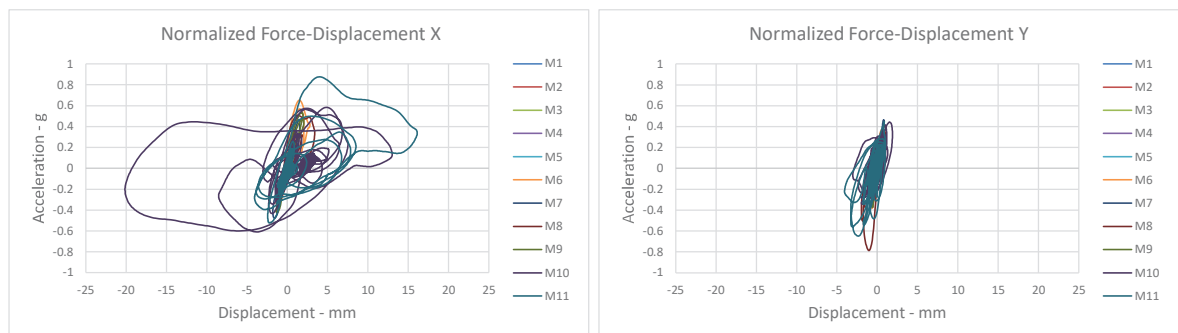


**Figure 16. Hysteretic curves defined at the effective height for the eleven original ground motion having the strongest motion orientated in the global X direction. Normalized force computed with Mass B.**

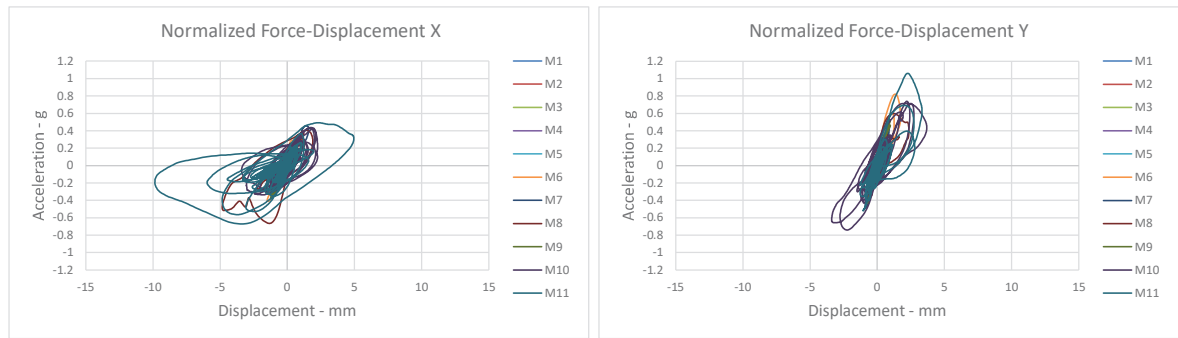


**Figure 17. Hysteretic curves defined at the effective height for the eleven original ground motion having the strongest motion orientated in the global Y direction. Normalized force computed with Mass B.**

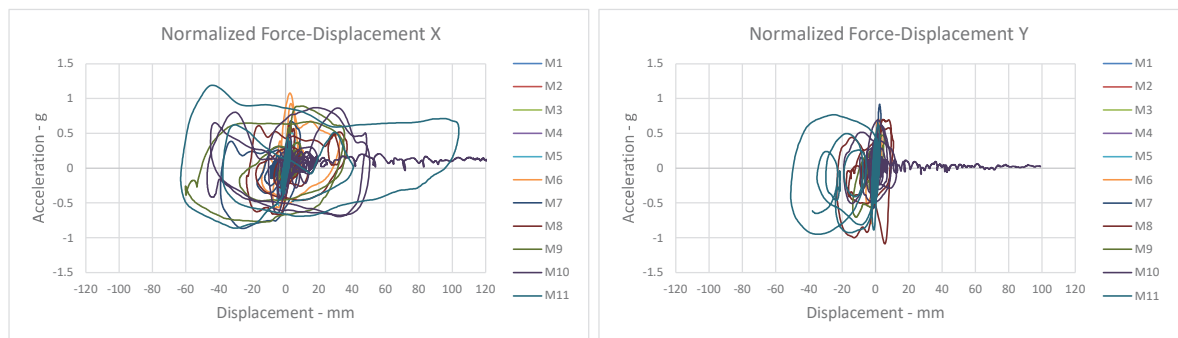


**Figure 18. Hysteretic curves defined at the effective height for the eleven scaled ground motion having the strongest motion orientated in the global X direction. Normalized force computed with Mass B.**

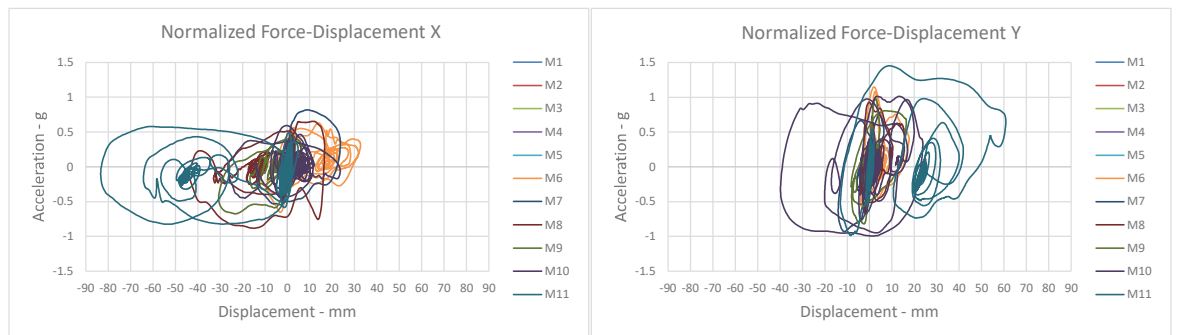


**Figure 19. Hysteretic curves defined at the effective height for the eleven scaled ground motion having the strongest motion orientated in the global Y direction. Normalized force computed with Mass B.**

Either in-plane or out-of-plane stop criteria are reached in various analyses; in some cases, almost at the same time. Regarding the OOP failure, that is mainly detected in four walls: one of the loadbearing internal walls (indicated with A in Figure 20), the wall at the North corner with the West façade (B) and both the North and South walls along the East side of the building (C and D). Examples of OOP failure are depicted in Figure 21. The in-plane is mainly distinguished in failure of part 1 (West side in Figure 20) or part 2 (East side). The in-plane behaviour is considered as ductile, due to the observed flexural cracks at the base of the piers which trigger rocking mechanisms which precede possible shear cracks. Examples of IP failures are shown in Figure 22. The failure types evaluated from the model for different motion series and time histories are summarized in Table 3 for the case of 100 mm OOP limit and Table 4 when a 60 mm OOP limit is selected. When the

strongest motion is applied in the Y direction, the most common failure mechanism is the out-of-plane of the internal wall A. However, Motion 8 shows in-plane failure of the East side of the structure, and Motion 11 a combination of IP and OOP failure. In the analyses for which the strongest motion is applied in the X direction, the collapse mechanism shifts towards the in-plane failure, although a combination of IP and OOP is found for motion 11 and the OOP failure of wall A is found for Motion 8. When considering the lower limit of 60 mm for the out-of-plane walls, the collapse is obtained earlier and concerns different load bearing walls, such as wall D, E, F (Figure 20). This is often the case for the amplified motion in X direction.

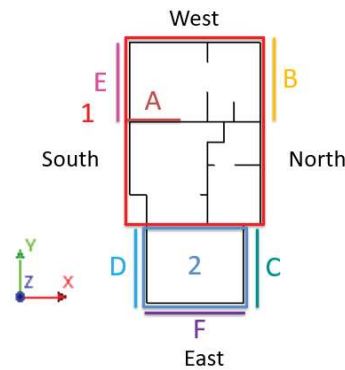


Figure 20. Location of OOP failures in the Wirdumerweg building.

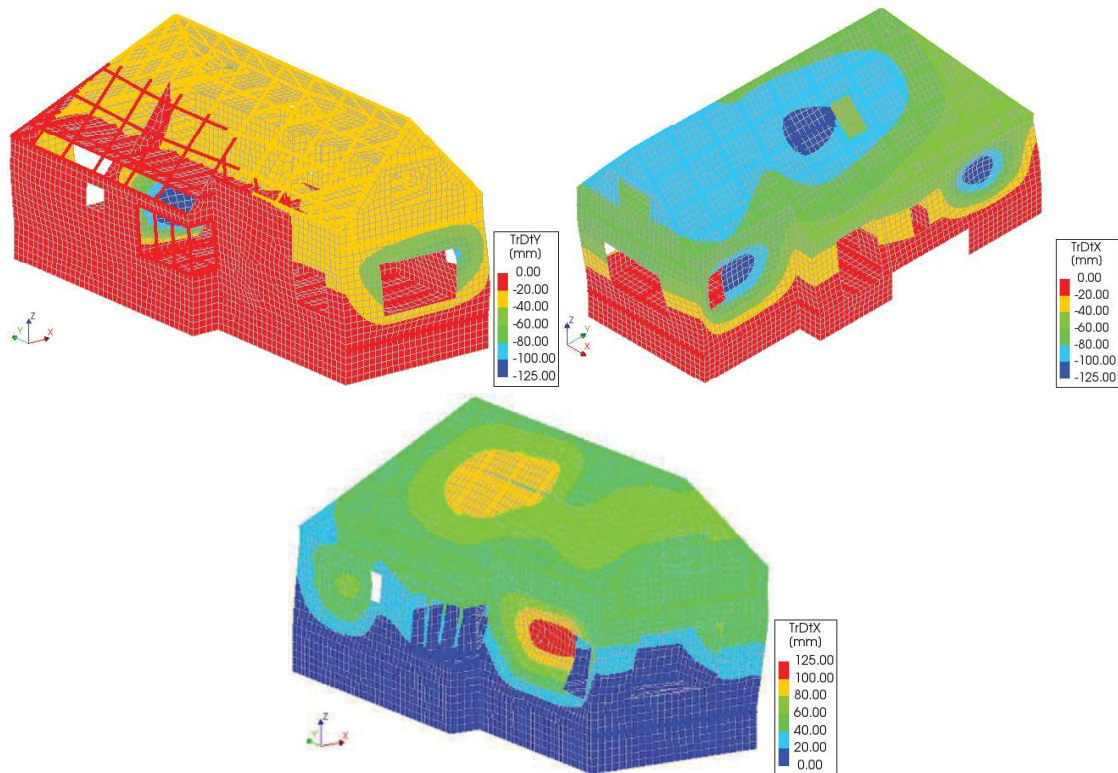


Figure 21. Typical OOP failures found in the Wirdumerweg building. Failure wall A (top-left), failure walls B and C (top-right), failure wall D (bottom).

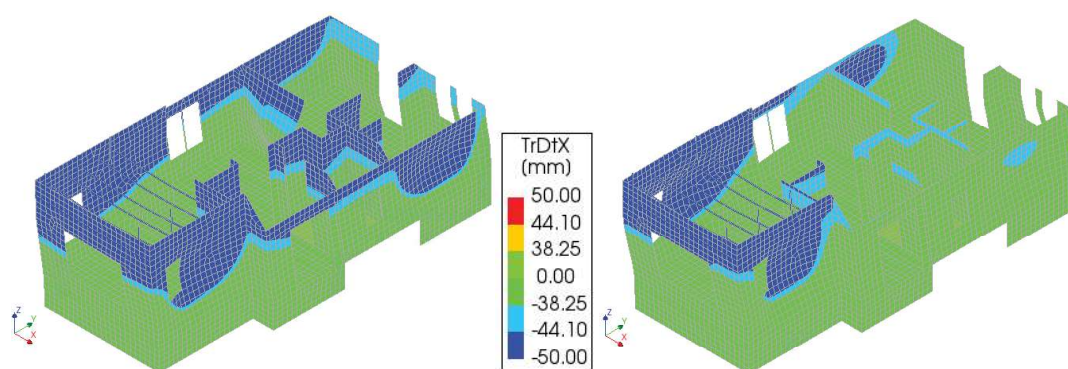


Figure 22. Typical IP failures found in the Wirdumerweg building. Failure part 1+2 (left), failure part 2 (right).

Table 3. Failure type of Wirdumerweg building for the four series of the 11 ground motions, without considering connection failure. OOP limit of 100 mm.

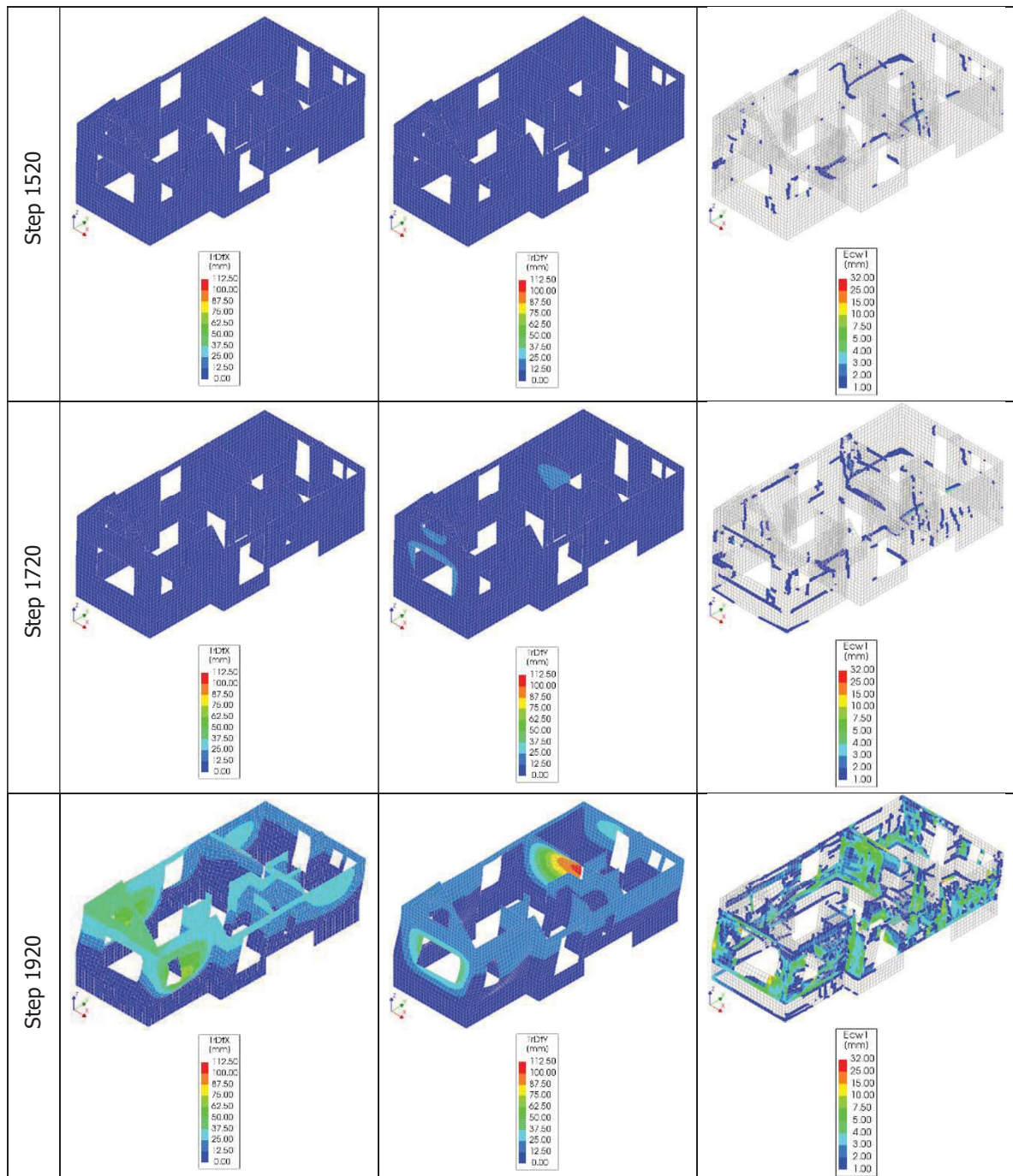
	M1	M2	M3	M4	M5	M6	M7	M8	M9	M10	M11
Strong Motion in X Original	-	-	-	-	-	-	-	-	-	-	-
Strong Motion in Y Original	-	-	-	-	-	-	-	-	-	-	-
Strong Motion in X PGA x 2	-	-	-	-	-	-	-	OOP A	IP 1,2	IP 2	IP 1,2 OOP A,B,C
Strong Motion in Y PGA x 2	-	-	-	-	-	OOP A	OOP A	IP 2	OOP A	OOP A	IP 1,2 OOP A

Table 4. Failure type of Wirdumerweg building for the four series of the 11 ground motions, without considering connection failure. OOP limit of 60 mm.

	M1	M2	M3	M4	M5	M6	M7	M8	M9	M10	M11
Strong Motion in X Original	-	-	-	-	-	-	-	-	-	-	-
Strong Motion in Y Original	-	-	-	-	-	-	-	-	-	-	-
Strong Motion in X PGA x 2	-	-	-	-	-	-	OOP C	OOP A	IP 1,2 OOP A,C,D	IP 2 OOP D	IP 1,2 OOP A,B,C,D,E,F
Strong Motion in Y PGA x 2	-	-	-	-	-	OOP A,C,D	OOP A	IP 2 OOP A,C,D,E	OOP A	OOP A,F	IP 1,2 OOP A,B,C,D,E

As described in section 3.1, the failure of the connections between masonry and timber beams can also determine the stop of the analyses. An average capacity is evaluated from the analyses that show collapse of the connection: the computed values of the average capped capacity in the X- and Y-direction are respectively 0.43 g and 0.59 g (considering effective mass B).

Figure 23 shows the evolution of the displacements and of the crack pattern of motion 6 (double PGA) when the earthquake is applied to the global Y direction. The resulting failure mechanism is localized to the internal wall A which deforms OOP with a displacement greater than 100 mm.



**Figure 23. Evolution of displacements, cracks of Wirdumerweg when subjected to motion 6 with high PGA applied in the Y direction. Maximum horizontal displacement (left), vertical displacement (middle) and maximum principal crack width (right) at step 1520 (top), 1720 (middle) and 1920 (bottom). Absolute deformation magnified 10 times.**

### 3.3 Backbone curves

The hysteretic curves defined for each analysis are used to determine the global backbone curve according to the procedure described in [3]. Two different curves are presented, according to the considered effective mass as presented in Table 1. The backbone curves for both X and Y direction when the 100 mm limit is considered for the OOP deformation are shown in Figure 25. Such backbones are the one obtained without considering the failure of the connections. However, such failure caps the capacity at an average value of 0.38 g for the X direction and 0.41 g for the Y direction (for effective mass B). The capped curves are depicted in Figure 26. The comparison between the backbones computed with different OOP criteria (100 mm vs 60 mm) is shown (for effective mass B) in Figure 29. Here the connection failure is not taken into account. The capped curves are shown in Figure 28. The summary of the initial stiffness, yield displacement and force, peak displacement and force, ultimate displacement, is tabulated in Table 5 for the case with 100 mm as OOP stop criteria and Table 6 for the 60 mm stop criteria. Figure 24 and Figure 25 show the curves obtained by considering either the effective mass A or B, to enhance the large impact that the choice of the effective mass has on the peak acceleration capacity of the building. The alternative OOP stop criteria (Figure 29) depicts, for the curve in the X direction, a small reduction (about 10%) of peak force, peak and ultimate displacement. In the Y direction instead, the difference is mainly localized at the ultimate displacement (reduction of about 40%).

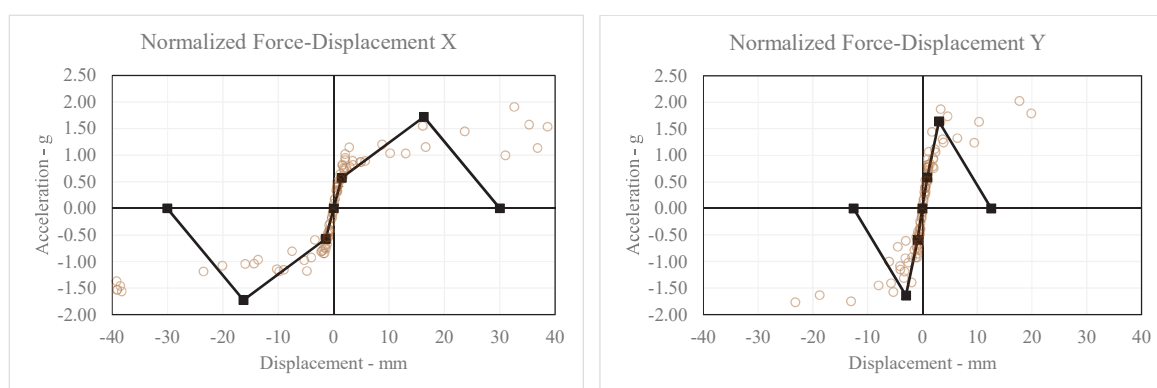


**Figure 24. Max normalized forces and displacements for each performed simulation, and corresponding backbone curve for both the X- and Y-direction (computed for the effective mass A, OOP limit of 100 mm).**

The results of the backbones, also summarised in Table 5 and Table 6, show the sensitivity of the backbone curve to the value selected for the effective mass and to the failure of the connections. As discussed in Appendix E, Mass A should be considered as effective mass to be consistent with the assumptions made by TU Delft for the study on Metselwerk 7 [3], and the approach followed by Eucentre for the index building Badweg 12 [9]. Direction X is the most flexible one, with displacement that ranges from 1.47 mm at the yielding point to 30.05 as ultimate displacement, where most of the analysis showed a stable behaviour. Peak displacement in X direction is detected at 16.3 mm. Peak and ultimate displacement reduces to 14.4 mm and 26.8 mm respectively when the stop criteria of 60 mm is considered. Capacity force in the X direction, referring to the Mass A case, is equal to 1.72 g (1.58 g for 60 mm OOP limit) without capping. Direction Y results in a much stiffer behaviour, with an initial stiffness which is almost twice as much respect to the one of the backbone in X direction (0.67 g/mm against 0.40 g/mm). The displacement ranges from 0.87 mm of the yield displacement to the 14.26 mm of the ultimate displacement (3.0 mm as displacement at the peak). The ultimate displacement reduces to 8.4 mm for OOP limit of 60 mm. When the failure of the connections is taken into account, the peak force drastically reduces in all cases. In fact, the connections at the first floor level fail when the strongest motions are applied. For direction X the reduction of the peak force is more than 50%. Peak force in direction Y reduces by almost 40%. This difference is sensible, since the beams span in the X-direction, so that the failure is expected to occur before in the case when the strongest motions are applied in the same direction. However, it should be noted that the walls which undergo out-of-plane collapse for the

analyses with the stronger motion in the Y-direction are not connected to the beams which fail. For this reason, such large reduction of capacity for these analyses may in fact not occur if the nonlinear behaviour of the connections would be modelled. The results presented can be therefore seen, for this aspect, as conservative with respect to this specific point.

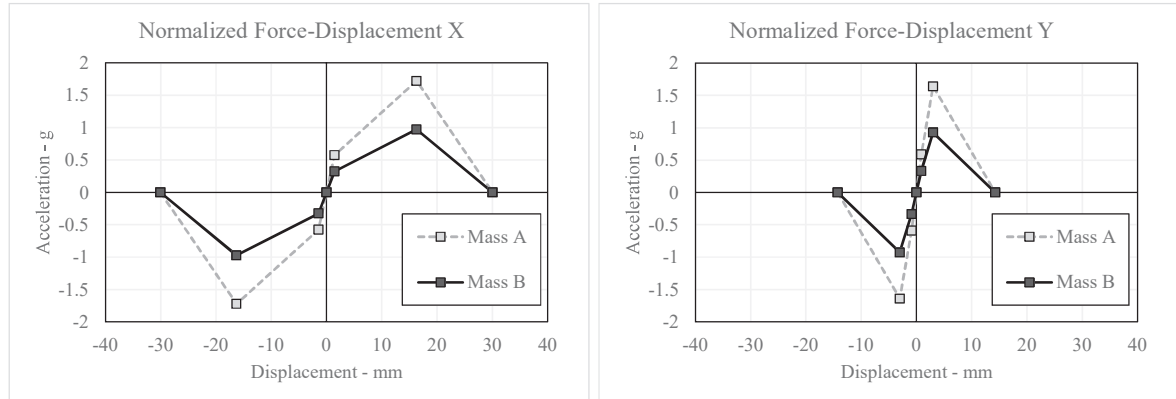


**Figure 25. Backbone curves for different effective masses without cap, 100 mm OOP stop criteria and for both the X- and Y-direction.**

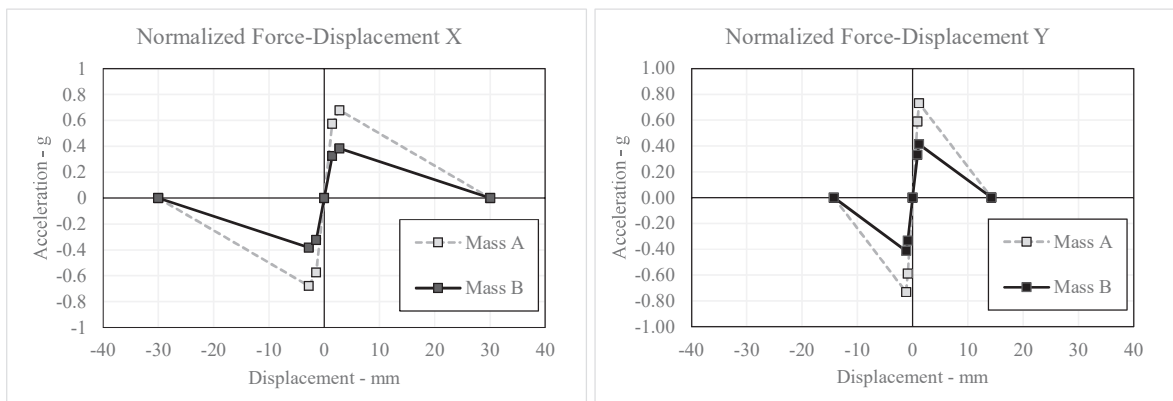


**Figure 26. Backbone curves capped by the failure of the connections, for different effective masses, 100 mm OOP stop criteria and for both the X- and Y-direction.**

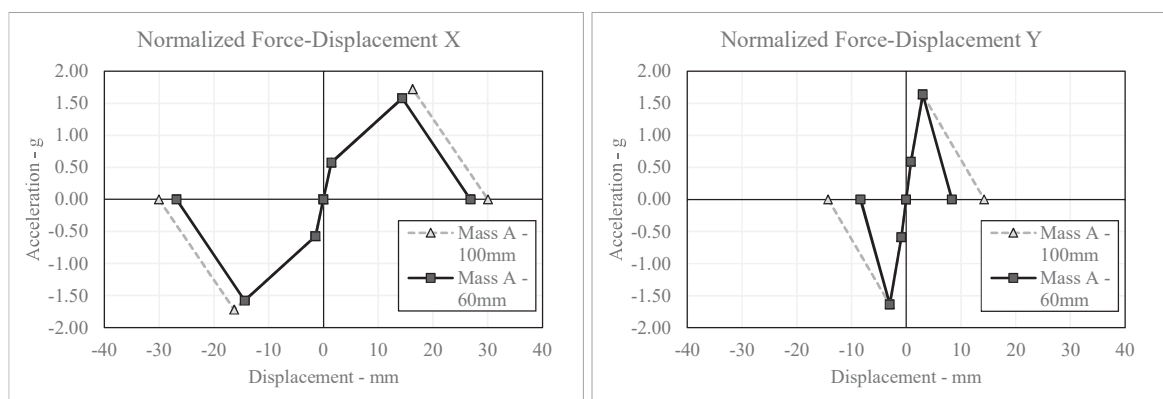


**Figure 27. Backbone curves for alternative OOP stop criteria without cap and for both the X- and Y-direction.**

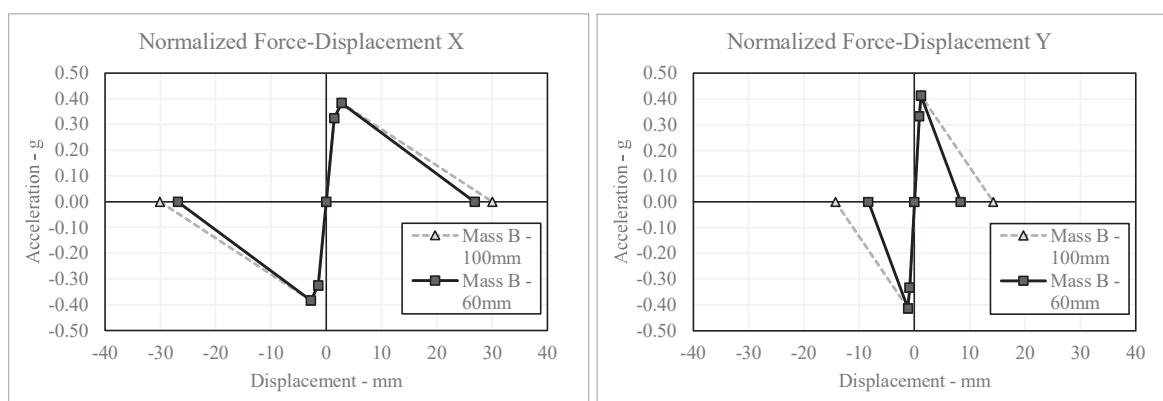


Figure 28. Backbone curves capped by the failure of the connections, for alternative OOP criteria and for both the X- and Y-direction.

Table 5. Summary table backbone curves for OOP stop criteria of 100 mm.

	Mass A No Cap	Mass B No Cap	Mass A With Cap	Mass B With Cap
Initial Stiffness X/Y [g/mm]	0.40 / 0.67	0.22 / 0.38	0.40 / 0.67	0.22 / 0.38
Yield Displacement X/Y [mm]	1.45 / 0.87	1.45 / 0.87	1.45 / 0.87	1.45 / 0.87
Yield Normalized Force X/Y [g]	0.57 / 0.59	0.32 / 0.33	0.57 / 0.59	0.32 / 0.33
Peak Displacement X/Y [mm]	16.30 / 3.00	16.30 / 3.00	2.79 / 1.16	2.79 / 1.16
Peak Normalized Force X/Y [g]	1.72 / 1.64	0.97 / 0.93	0.68 / 0.73	0.38 / 0.41
Ultimate Displacement X/Y [mm]	30.05 / 14.26	30.05 / 14.26	30.05 / 14.26	30.05 / 14.26

Table 6. Summary table backbone curves for OOP stop criteria of 60 mm.

	Mass A No Cap	Mass B No Cap	Mass A With Cap	Mass B With Cap
Initial Stiffness X/Y [g/mm]	0.40 / 0.67	0.22 / 0.38	0.40 / 0.67	0.22 / 0.38
Yield Displacement X/Y [mm]	1.45 / 0.87	1.45 / 0.87	1.45 / 0.87	1.45 / 0.87
Yield Normalized Force X/Y [g]	0.57 / 0.59	0.32 / 0.33	0.57 / 0.59	0.32 / 0.33
Peak Displacement X/Y [mm]	14.39 / 3.02	14.39 / 3.02	2.78 / 1.17	2.78 / 1.17
Peak Normalized Force X/Y [g]	1.58 / 1.64	0.89 / 0.93	0.68 / 0.73	0.38 / 0.41
Ultimate Displacement X/Y [mm]	26.84 / 8.35	26.84 / 8.35	26.84 / 8.35	26.84 / 8.35

## 4 Conclusions

In this case study, the structural behaviour of the two storey detached house Wirdumerweg subjected to non-linear time history (NLTH) analyses is investigated. The calculations are conducted employing the Finite Element software package DIANA FEA version 10.4 [1]. The hysteretic behaviour of the building, the governing failure mechanism and the global backbone curves in the two main directions of the building are derived and presented. Four series of 11 ground motions are considered, by varying the main direction of the stronger base acceleration and the amplitude (the original accelerations are scaled by a factor 2).

Different stop criteria are selected for the analyses, namely:

1. In-plane (IP) limit as the 1.5% of the inter-storey drift;
2. Out-of-plane (OOP) displacement of masonry walls limited to 100 mm (wall thickness). A variation study considering 60 mm is also conducted;
3. Connection failure between masonry and timber beams, computed based on a frictional force criterion evaluated in the post-processing of the analyses.

The following is observed:

- The collapse of the buildings is governed mainly by OOP collapse of an internal wall and of the East façade in the global Y-direction, and of the North and South walls in the global X-direction. In some cases, the IP criteria is also reached in combination with OOP in the X direction.
- Connection failure is obtained at the connection between North/South masonry piers and beam elements of the first floor. The failure of the connections limit the capacity of the building.
- The minimum input PGA that leads to collapse is equal to 1.07 g.
- Considering an effective mass consistent with the TU Delft study on Metselwerk 7 and the index building Badweg 12 (mass A), the peak normalized forces are 0.68g and 0.73g for the X- and Y-direction (when the limitation determined by the failure of the connections is taken into account).
- Large ultimate displacements are achieved in the X-direction (30.05 mm), whereas more brittle failure is achieved in the Y-direction (14.26 mm).
- A stricter OOP stop criteria (60 mm) reduces both the peak force capacity the peak and ultimate displacement of the structure of about 10% in the X direction. A reduction of about 40% is evaluated in the ultimate displacement in the Y direction.

The plot of the final backbone curves and the values of the points of such curves are shown in Figure 29 and reported in Table 7, respectively.

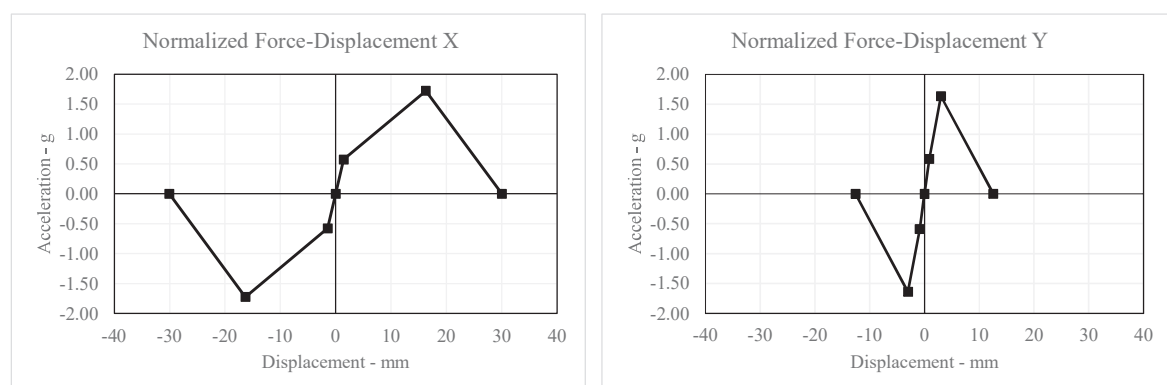


**Figure 29. Final backbone curves (for the effective mass A, OOP stop criteria of 100 mm and considering the failure of the connections) for both the X- and Y-direction.**

**Table 7. Summary table for the final backbone curve**

	<b>Final backbone curve</b>
<b>Initial Stiffness X/Y [g/mm]</b>	0.40 / 0.67
<b>Yield Displacement X/Y [mm]</b>	1.45 / 0.87
<b>Yield Normalized Force X/Y [g]</b>	0.57 / 0.59
<b>Peak Displacement X/Y [mm]</b>	2.78 / 1.17
<b>Peak Normalized Force X/Y [g]</b>	0.68 / 0.73
<b>Ultimate Displacement X/Y [mm]</b>	26.84 / 8.35

## References

- [1] Diana User's Manual -- Release 10.4, 2020; <https://dianafea.com/manuals/d104/Diana.html>
- [2] Schreppers, G.M.A., Garofano, A., Messali, F., Rots, J.G. (2017). DIANA Validation report for Masonry modelling. Report *DIANA FEA BV & TU Delft*, 15 February 2017
- [3] Messali, F., Longo, M. (2020). A numerical investigation of building typology 'Metselwerk 7'. Delft University of Technology. Report number 03, Version 01, 19 June 2020.
- [4] Mirra, M., & Ravenshorst, G. (2019). Seismic characterization of timber-masonry connections based on experimental results. Delft University of Technology
- [5] Messali, F., Ravenshorst, G.J.P. (2019). Database of connections: characteristics and properties. Delft University of Technology. Report number CM1B05-WP1-2.3, Final version, 03/12/2019.
- [6] Messali, F., Longo, M. (2020). Study of a median backbone curve and of the building to building variability for typology 'Metselwerk 1'. Delft University of Technology. Report number 02, Version 01, 07 May 2020.
- [7] Messali, F., Longo, M. (2020). Definition of a consistent backbone curve for typology 'Metselwerk 2'. Delft University of Technology. Report number 01, Version 02, 15 April 2020.
- [8] European Committee for Standardization (2005). Eurocode 8: Design of structures for earthquake resistance-part 1: general rules, seismic actions and rules for buildings.
- [9] Crowley, H., Pinho, R. (2020). Report on the Fragility and Consequence Models for the Groningen Field (Version 7)
- [10] ARUP (2017), Typology Modelling: Analysis Results in Support of Fragility Functions – 2017 Batch Results. Arup Project Title: Groningen Earthquakes - Structural Upgrading

## Appendix A: Material properties

The material parameters used in the model are listed below:

### 1. MASONRY

The Engineering Masonry Model [2] is used as material model for piers, bank, spandrel, gables and foots. Both internal and external walls have the same properties. Masonry is modelled with a thickness of 100 mm. Local y axis is aligned to the global Z axis in order to define the bed joint orientation. Local x axis is aligned to the in-plane direction of the elements. For the NLTH calculations the elastic properties are halved in order to properly capture the cyclic strength degradation, not explicitly described by the EMM. Besides, the same assumption has been already employed in other calibration/validation studies of URM buildings to overcome the global rigidity given by local connections which results in over stiff results.

**Table 8. Masonry material properties employed in the model.**

EMM	Clay
$E_y$ [MPa]	3000
$E_x$ [MPa]	1500
$G$ [MPa]	1250
Density [Kg/m <sup>3</sup> ]	1950
$f_y$ [MPa]	0.30
Min $f_x$ [MPa]	0.90
$G_{f,t}$ [N/m]	10
$\alpha$ [rad]	0.58
$f_c$ [MPa]	10.0
$G_c$ [N/m]	15000
$\phi$ [rad]	0.643
$c$ [MPa]	0.40
$G_s$ [N/m]	200

### 2. TIMBER PLANKS

An orthotropic behaviour, whose properties are calibrated according to past laboratory experiment, is assigned to timber planks of the ground, first and attic floor. The local x axis is aligned with the global Y. The properties are tabulated in Table 9.

**Table 9. Ground, first and attic floor timber diaphragm material properties employed in the model.**

Linear Elastic Orthotropic	Timber C18 - Plates
$E_x$ [MPa]	1.5
$E_y$ [MPa]	11
$E_z$ [MPa]	400
Density [Kg/m <sup>3</sup> ]	380
$\nu$ [-]	0.00
$G_{xy}$ [MPa]	1100
$G_{yz}$ [MPa]	1100
$G_{xz}$ [MPa]	500

### 3. TIMBER BEAMS

Beam properties are considered as isotropic linear elastic. Timber C14 is assigned as material to internal walls at first floor, purlins, rafters, joists, wall plates and ridge beams. The timber frame of the ground floor window is modelled with timber C18. The material parameters are listed in Table 10.

**Table 10. Timber beams properties employed in the model.**

Linear Elastic Isotropic	Timber C14	Timber C18
E [MPa]	7000	9000
Density [Kg/m <sup>3</sup> ]	290	320
$\nu$ [-]	0.3	0.3

### 4. REINFORCED CONCRETE

Floor material is modelled as linear elastic isotropic model. The properties are listed in Table 11.

**Table 11. Reinforced concrete properties employed in the model.**

Linear Elastic Isotropic	Concrete	Cement
E [MPa]	27000	15000
Density [Kg/m <sup>3</sup> ]	2500	2300
$\nu$ [-]	0.2	0.2

### 5. STEEL

Lintel material is modelled as linear elastic. Material properties are reported in Table 12.

**Table 12. Steel properties employed in the model.**

Linear Elastic Isotropic	Steel
E [MPa]	210000
Density [Kg/m <sup>3</sup> ]	7800
$\nu$ [-]	0.3

## Appendix B: original motions (stronger X-direction)

Appendix B reports the hysteretic curves measured at the effective height for the *original* motions applied to the building considering the strongest PGA in the *global X direction*. In addition, also displacements plots of attic floor and roof are reported. The hysteretic curves are reported for the three different effective masses.

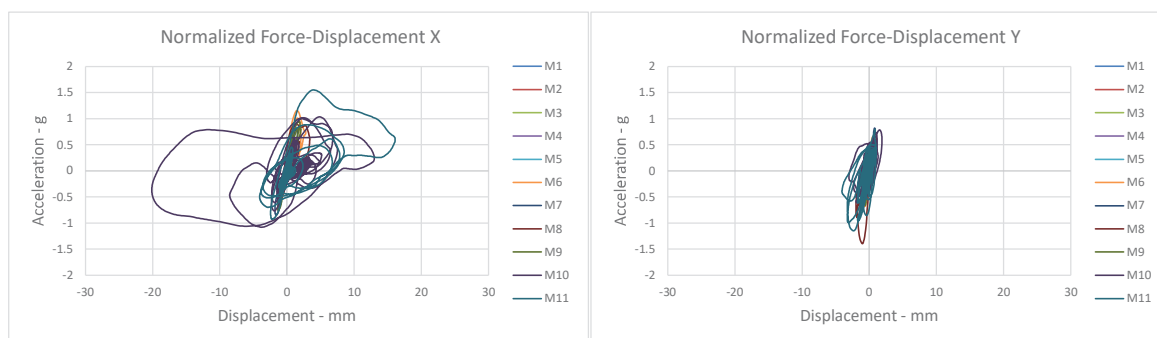


**Figure 30.** Hysteretic curves defined at the effective height for the eleven original ground motion having the strongest motion orientated in the global X direction. Normalized force computed with Mass A.

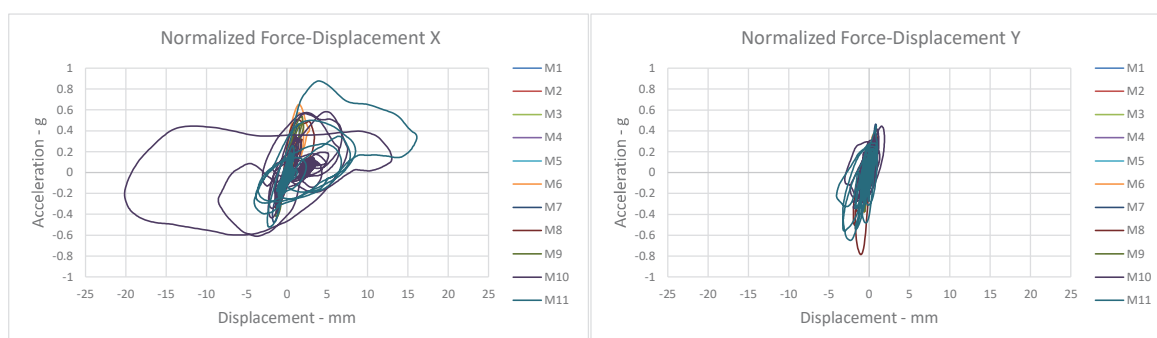


**Figure 31.** Hysteretic curves defined at the effective height for the eleven original ground motion having the strongest motion orientated in the global X direction. Normalized force computed with Mass B.

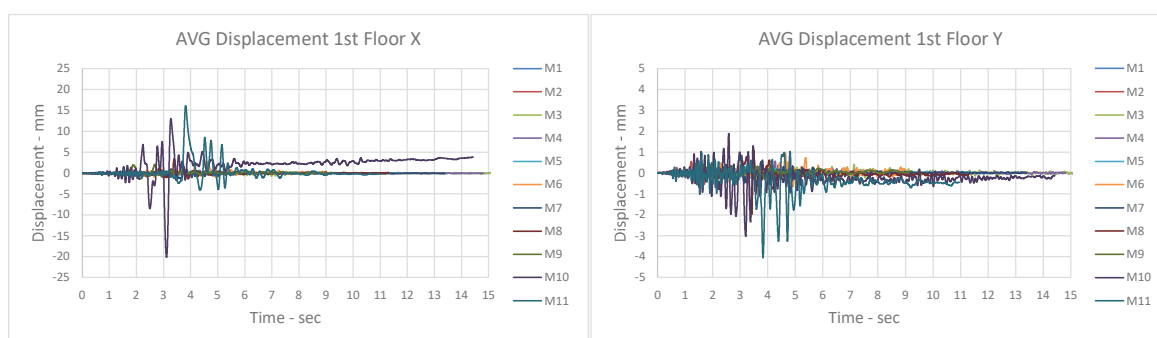


**Figure 32.** Average displacement defined at the effective height for the eleven original ground motion having the strongest motion orientated in the global X direction.

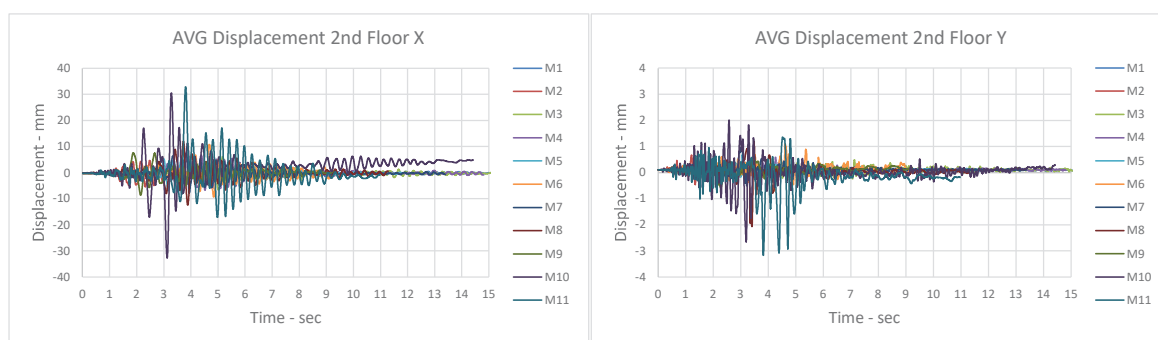


**Figure 33. Average displacement defined at the second floor height for the eleven original ground motion having the strongest motion orientated in the global X direction.**

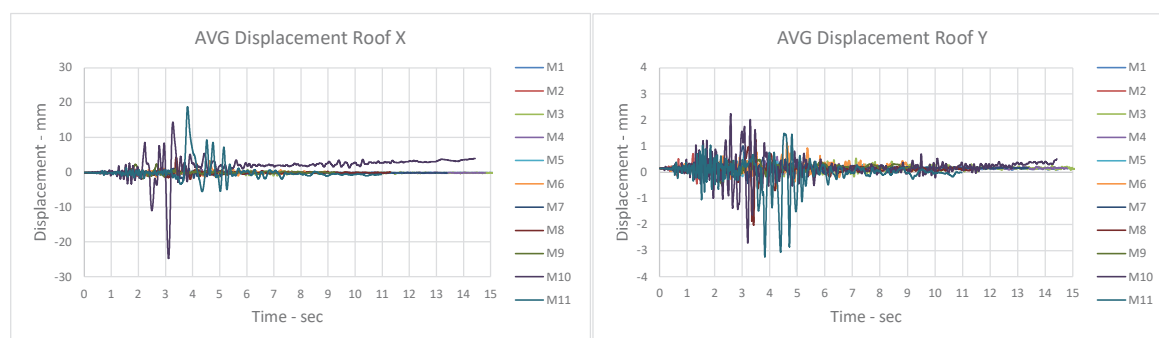


**Figure 34. Average displacement defined at the roof height for the eleven original ground motion having the strongest motion orientated in the global X direction.**

## Appendix C: original motions (stronger Y-direction)

Appendix C reports the hysteretic curves measured at the effective height for the *original* motions applied to the building considering the strongest PGA in the *global Y direction*. In addition, also displacements plots of attic floor and roof are reported. The hysteretic curves are reported for the three different effective masses.

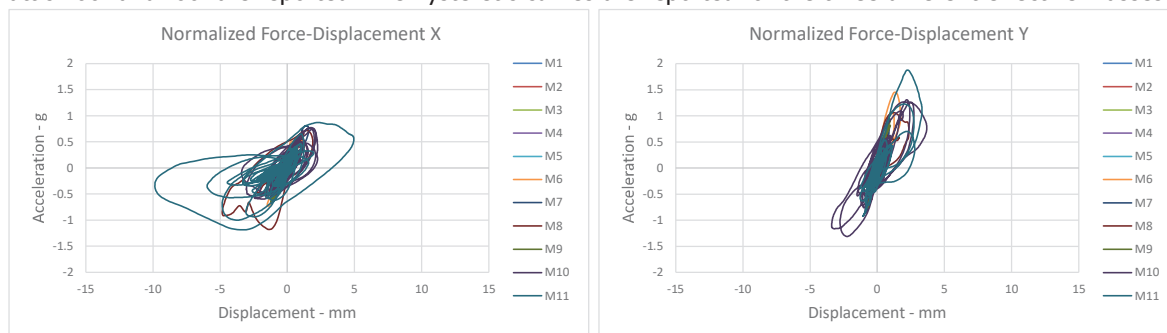


**Figure 35.** Hysteretic curves defined at the effective height for the eleven original ground motion having the strongest motion orientated in the global Y direction. Normalized force computed with Mass A.

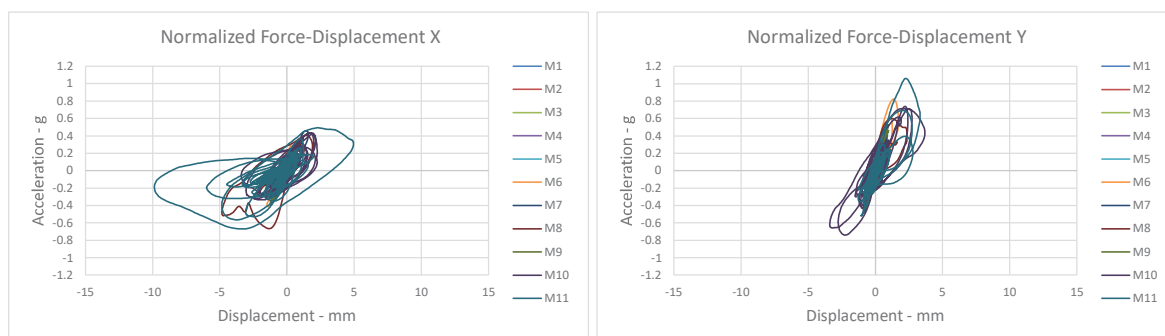


**Figure 36.** Hysteretic curves defined at the effective height for the eleven original ground motion having the strongest motion orientated in the global Y direction. Normalized force computed with Mass B.

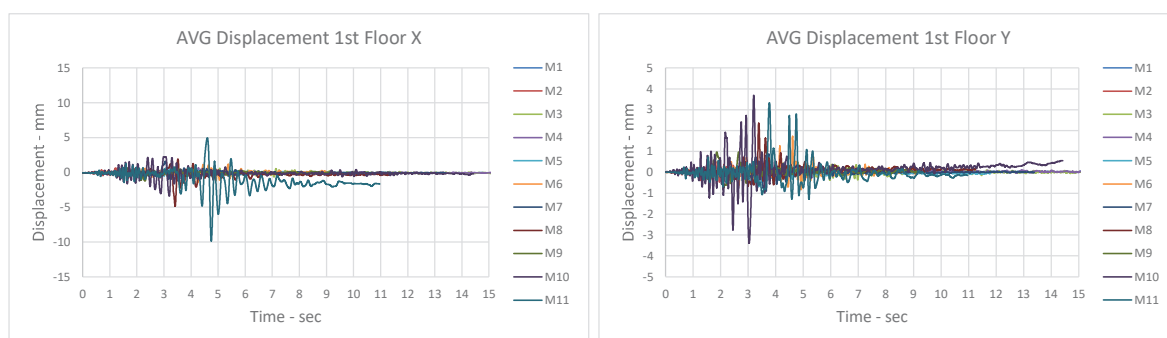


**Figure 37.** Average displacement defined at the effective height for the eleven original ground motion having the strongest motion orientated in the global Y direction.

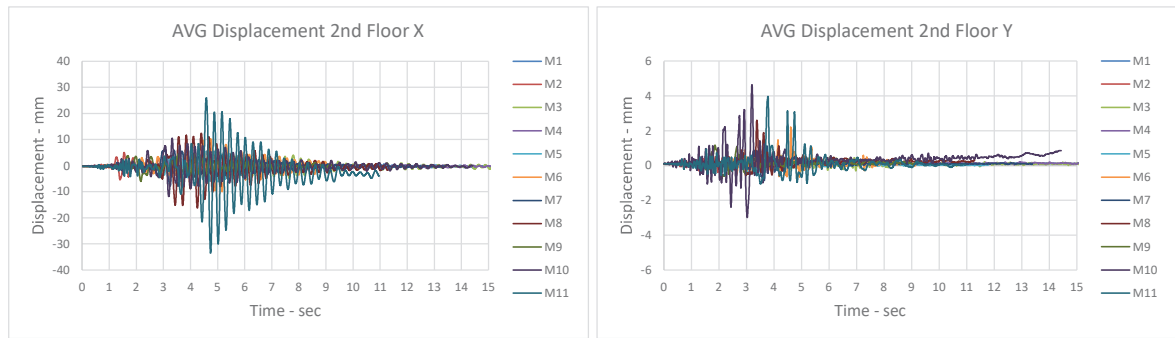


**Figure 38. Average displacement defined at the second floor height for the eleven original ground motion having the strongest motion orientated in the global Y direction.**

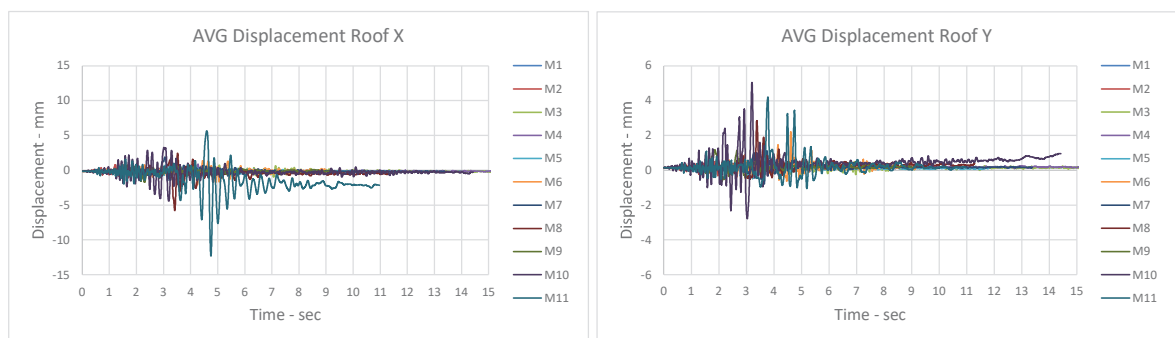


**Figure 39. Average displacement defined at the roof height for the eleven original ground motion having the strongest motion orientated in the global Y direction.**

## Appendix D: scaled motions (stronger X-direction)

Appendix D reports the hysteretic curves measured at the effective height for the *scaled* motions applied to the building considering the strongest PGA in the *global X direction*. In addition, also displacements plots of attic floor and roof are reported. The hysteretic curves are reported for the three different effective masses.

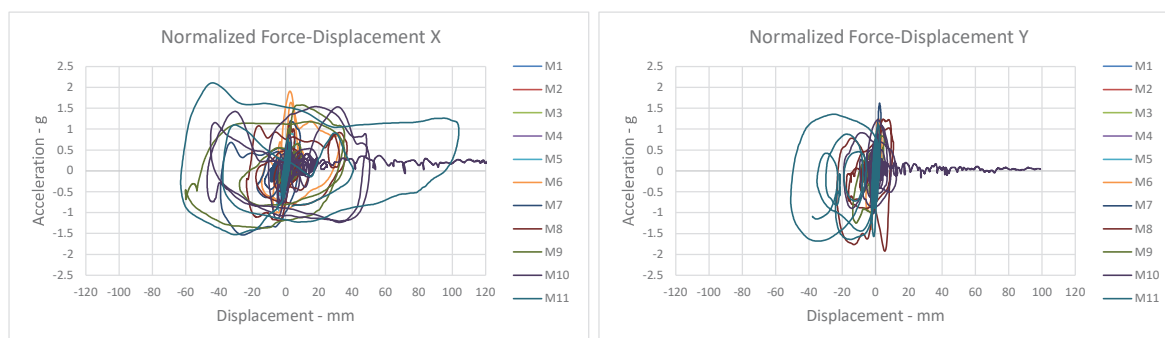


**Figure 40.** Hysteretic curves defined at the effective height for the eleven scaled ground motion having the strongest motion orientated in the global X direction. Normalized force computed with Mass A.

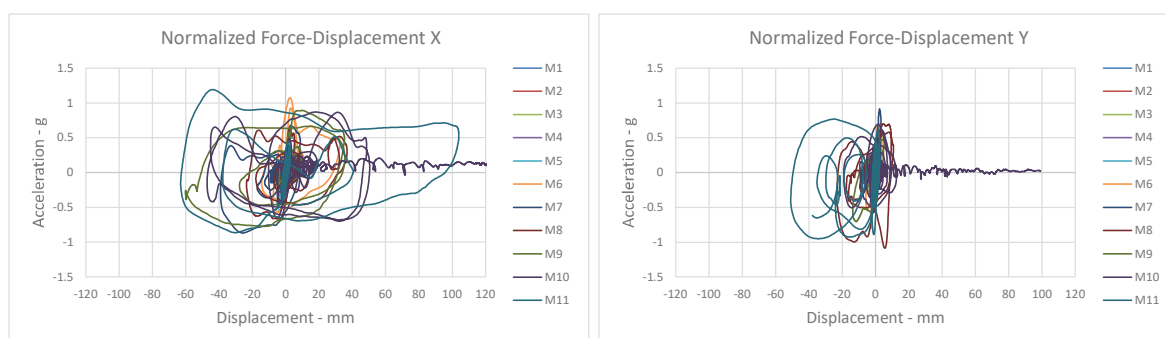


**Figure 41.** Hysteretic curves defined at the effective height for the eleven scaled ground motion having the strongest motion orientated in the global X direction. Normalized force computed with Mass B.

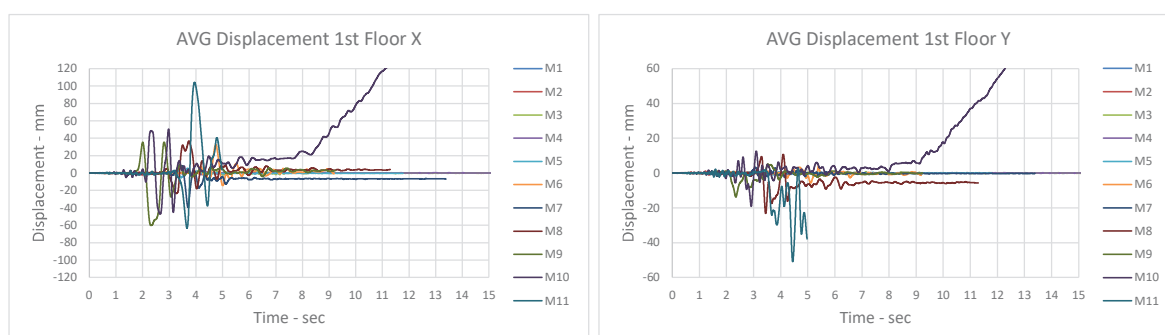


**Figure 42.** Average displacement defined at the effective height for the eleven scaled ground motion having the strongest motion orientated in the global X direction.

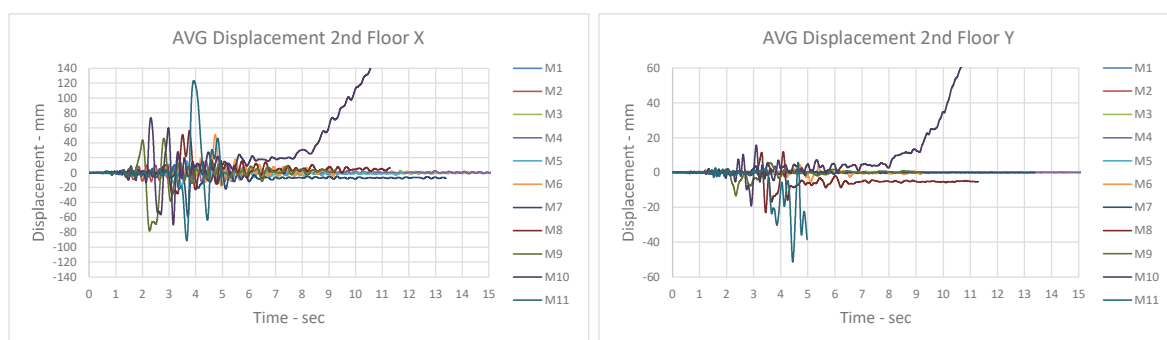


**Figure 43. Average displacement defined at the second floor height for the eleven scaled ground motion having the strongest motion orientated in the global X direction.**

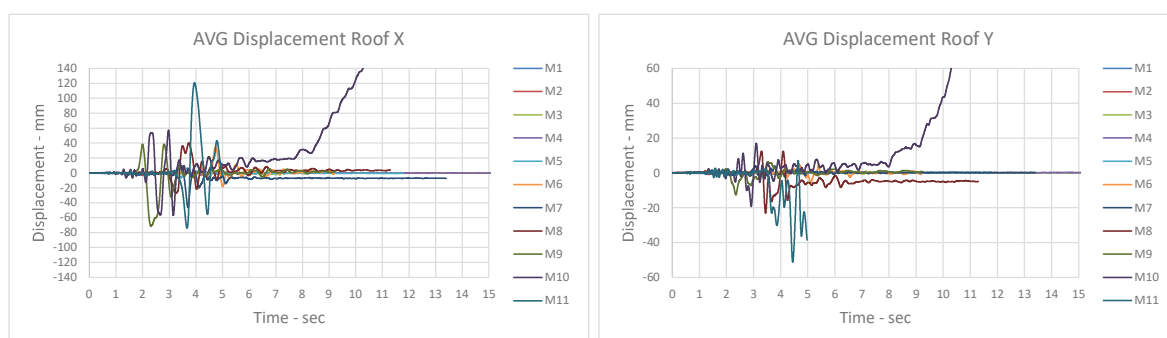


**Figure 44. Average displacement defined at the roof height for the eleven scaled ground motion having the strongest motion orientated in the global X direction.**

## Appendix E: scaled motions (stronger Y-direction)

Appendix E reports the hysteretic curves measured at the effective height for the *scaled* motions applied to the building considering the strongest PGA in the *global Y direction*. In addition, also displacements plots of attic floor and roof are reported. The hysteretic curves are reported for the three different effective masses.

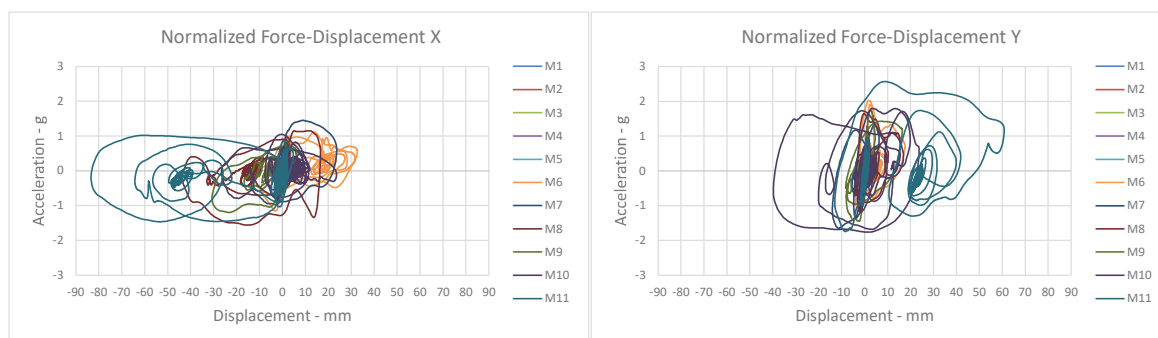


**Figure 45.** Hysteretic curves defined at the effective height for the eleven scaled ground motion having the strongest motion orientated in the global Y direction. Normalized force computed with Mass A.

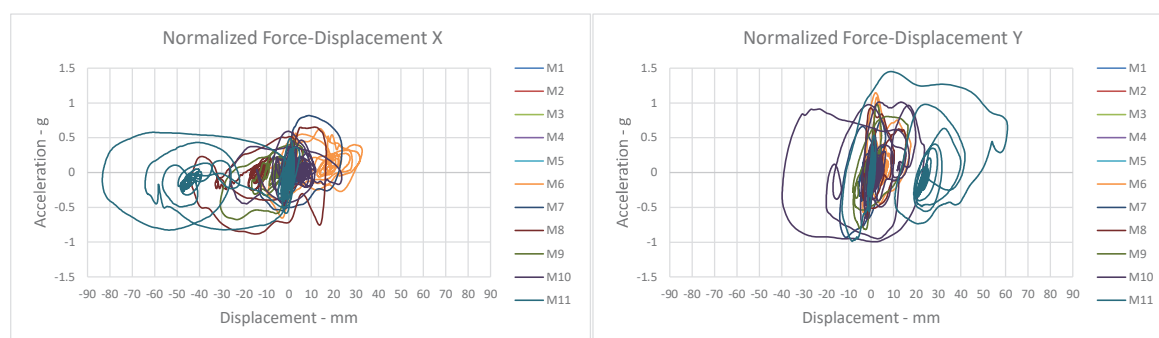


**Figure 46.** Hysteretic curves defined at the effective height for the eleven scaled ground motion having the strongest motion orientated in the global Y direction. Normalized force computed with Mass B.

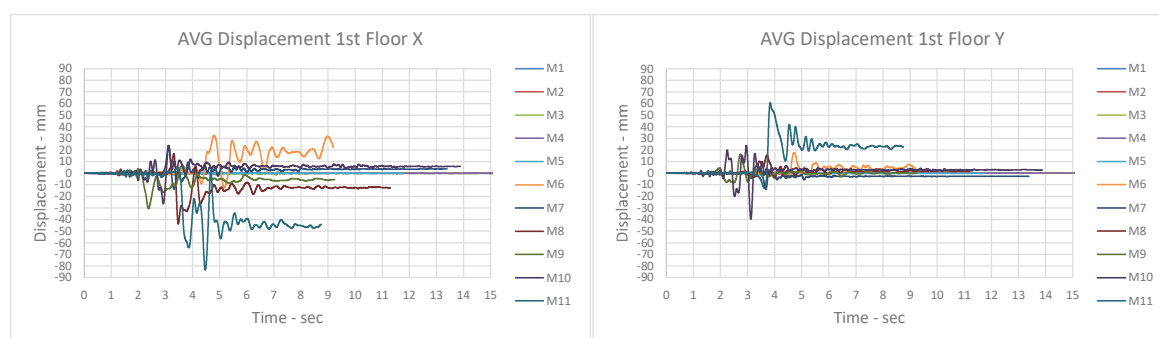


**Figure 47.** Average displacement defined at the effective height for the eleven scaled ground motion having the strongest motion orientated in the global Y direction.

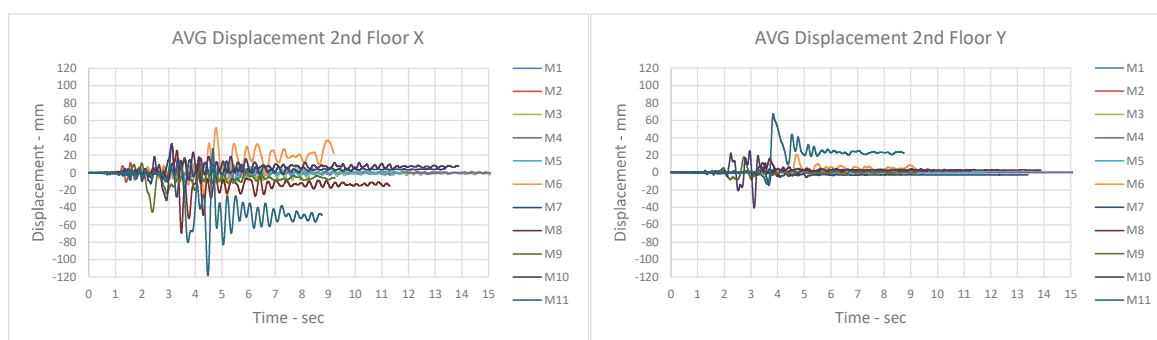


**Figure 48. Average displacement defined at the second floor height for the eleven scaled ground motion having the strongest motion orientated in the global Y direction.**

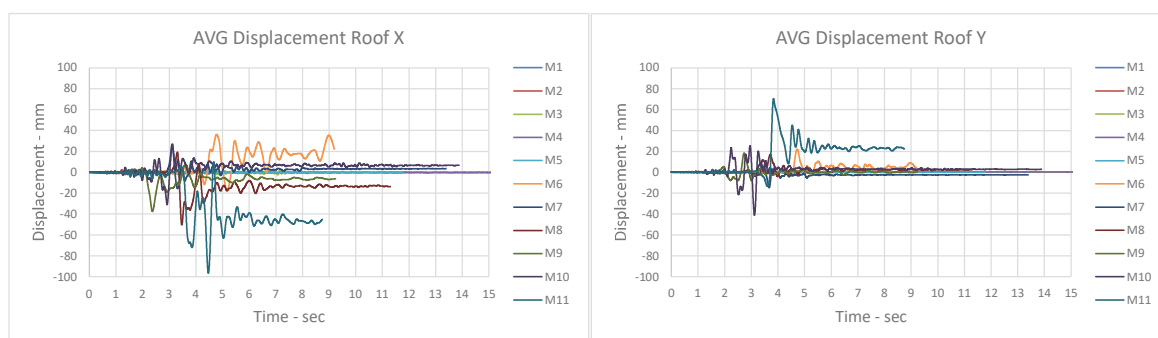


**Figure 49. Average displacement defined at the roof height for the eleven scaled ground motion having the strongest motion orientated in the global Y direction.**

## Appendix E: consistency of the definition of the effective mass with ‘Badweg 12’

The effective mass is a critical parameter that largely influences the normalized base shear capacity of a building. In the variation study performed for typology Metselwerk 7, the effective mass is defined as the mass of the building located above the mid-height of the masonry piers of the ground-storey level. In the case of the building located at Wirdumerweg 4 (Wirdum), described in this report, the presence of high foundation walls suggested that also the lower part of the ground-storey level might be partly excited by the seismic action, as reported in Section 2. For this reason, the two masses “A” and “B” are considered as alternative definitions of the effective mass (Figure 10). Compared to Mass A, Mass B includes the lower half of the ground-storey level (inclusive of the ground floor).

The fundamental modes in the X- and Y-directions (Figure 50) show that the superior portion of the structure largely deforms, whereas the lower part (including the ground-floor) displaces little. Similarly, the failure mechanisms at collapse (Figure 51) involve almost exclusively the portion of the building included in the calculation of Mass A. The minimum PGA of a ground motion that determines the collapse of the building is 0.535g (in Y-direction, as reported in Table 13), a value that is almost the average between the normalized base shear capacity values obtained for Mass A and Mass B. A higher PGA value is found in the X-direction (0.710g), in line with the normalized accelerations measured for the building in that loading direction for mass A. Finally, the effective mass is defined for pushover analyses according to Equation 1 (as in Appendix B of Eurocode 8 [8]):

$$m_{eff} = \sum m_i \phi_{it} \quad (1)$$

where  $m_i$  is the mass of the  $i$ -th storey and  $\phi_{it}$  the displacements normalized (so that  $\phi_{it}$  of the top storey is equal to 1). The normalized displacements of the mass of the lower part of the ground storey (and especially the ground floor) are negligible, so that this portion of the building can be excluded from the calculation of the effective mass. The value of the effective mass of the building is therefore close to the value computed for Mass A, because the additional portion of buildings included in Mass B (the lower half of the ground-storey level inclusive of the ground floor) is scarcely activated by the seismic motion at collapse of the building.

An equivalent approach is followed by Eucentre for the index building Badweg 12 [9]. The effective mass of the building is taken equal to 44 t, which is the sum of the masses located above the mid-height of the piers of the ground storey level, as shown in Figure 52 (1<sup>st</sup> floor – 36 t – and roof – 8 t).

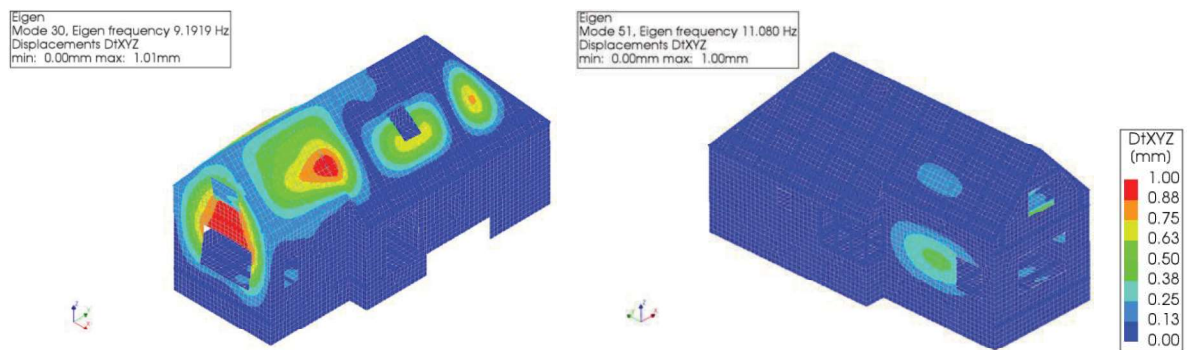


Figure 50. Fundamental eigenmodes (no. 30, in the Y-direction, and no. 51, in the X-direction).

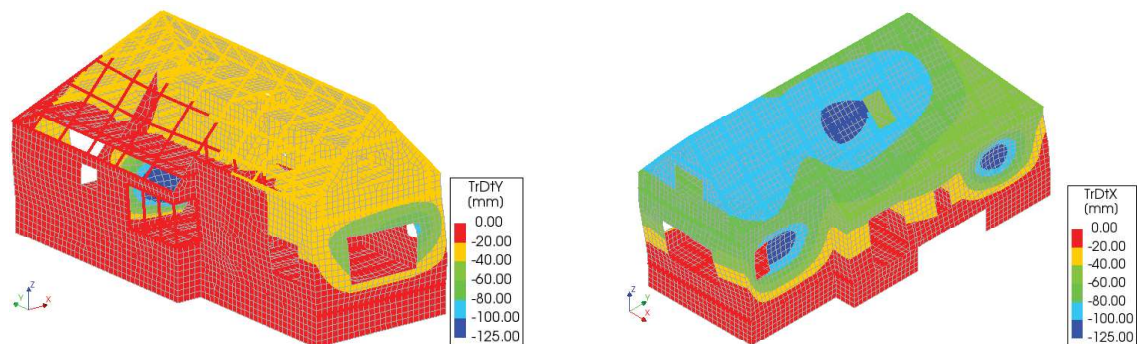


Figure 51. Failure mechanisms at collapse in the Y-direction and X-direction.

Table 13. Failure type of Wirdumerweg building for the four series of the 11 ground motions for an OOP limit of 100 mm.

	M1	M2	M3	M4	M5	M6	M7	M8	M9	M10	M11
PGA strong dir [g]	0.061	0.317	0.215	0.136	0.191	0.416	0.505	<b>1.021</b>	0.403	0.422	<b>0.710</b>
PGA weak dir [g]	0.090	0.192	0.237	0.245	0.257	<b>0.948</b>	<b>0.542</b>	0.780	<b>0.535</b>	<b>0.843</b>	<b>1.302</b>
PGA vertical dir [g]	0.034	0.099	0.080	0.182	0.168	0.315	0.196	0.401	0.461	0.503	0.386
Strong Motion in X PGA x 2	-	-	-	-	-	-	-	<b>OOP A</b>	(IP 1,2)*	(IP 2)*	(IP 1,2)* <b>OOP A,B,C</b>
Strong Motion in Y PGA x 2	-	-	-	-	-	<b>OOP A</b>	<b>OOP A</b>	(IP 2)*	<b>OOP A</b>	<b>OOP A</b>	(IP 1,2)* <b>OOP A</b>

\*the in-plane limits are not considered in this case because they refer to the characteristic behaviour of the structure and not to the median behaviour.

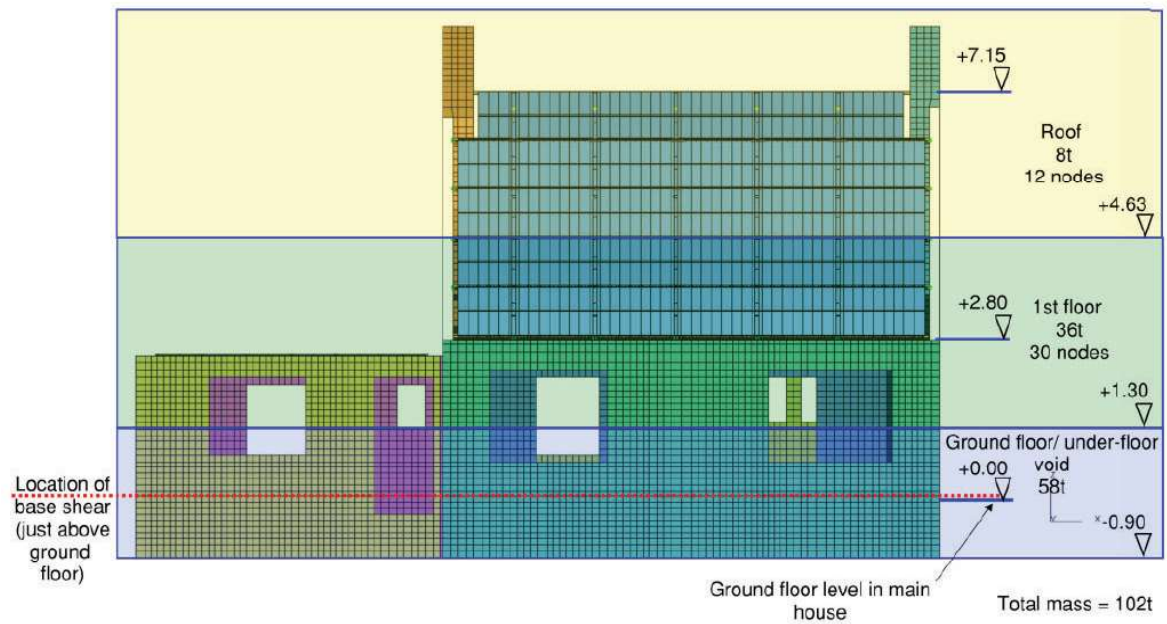


Figure 52. Mass distribution of Badweg 12 (extracted from [10]).

Project	Typology based assessment
Report number	08
Internal Reference	B2B-R08
Date	April 12, 2021
Version	01
Status	Draft


# **SEISMIC PERFORMANCE OF A DETACHED HOUSE: CASE STUDY DAMSTERWEG 37, STEENDAM**

*A quick, safe and validated typology based seismic assessment of  
buildings*

Client: Ministerie van Economische Zaken en Klimaat (EZK)

Authors  
Francesco Messali  
[F.Messali@tudelft.nl](mailto:F.Messali@tudelft.nl)  
Michele Longo  
[M.Longo@tudelft.nl](mailto:M.Longo@tudelft.nl)  
Anmol Singla  
[A.Singla@tudelft.nl](mailto:A.Singla@tudelft.nl)

Address  
Delft University of Technology  
Faculty of Civil Engineering and Geosciences  
Stevinweg 1, 2628 CN, Delft

 <p>Faculty of Civil Engineering and Geosciences Stevinweg 1 2628 CN Delft PO 5048 2600 GA Delft <a href="http://www.citg.tudelft.nl">www.citg.tudelft.nl</a></p>	<b>Report</b>	
	<i>Title:</i> Seismic performance of a detached house: case study Damsterweg 37, Steendam	
	<i>Author(s):</i> Francesco Messali Michele Longo Anmol Singla	
	<i>Date:</i> 12/04/2021	
<i>Client(s):</i> Ministerie van Economische Zaken en Klimaat (EZK)	<i>Version:</i> 01	<i>Status:</i> Draft
<i>Project number:</i> TBA-20/21	<i>Project name:</i> A quick, safe and validated typology based seismic assessment of buildings	<i>File reference:</i> B2B-R08
<i>Cite as:</i> Messali, F., Longo, M., Singla, A. (2021). Seismic performance of a detached house: case study Damsterweg 37, Steendam. Delft University of Technology. Report number 08, Version 01, 12 April 2021.		

### **Copyright statement**

All rights reserved. No part of this publication may be reproduced, stored in a retrieval system of any nature, or transmitted, in any form or by any means, electronic, mechanical, photocopying, recording or otherwise, without the prior written permission of TU Delft.

### **Liability statement**

TU Delft and those who have contributed to this publication did exercise the greatest care in putting together this publication. However, the possibility should not be excluded that it contains errors and imperfections. Any use of this publication and data from it is entirely on the own responsibility of the user. For everybody who has contributed to this publication, TU Delft disclaims any liability for damage that could result from the use of this publication and data from it, unless the damage results from malice or gross negligence on the part of TU Delft and/or those who have contributed to this publication.

## Table of Contents

1	Introduction .....	4
2	Building and model description.....	5
3	Results .....	10
3.1	Failure (stop) criteria .....	10
3.2	Analyses Results.....	11
3.3	Backbone capacity curve.....	16
4	Conclusions.....	18
	References.....	20
	Appendix A .....	21
	Appendix B: original motions.....	24
	Appendix C: scaled motions .....	26
	Appendix D: comparison timber beam variation.....	28

## 1 Introduction

This report summarizes the results of the numerical simulations performed to define the seismic performance of the detached house located in Damsterweg 37, 9629 PB in Steendam (hereinafter named Damsterweg only, for the sake of simplicity). Non-linear time history (NLTH) analyses are carried out. A set of 11 ground motions having different intensities is used.

A backbone curve representative of the global behavior of the building is built from the entire set of analyses results. Both local and global failure mechanisms are considered to define the base shear capacity and the ultimate displacement of the building. The possible failure of the timber beam-masonry connections is also taken into account in the definition of the capacity of the building.

The analyses are conducted by employing the Finite Element software DIANA FEA version 10.4 [1].

## 2 Building and model description

The Damsterweg building is a two-storey (plus attic) detached house with the gutter line at the level of the first floor, built in 1936 and belonging to the typology Metselwerk 7. The building is partially made of unreinforced masonry (URM) cavity walls and partially made of single leaf clay walls. A picture and a plan section of the building is shown in Figure 1. The cavity wall system consists of clay bricks for both the inner and outer leaf. The building has a height of 8.07 m measured at the ridge beam. The ground floor is built with two different materials. The South-West side is made of timber beams and chipboard panels while the North-East part is made of pre-cast concrete. At the 1<sup>st</sup> floor and at the attic floor, the timber beams spanning in the X-direction (North-South) are connected with chipboard panels. The roof is composed by timber purlins and rafters, connected with chipboard panels.

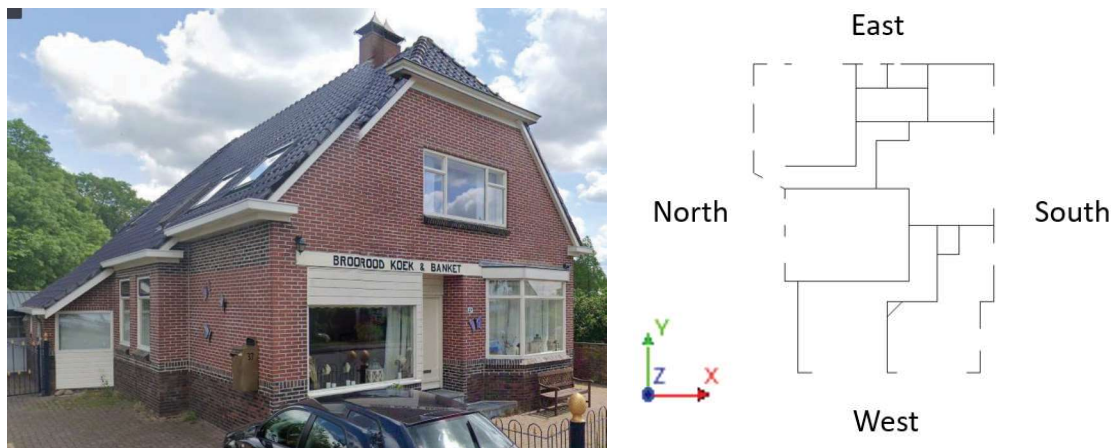


**Figure 1. Damsterweg detached house. North-West façade view (left) and plan view (right).**

The detached house is numerically modelled in 3D by means of the software Diana 10.4. A representation of the model used for the simulations is shown in Figure 2.

The cavity wall system is implemented by explicitly modelling the inner leaf and considering the outer leaf as dynamic mass acting in the horizontal direction perpendicular to the wall plane. This implies the assumption that the wall ties are unable to transfer any shear force. The overview of the modelled inner leaf is depicted in Figure 3. Lintels above the openings are modelled as linear concrete elements. The internal partition walls at the ground floor are made of two materials, clay brick masonry or aerated concrete masonry, and bear the first floor: namely, they are directly connected to the timber beams of the floor, but they are disconnected from the floor planks. Some of the partition walls at the first storey level are also made of aerated concrete, but they are not load bearing. In addition, partitions made of timber are also present at the first storey level and they are not load bearing. In practice, the lateral connection between internal and external walls is done by a vertical mortar joint. Such connection is modelled with a strip of weak elements that simulates a vertical mortar joints. An overview of the walls is shown in Figure 4. Both internal and external masonry walls are modelled using the Engineering Masonry Model [2]. For the aerated concrete walls, the Total Strain Rotating Crack model is employed. The timber walls are modelled as linear elastic. The weak elements representing the vertical joint between the internal and external walls are also modelled with the Engineering Masonry Model, but the local axes are rotated and both elastic and nonlinear properties are reduced by 30%.

The precast concrete ground floor and the timber at the ground, first and attic floors are modelled as linear elements (Figure 5). The timber beams spanning in the X-direction (North-South) which are part of the attic floor sheets, are shown in Figure 6. They are also modelled as linear elastic material.

The roof purlins, struts, rafter, wall plates and ridge beam are modelled with beam elements using a linear elastic isotropic material (Figure 7). Non-linear point interfaces are used to model the pocket connections between the beams of the first floor and the masonry walls, and between the purlins and the masonry gables. A coulomb-friction model is employed for the interfaces. The locations of the point interfaces are shown in Figure 8. The timber boards, representing the roof structure are modelled as shell elements using linear elastic orthotropic material (Figure 9).

A full list of the material properties used in the model is provided in Appendix A.

The total dynamic mass (the one which is acting during the motion) of the model is equal to 119 tons. Two variations of the effective mass are proposed and implemented in the computation of the normalized force. Mass A considers the participation of the building above half of the ground storey height, consistently to the criterion adopted for the analyses performed in support of the Typology based assessment. However, unlike the buildings studied for Metselwerk 7 [3], the current building presents high foundations, so that it is expected that the mass of the ground floor too is activated by the ground motions. For this reason, a second effective mass, Mass B, is computed taking into account the mass of the entire ground storey (including the floor mass). An overview of the selected effective mass is depicted in Figure 10 and listed in Table 1. The effective height is considered at the location of the first floor height, equal to 2.9 m from the ground floor.

Quadratic 8-noded curved shell elements (CQ40S and CT30S) are used to model the walls, floors and lintels of the 3D building. The timber beams are modelled with Class-III beam element (CL18B). The timber-masonry connection is modelled with point interfaces (N6IF). The model is assumed to be fixed-base (no soil-structure interaction is considered), so that it is fully restrained at the bottom from translations and rotations. The elements are meshed with an average size of 200x200 mm (Figure 2).

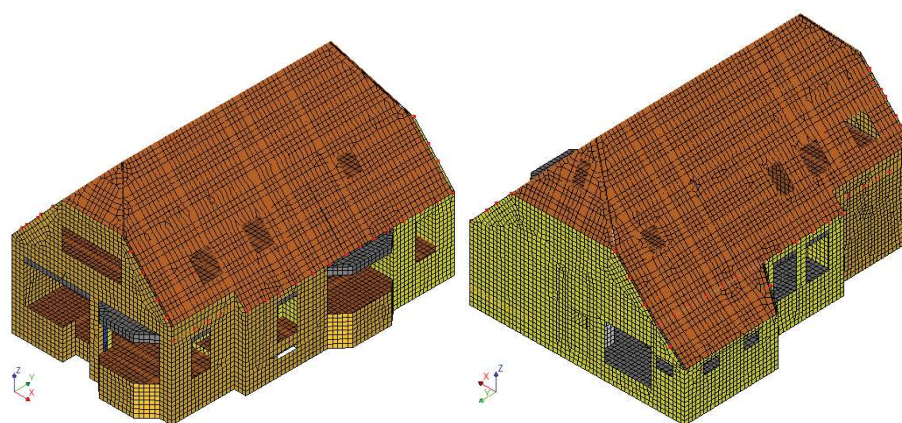


**Figure 2. Diana model of Damsterweg. South-West view (left) and North-East view (right).**

Non Linear Time History (NLTH) analyses are performed. The model is first subjected to gravity loads, applied in ten equal steps. Afterwards, live loads at floor levels, and additional roof masses are applied in ten steps. Then, the different acceleration motions are applied in the longitudinal, transversal and vertical direction at the base nodes, using a time step of 2.5 milliseconds. A Rayleigh damping of 2% is accounted for in the calculations. The Secant BFGS (Quasi-Newton) method is employed as iterative method. Energy norm must be satisfied during the iterative procedure with a tolerance of 0.01%. The Parallel Direct Sparse method is employed to solve the system of equations. The second order effects are accounted via the Total Lagrange geometrical nonlinearity.

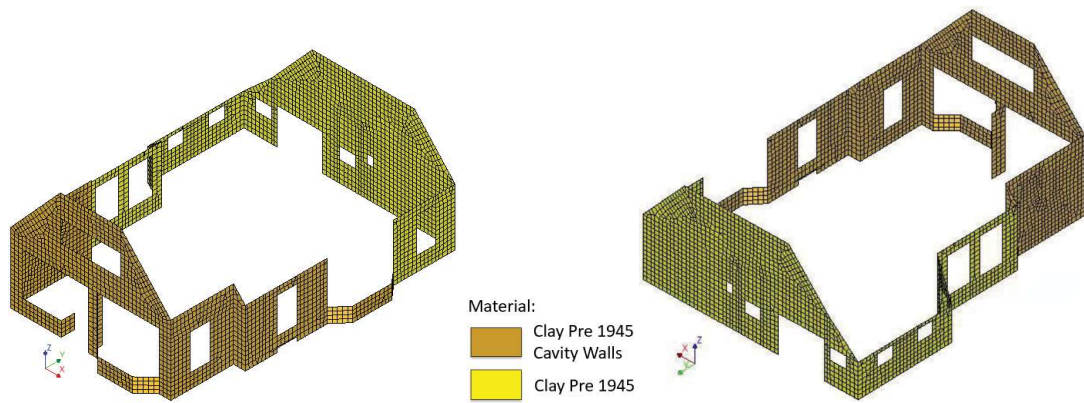


Figure 3. External walls material. South-West view (left) and North-East view (right).

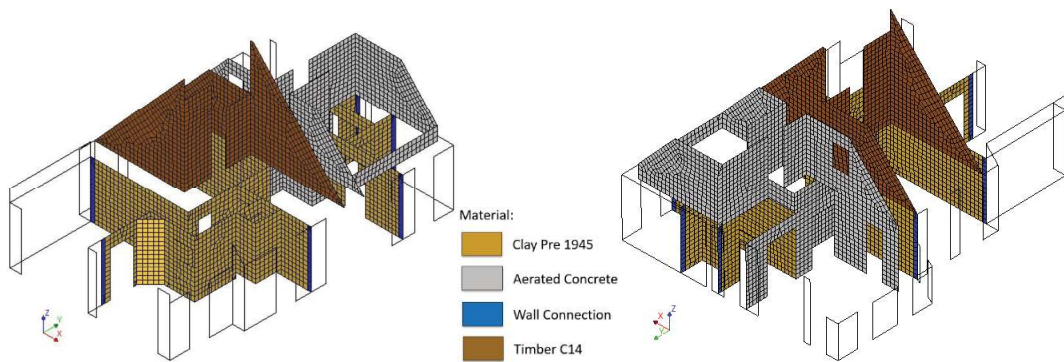


Figure 4. Internal walls material. South-West view (left) and North-East view (right).

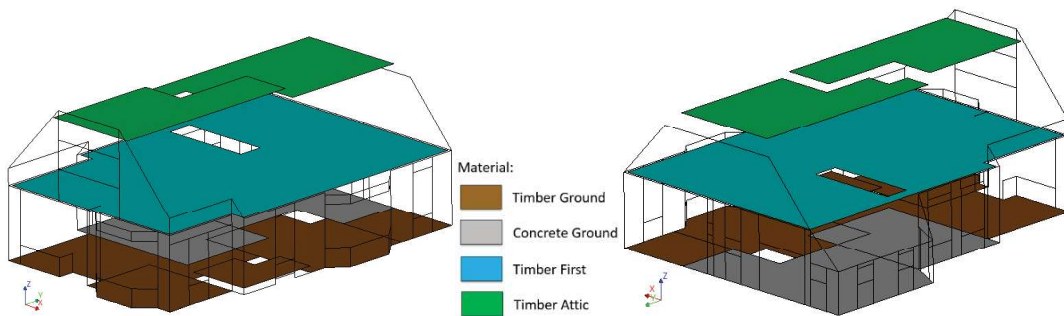


Figure 5. Floor material. South-West view (left) and North-East view (right).

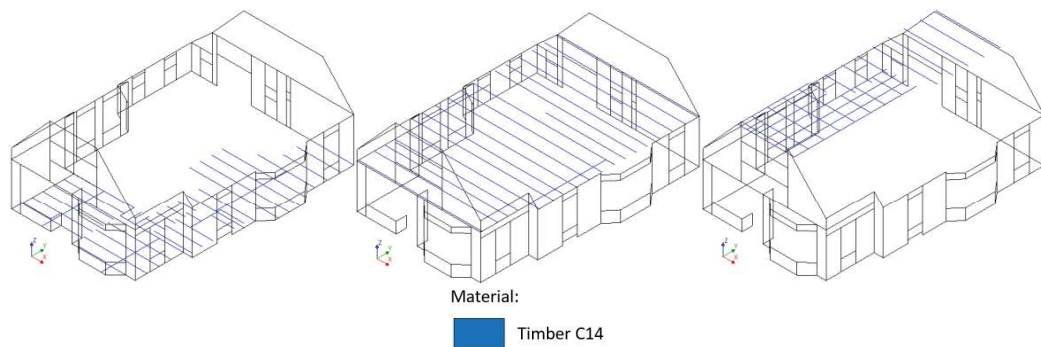


Figure 6. Floor timber beams. Ground (left), first (middle) and attic (right) floor. South-West view.

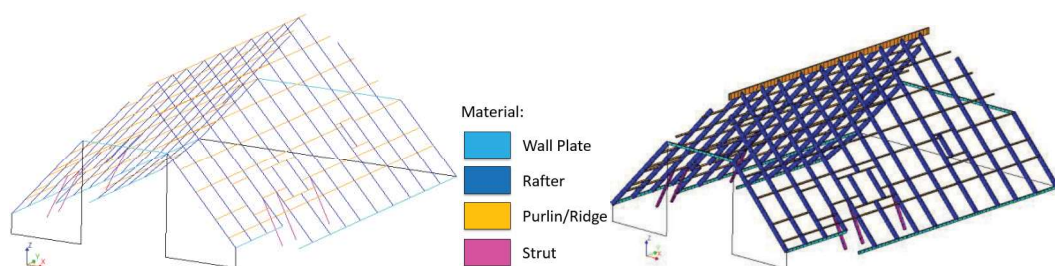


Figure 7. Roof beam structure. South-West view.

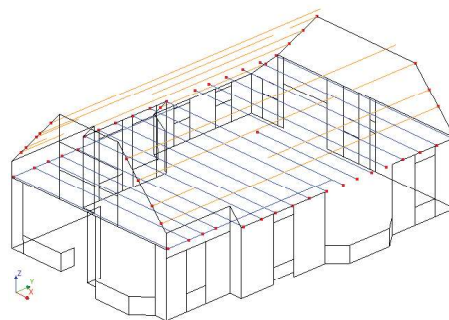


Figure 8. Interface location. South-West view.

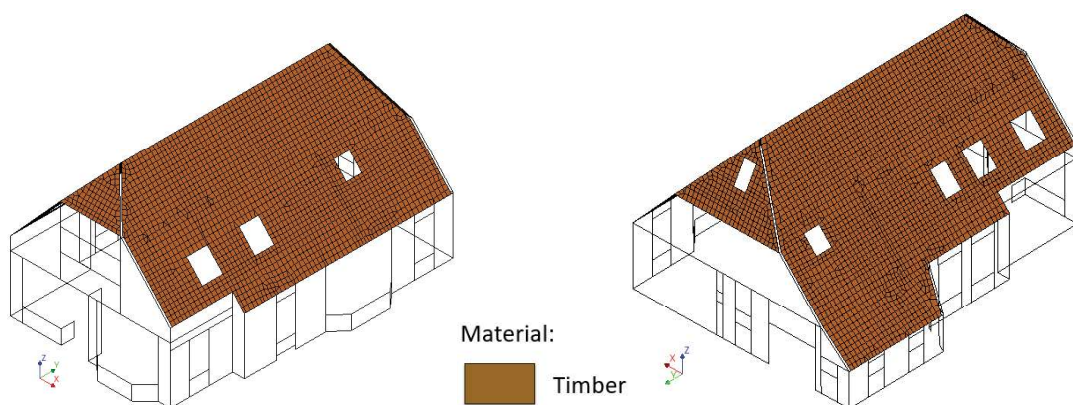


Figure 9. Roof boards. South-West view (left) and North-East view (right).

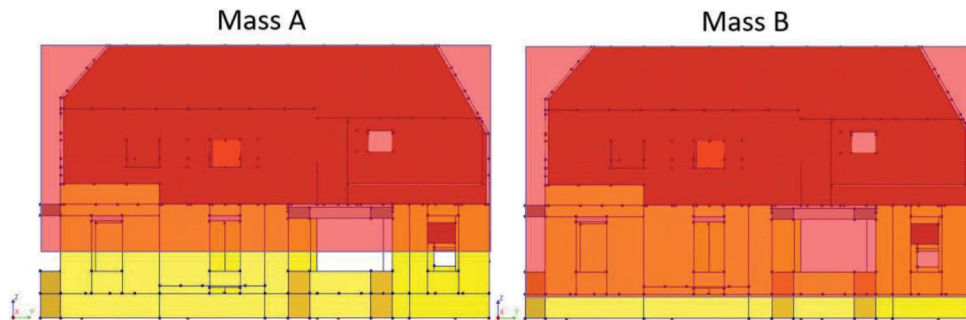


Figure 10. Considered effective masses (highlighted in red).

Table 1. Values of the two considered effective masses.

	Mass A	Mass B	Total Mass
Effective Mass [ton]	53.3	99.1	119.0

The seismic input is described by 11 different ground motions applied in the three directions. The strongest horizontal motion (indicated as "weak direction" motion) is applied in the global Y-direction. Table 2 lists the PGAs for different earthquakes in different directions. Since the original series of ground motions did not allowed to determine the ultimate displacement capacity of the building, a second series of motions was considered, with the original PGAs scaled up by a factor two for all three motion directions. The complete ground motions used for the simulations are reported in [3].

Table 2. PGAs of the 11 selected ground motion.

	M1	M2	M3	M4	M5	M6	M7	M8	M9	M10	M11
PGA strong dir [g]	0.061	0.317	0.215	0.136	0.191	0.416	0.505	1.021	0.403	0.422	0.710
PGA weak dir [g]	<b>0.090</b>	<b>0.192</b>	<b>0.237</b>	<b>0.245</b>	<b>0.257</b>	<b>0.948</b>	<b>0.542</b>	<b>0.780</b>	<b>0.535</b>	<b>0.843</b>	<b>1.302</b>
PGA vertical dir [g]	0.034	0.099	0.080	0.182	0.168	0.315	0.196	0.401	0.461	0.503	0.386

## 3 Results

### 3.1 Failure (stop) criteria

Due to the implicit nature of the time history calculations performed with Diana, a set of “stop criteria” are implemented in order to cap the capacity and the ultimate displacement of the analyses. Different criteria are selected:

- **In-Plane (IP) failure:** the maximum allowable drift limit for the masonry piers in the in-plane direction is set to 1.5% for ductile mechanism and to 0.6% for a brittle (shear type) failure, in line with the values recommended in NPR 9998:2020. Such drift values corresponds to displacements equal to 43.5 mm and 17.4 mm, respectively, for ductile and brittle type failure. In-Plane limits are only computed at the ground floor (to all load bearing piers, Figure 11). The criteria are selected conservatively, since the standard NPR 9998 refers to the characteristic and not the mean capacity of the building. A correction factor (for instance similar to that used in [6] and [7] for the SLAMA analyses) may be applied to increase the limits; however, this would not influence the definition of the backbone curve, since the collapse is governed by the out-of-plane of an internal loadbearing wall at the ground storey level. For this reason, such factor is omitted.
- **Out-Of-Plane (OOP) failure:** the maximum permitted OOP displacement for all load-bearing-walls is set to 100 mm. A variation study is made, by considering a limit of 60 mm. It should be noted that the collapse of the West gable is considered as local failure, since it is not bearing the attic floor nor the roof, which are supported by the rafter structure (Figure 12).
- **Connection failure:** the nonlinear behaviour of the connections between masonry and timber beams at roof and attic floor level (Figure 8) is considered. However, the elements do not have an explicit deformation limit, so that the relative displacements between the beams and the masonry walls are checked during the entire dynamic motion. The axial relative displacement generated at the interface is assessed according to the available support provided by the masonry wall. A conservative value of 0.6 times the masonry thickness is selected (thus, equal to 60 mm). In that situation the overall failure of the building is considered due to the failure of the connections. According to the moment of failure, the maximum normalized force at connection failure (averaged over the entire set of analyses), is used to cap the capacity of the backbone curves.

Displacement at different floors and roof level are computed at the location represented in Figure 13 and then averaged to a single value. It must be noted that the floor node at the first and second floor at the East and West side coincide with the node of the masonry East and West façade.

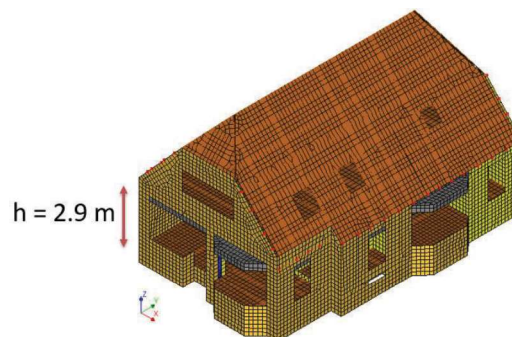


Figure 11. Inter-storey height of the building.

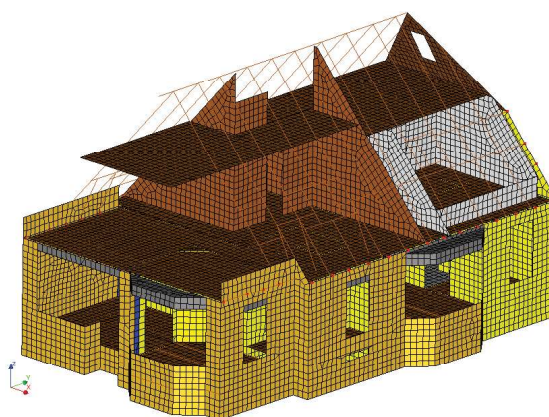


Figure 12. Model overview without West gable and its connected elements.

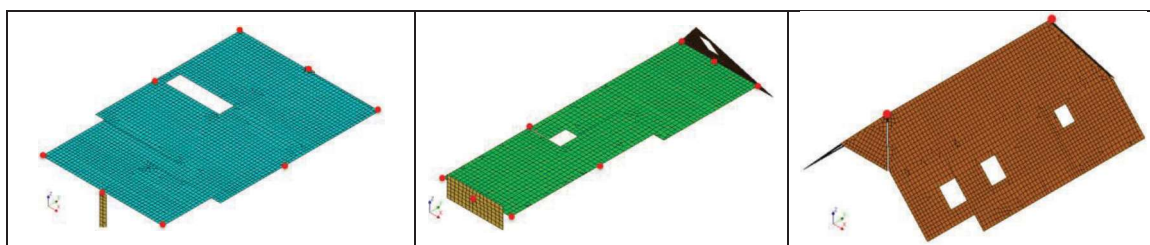
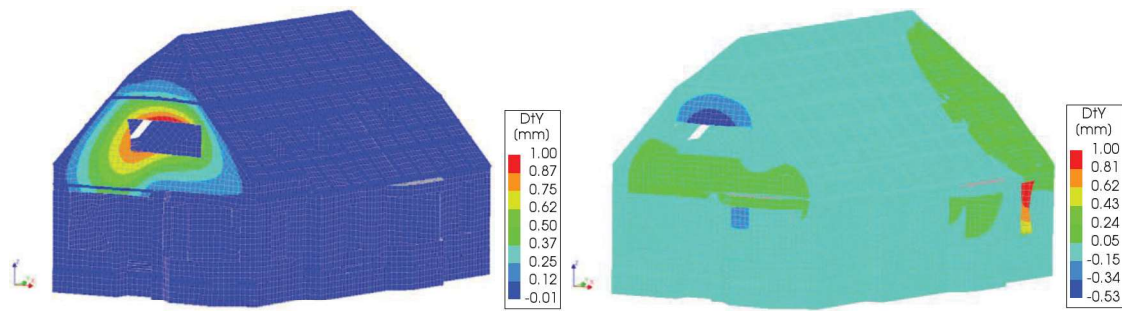


Figure 13. Output location for Damsterweg building. First floor/effective height (left), attic floor (middle) and roof (right).

### 3.2 Analyses Results

Before running the NLTH calculation, an analysis of the eigen modes of the structure is performed. An overview of the main frequencies is shown in Figure 14 for the two modes with highest participation mass, which are also selected to compute the Rayleigh damping coefficients.

The hysteresis plots (normalized base shear force vs. first floor displacement) computed for the two motion series, namely with the original PGA and with a PGA scaled by a factor 2 (both with the strongest motion applied in Y direction), are depicted in Figure 15. Such plots show the entire time history up to the last converging step of each analysis and they are not limited by the failure criteria described in section 3.1: the criteria are applied directly to when the backbone curve of the building is computed. All the hysteretic curves are shown in Appendix B and Appendix C. When the analyses with the original PGA are run the maximum average displacement reached at the effective height in the Y-direction is around 5 mm with a maximum normalized force of 1.15 g (computed by considering Mass B). When the stronger input motions are applied, the maximum normalized force does not increase, but the maximum average displacements increases up to almost 10 mm. The stop criteria of the different analyses are reported in Table 3 (original motions) and Table 4 (scaled motions).



**Figure 14. Eigen modes for Damsterweg building. Mode 4 (left), mode 20 (right).**

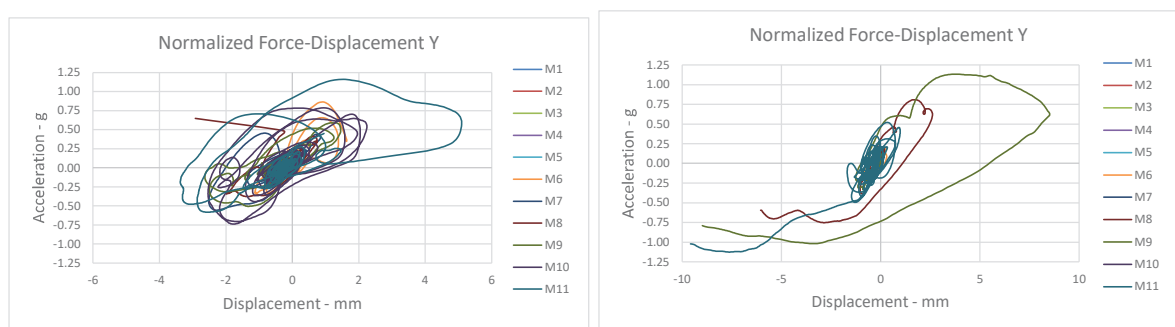


**Figure 15. Hysteretic curves defined at the effective height in the Y direction for the original PGA motions (left) and the scaled PGA motions (right). Normalized force computed using Mass B.**

The global OOP stop criterion is reached for the amplified motion M9, for which both the West façade and a load bearing internal wall at the ground floor (indicated with A and B in Figure 16) exceed the limit of 100 mm and 60 mm, respectively. Due to numerical instability it was not possible to reach larger displacements of the internal wall, so that the global stop criteria is conservatively taken as 60 mm. The local failure of the West façade is observed also in the original ground motions M10 and M11, and for the scaled motions M8 and M11 (considering 100 mm limit). Examples of OOP failure are depicted in Figure 17. As reported in section 3.1, only the collapse of wall B is considered for the stop criterion, since it involves a load bearing wall whose collapse would determine the consequent collapse of the floor structure above.

In-plane mechanisms are not observed and the displacement are for all cases below the selected limits. Also in the X-direction maximum displacements of about 20 mm at the South-West corner are detected (Figure 18) which do not cause any OOP failure nor it exceeds the IP global limit (considering that such deformation is achieved after the activation of a ductile flexural mechanism of the slender piers on the West façade).

The failures observed for each ground motion are summarized in Table 3 (original motions) and Table 4 (scaled motions). Few original motions with low PGA have not been analysed since the focus of this investigation is on the ultimate limit state of the building. On the opposite, such motions would only influence the initial stiffness of the backbone curve.

As described above, the OOP displacement of the internal wall (B) is the governing failure mechanism associated to the global collapse of the building. The local failure of the West façade is reached for lower PGAs (0.53 g when the 60 mm limit is considered).

As described in section 3.1, the failure of the connections between masonry and timber beams may also determine the stop of the analyses. However, the minimum or maximum relative displacement of the interface elements is 41 mm, smaller than the corresponding limit (Figure 19).

Figure 20 shows the evolution of the displacements and of the crack pattern of scaled motion 9. The resulting failure mechanism is localized on the West façade A and its connection to the South façade. Two way bending failure is also observed for wall B, which deforms in the OOP direction with a maximum displacement of about 67 mm.

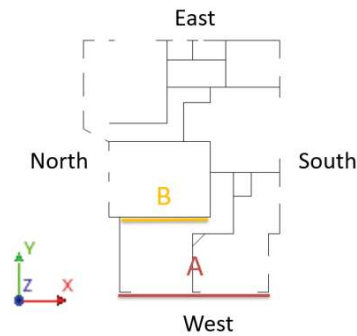


**Figure 16. Location of OOP mechanisms in the Damsterweg building.**

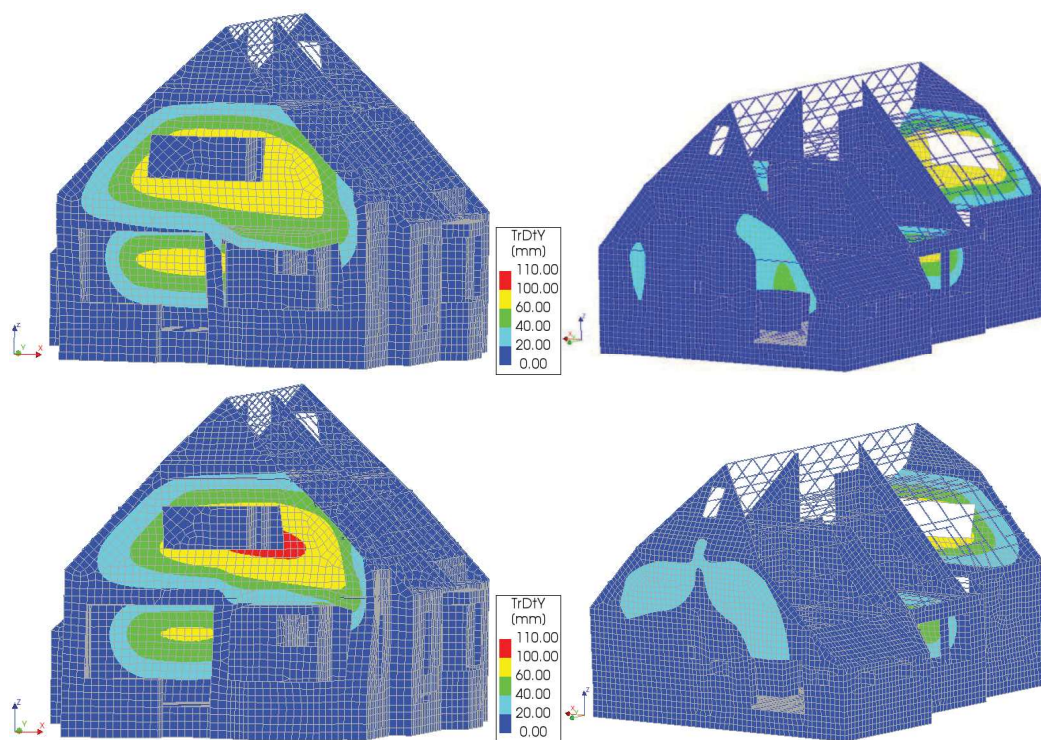


**Figure 17. Typical OOP mechanisms observed in the Damsterweg building at step 894 of scaled motion 9. Failure wall A-B. Minimum (top) and maximum (bottom) Y-displacement. South-West view (left) and North-East view (right).**

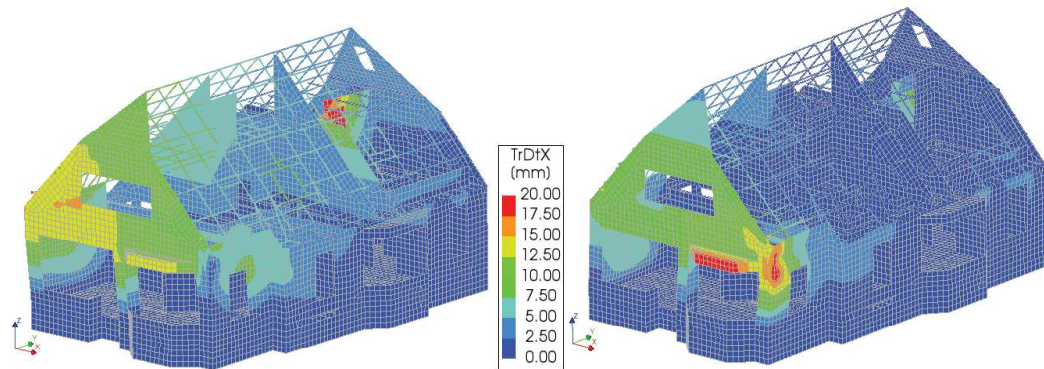


Figure 18. Displacement X-direction at step 894 of scaled motion 9 Damsterweg building. Minimum (left) and maximum (right) displacement.

Table 3. Failure type of Damsterweg building for the original motions for different OOP stop criteria.

Original Motion	M2	M5	M6	M7	M8	M9	M10	M11
OOP Criteria 100 mm	-	-	-	-	-	-	Local OOP A	Local OOP A
Step at Failure							1320	1620
OOP Criteria 60 mm	-	-	-	-	-	Local OOP A	Local OOP A	Local OOP A
Step at Failure						1220	1020	1620

Table 4. Failure type of Damsterweg building for the scaled motions for different OOP stop criteria.

Scaled Motion	M6	M8	M9	M11
OOP Criteria 100 mm	-	Local OOP A	Local OOP A	Local OOP A
Step at Failure		1300	820	1420
OOP Criteria 60 mm	-	Local OOP A	Local OOP A; OOP B	Local OOP A
Step at Failure		1300	820; 894	1420

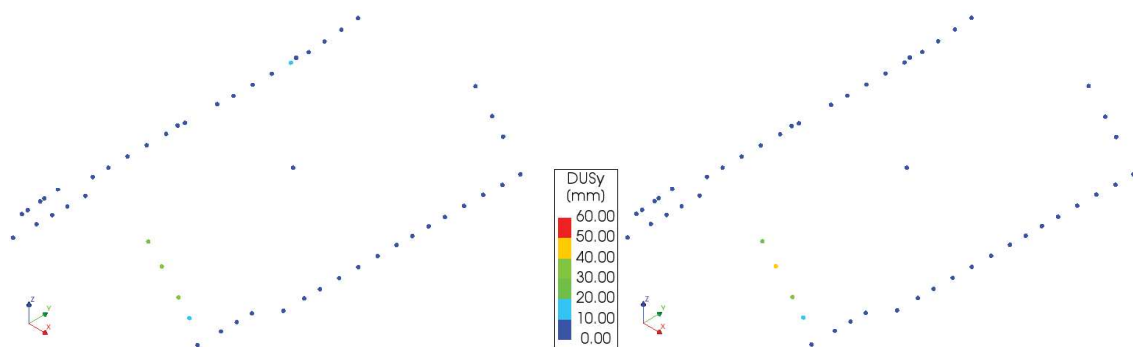
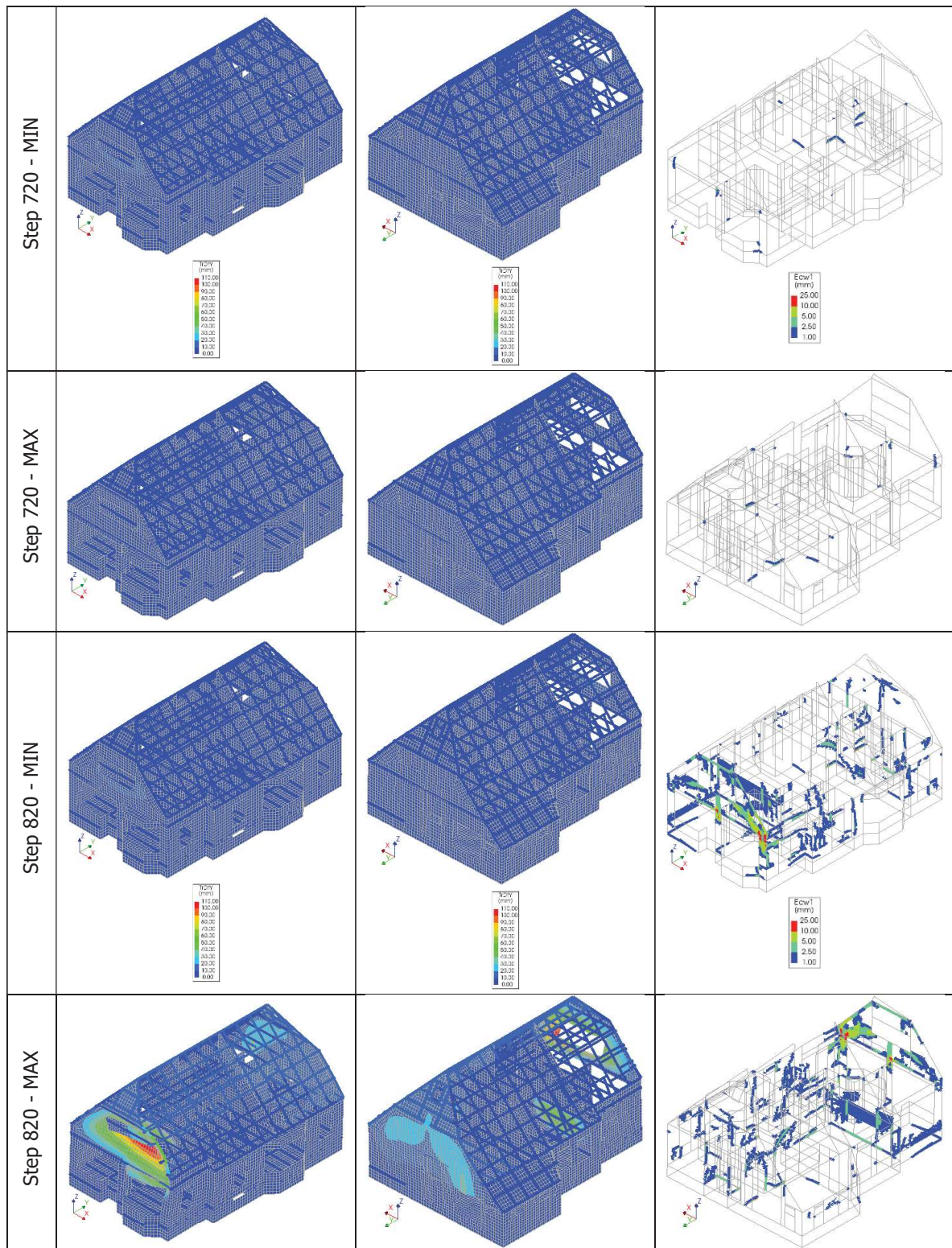
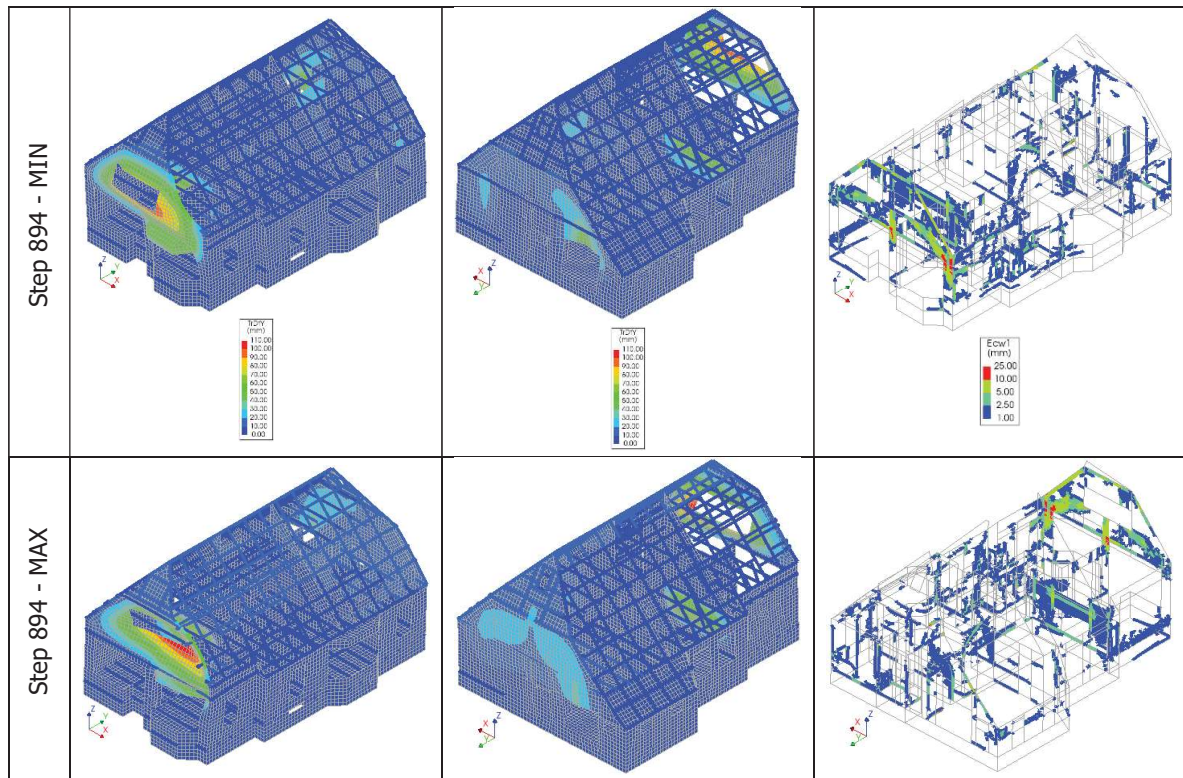


Figure 19. Minimum (left) and maximum (right) relative interface displacement in Y-direction observed in the Damsterweg building at step 894 of scaled motion 9.





**Figure 20. Evolution of displacements Y-direction, cracks of Damsterweg when subjected to scaled motion 9. Minimum and maximum y-direction displacement, South-West view (left), North-East view (middle) and maximum principal crack width (right) at step 720 (top), 820 (middle) and 894 (bottom).**

### 3.3 Backbone capacity curve

The hysteretic curves defined for each analysis are used to determine the global backbone capacity curve of the building according to the procedure described in [3]. Since the capacity of the building is governed by the performance of the building in the Y-direction (East-West), the backbone is based on the hysteretic curves defined in this direction. The backbone capacity curve is shown in Figure 21a, whereas Figure 21b shows a comparison between the backbones computed with different effective mass (Mass A vs Mass B). The values of the initial stiffness, yield displacement and force, peak displacement and force, and ultimate displacement are listed in Table 5.

As described above, direction Y is the predominant direction for this building, due to limited vertical compression acting on the West and East façades that makes the two walls more vulnerable to the out-of-plane collapse. In addition, the presence of the large openings on the West façade localizes the failure at the gable level. Due to the local OOP mechanism, the obtained backbone is relatively stiff and the ultimate displacement small (lower than 10 mm). Such displacement is evaluated considering the exceedance of the limit value 60 mm for the OOP failure criterion. Larger OOP displacements of wall B would be expected if the analyses could continue to run, but that was not possible due to numerical instability. In fact, part of the timber roof and floor structure showed inconsistent large local deformations which eventually led to divergence. Attempts to fix such numerical problems were made by increasing the stiffness of such elements, as described in Appendix D. Such modifications allowed to obtain more stable analyses and to observe the exceedance of the 60 mm OOP limit, but not to make the analyses running further.

For this reason, it was not possible to define a backbone curve considering the 100 mm OOP failure criterion, and the presented curve can be considered only a lower bound for it. Based on analyses performed for other buildings belonging to the same typology, an increment of approximately 25-30% would be expected.

The low value of displacement are due to fact that the North and South façades mainly behave linearly with limited damage (as shown by Figure 20 too) and the collapse is only reached in walls A and B, which little contribute to the average building deformation, and therefore to the ultimate displacement value of the backbone. The computed peak force is equal to 0.94 g when Mass B is used to normalize the base shear; if Mass A would be considered much higher (1.75g) values would be achieved.

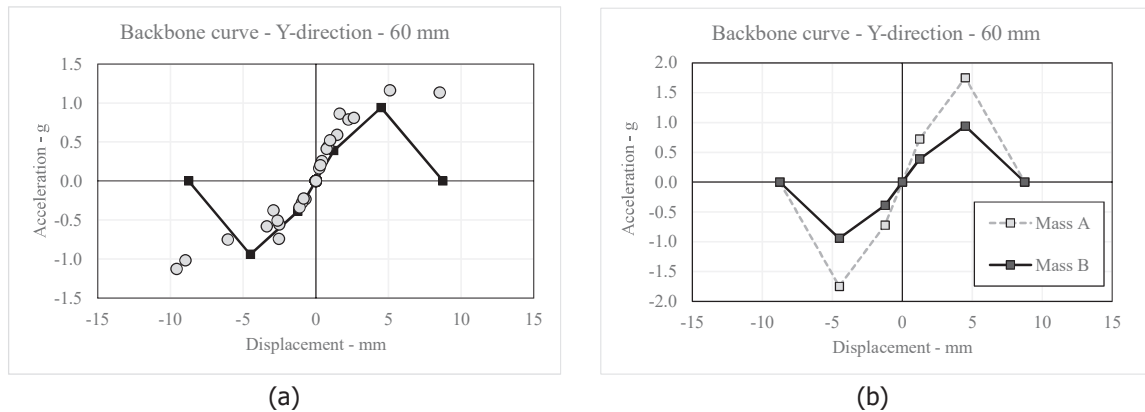


Figure 21. Max normalized forces and displacements for each performed simulation, and corresponding backbone curve for the Y-direction and Mass B (a). Backbone curves for alternative mass (b).

Table 5. Summary table backbone curves

	Mass A - Y	Mass B - Y
Initial Stiffness [g/mm]	0.58	0.31 (-46%)
Yield Displacement [mm]	1.24	1.24 (-)
Yield Normalized Force [g]	0.72	0.39 (-46%)
Peak Displacement [mm]	4.50	4.50 (-)
Peak Normalized Force [g]	1.75	0.94 (-46%)
Ultimate Displacement [mm]	8.75	8.75 (-)

## 4 Conclusions

In this case study, the structural behaviour of the two-storey detached house Damsterweg 37, Steendam is investigated by performing a set of nonlinear time history (NLTH) analyses. The calculations are conducted by employing the Finite Element software package DIANA FEA version 10.4 [1]. The hysteretic behaviour of the building, the governing failure mechanisms, and the global backbone capacity curve are computed. A series of 11 ground motions with increasing values of PGA is considered. An additional set of scaled motions is also employed to evaluate the ultimate displacement capacity of the building.

Different stop criteria are selected for the analyses, namely:

1. In-plane (IP) displacements of masonry walls: 1.5% of the inter-storey drift, or 0.8% of the effective height drift (both for ductile mechanisms, as observed for the structure);
2. Out-of-plane (OOP) displacement of masonry walls: 100 mm or 60 mm.
3. Failure of the connections between masonry and timber beams: a maximum relative displacement in the axial direction of the beams of 60 mm (either in compression or in tension).

The following is observed:

- The collapse of the buildings is governed mainly by the OOP collapse of an internal wall, located at the West side of the building. The local failure of the West gable precedes the collapse of the internal wall, but it is estimated not to lead to the global collapse of the building, since the rafters (which support both the roof and the attic floor) are supported on the North and South walls, and only the purlins are connected to the West façade.
- The failure of the connections is not achieved, although large relative displacements between the timber purlins and the masonry wall are observed, with a maximum unity check of about 0.69.
- The lowest PGA value of a ground motion that leads to local collapse of the West façade is 0.535 g. The global collapse of the building due to failure of an internal load bearing wall is obtained for an analysis with a larger PGA equal to 1.07 g.
- Considering an effective mass that accounts for the entire building except the footings (mass B), the peak normalized force in the Y-direction is 0.94 g.
- The ultimate displacement achieved in the Y-direction is equal to 8.75 mm. Such value is obtained by considering 60 mm as threshold limit for the OOP criterion. This value represents a lower bound for the curve computed for the 100 mm OOP limit: a more precise value could not be found, although it is expected to be approximately 25-30% higher based on calculations made for other buildings belonging to the same typology.

The plot of the final backbone curve and the values of the points of such curve are shown in Figure 22 and listed in Table 6, respectively.

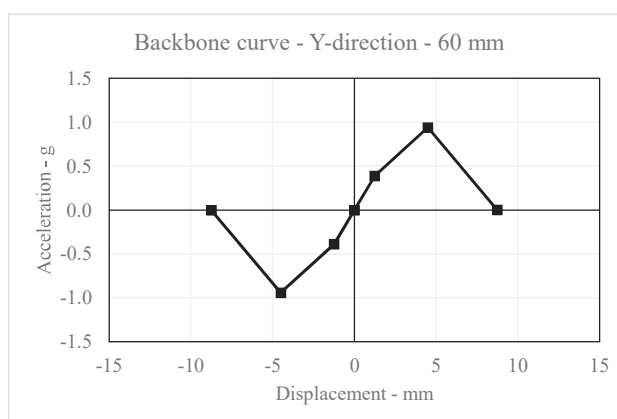


Figure 22. Final backbone curve (considering 60 mm as OOP stop criteria and Mass B) for Y-direction.

Table 6. Summary table for the final backbone curve

	Final backbone curve
Initial Stiffness [g/mm]	0.31
Yield Displacement [mm]	1.24
Yield Normalized Force [g]	0.39
Peak Displacement [mm]	4.50
Peak Normalized Force [g]	0.94
Ultimate Displacement [mm]	8.75

## References

- [1] Diana User's Manual -- Release 10.4, 2020; <https://dianafea.com/manuals/d104/Diana.html>
- [2] Schreppers, G.M.A., Garofano, A., Messali, F., Rots, J.G. (2017). DIANA Validation report for Masonry modelling. Report *DIANA FEA BV & TU Delft*, 15 February 2017
- [3] Messali, F., Longo, M. (2020). A numerical investigation of building typology 'Metselwerk 7'. Delft University of Technology. Report number 03, Version 01, 19 June 2020.
- [4] Mirra, M., & Ravenshorst, G. (2019). Seismic characterization of timber-masonry connections based on experimental results. Delft University of Technology
- [5] Messali, F., Ravenshorst, G.J.P. (2019). Database of connections: characteristics and properties. Delft University of Technology. Report number CM1B05-WP1-2.3, Final version, 03/12/2019.
- [6] Messali, F., Longo, M. (2020). Study of a median backbone curve and of the building to building variability for typology 'Metselwerk 1'. Delft University of Technology. Report number 02, Version 01, 07 May 2020.
- [7] Messali, F., Longo, M. (2020). Definition of a consistent backbone curve for typology 'Metselwerk 2'. Delft University of Technology. Report number 01, Version 02, 15 April 2020.

## Appendix A

The material parameters used in the model are listed below:

### 1. MASONRY

The Engineering Masonry Model [2] is used as material model for piers, bank, spandrel, gables and foots. Both internal and external walls have the same properties, except for the inertia mass, which is only added to the inner leaf walls and not to the internal walls. Masonry is modelled with a thickness of 100 mm. Local y axis is aligned to the global Z axis in order to define the bed joint orientation. Local x axis is aligned to the in-plane direction of the elements. The element for modelling the weak connection between internal and external walls is modelled by reducing the elastic, tensile and shear properties by 30%. In addition, the local y axis is aligned to the in-plane direction to simulate the vertical connection joint. For the NLTH calculations the elastic properties are halved in order to properly capture the cyclic strength degradation, not explicitly described by the EMM. Besides, the same assumption has been already employed in other calibration/validation studies of URM buildings to overcome the global rigidity given by local connections which results in over stiff results.

**Table 7. Masonry material properties employed in the model.**

EMM	Clay	Clay Weak
$E_y$ [MPa]	2500	1750
$E_x$ [MPa]	1667	1167
$G$ [MPa]	1000	700
Density [Kg/m <sup>3</sup> ]	1950	1950
$f_y$ [MPa]	0.15	0.10
Min $f_x$ [MPa]	0.45	0.30
$G_{r,l}$ [N/m]	10	8
$\alpha$ [rad]	0.58	0.58
$f_c$ [MPa]	8.5	8.5
$G_c$ [N/m]	20000	20000
$\phi$ [rad]	0.643	0.643
$c$ [MPa]	0.30	0.21
$G_s$ [N/m]	100	100

### 2. AERATED CONCRETE

The Total Strain Rotating Crack model is used as material model for the internal piers, bank and spandrel made by aerated concrete.

**Table 8. Aerated concrete material properties employed in the model.**

TSRCM	Aerated Concrete
$E$ [MPa]	1800
Density [Kg/m <sup>3</sup> ]	500
$\nu$ [-]	0.25
$f_t$ [MPa]	0.15
$G_{r,l}$ [N/m]	40
$f_c$ [MPa]	3.6
$G_c$ [N/m]	10000

### 3. TIMBER PLANKS

An orthotropic behaviour, whose properties are calibrated according to past laboratory experiment, is assigned to timber planks of the timber floors (ground, first and attic) and roof. The local x axis is aligned with the global Y. The properties are tabulated in Table 9.

**Table 9. Attic floor and roof timber diaphragm material properties employed in the model.**

Linear Elastic Orthotropic	Timber C18 - Plates
$E_x$ [MPa]	1.5
$E_y$ [MPa]	11
$E_z$ [MPa]	400
Density [Kg/m <sup>3</sup> ]	380
$\nu$ [-]	0.00
$G_{xy}$ [MPa]	1100
$G_{yz}$ [MPa]	1100
$G_{xz}$ [MPa]	500

### 4. TIMBER BEAMS

Beam properties are considered as isotropic linear elastic. Timber C18 is assigned as material to internal walls at attic floor, purlins, rafters, struts, wall plates and ridge beams. The material parameters are listed in Table 10. Must be noted that the timber beam properties are increased from 7 GPa to 14 GPa due to numerical instability. A comparison between the different results are provided in Appendix D.

**Table 10. Timber beams properties employed in the model.**

Linear Elastic Isotropic	Timber C18
$E$ [MPa]	9000
Density [Kg/m <sup>3</sup> ]	380
$\nu$ [-]	0.35

### 5. REINFORCED CONCRETE

Ground floor material and lintels are modelled as linear elastic. The properties are listed in Table 11.

**Table 11. Reinforced concrete properties employed in the model.**

Linear Elastic Isotropic	C 20-25
$E$ [MPa]	27100
Density [Kg/m <sup>3</sup> ]	2500
$\nu$ [-]	0.15

### 6. TIMBER-MASONRY CONNECTION

Timber-masonry connection is modelled via non-linear point interface. A Coulomb-friction model is used. The properties are listed in Table 12.

**Table 12. Interface properties employed in the model.**

<b>Coulomb-Friction</b>	<b>Interface</b>
$k_n$ [N/mm <sup>3</sup> ]	1000
$k_{ty}$ [N/mm <sup>3</sup> ]	100
$k_{tz}$ [N/mm <sup>3</sup> ]	100
$c$ [MPa]	0.02
$\phi$ [rad]	0.54
$\psi$ [rad]	0.00

## Appendix B: original motions

Appendix B reports the hysteretic curves measured at the effective height for original motions applied to the building. In addition, also displacements plots of attic floor and roof are reported. The hysteretic curves are reported for the two different effective masses.

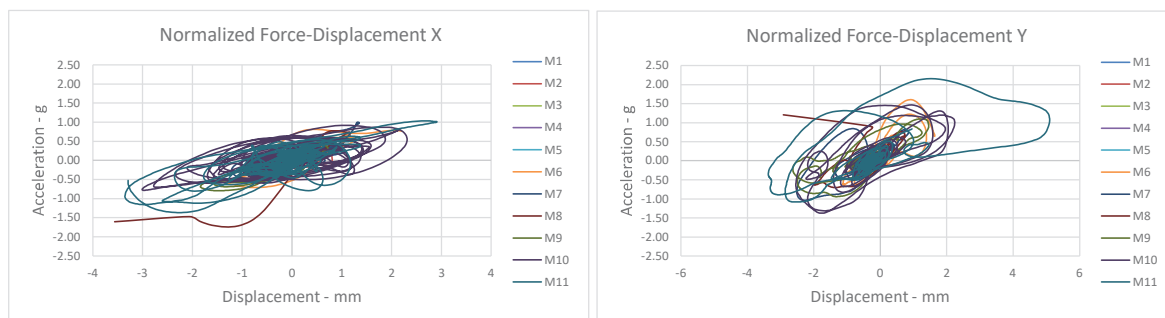


**Figure 23. Hysteretic curves defined at the effective height for the original motion. Normalized force computed with Mass A.**

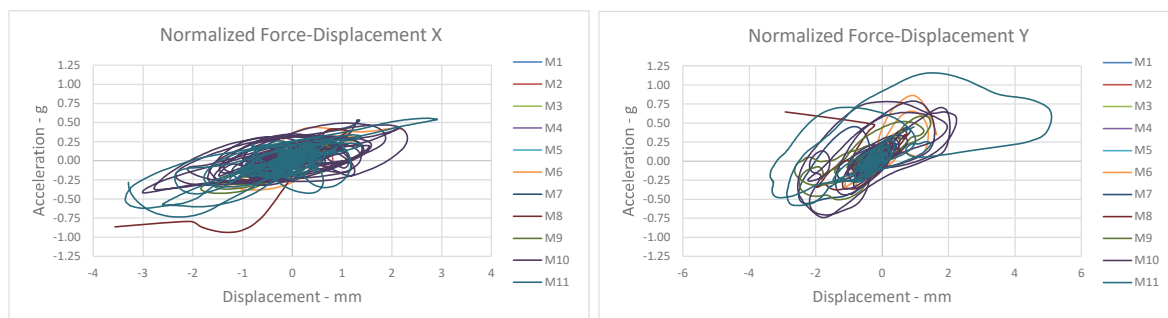


**Figure 24. Hysteretic curves defined at the effective height for the original motion. Normalized force computed with Mass B.**

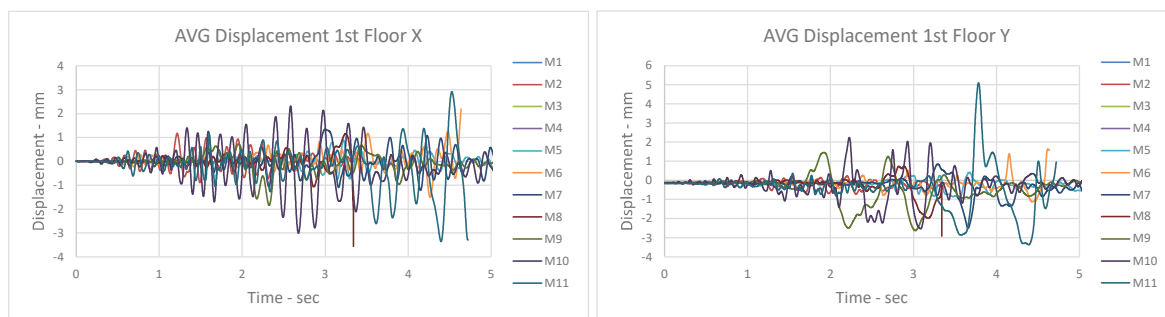


**Figure 25. Average displacement defined at the effective height for the original motion.**

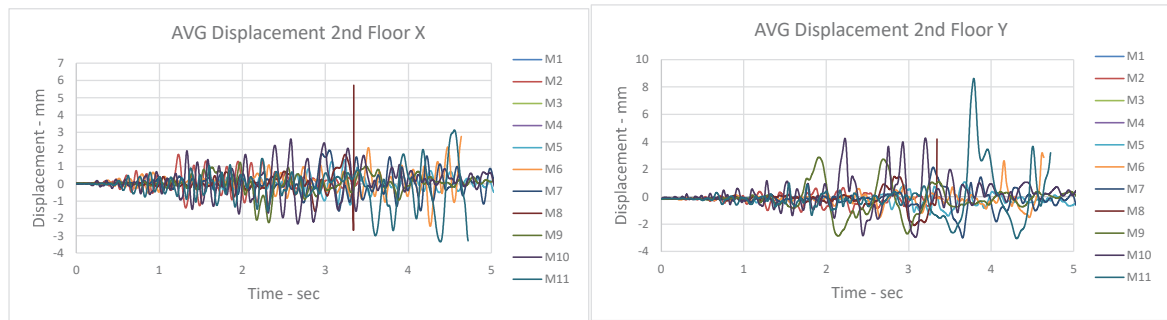


**Figure 26. Average displacement defined at the attic floor height for the original motion.**

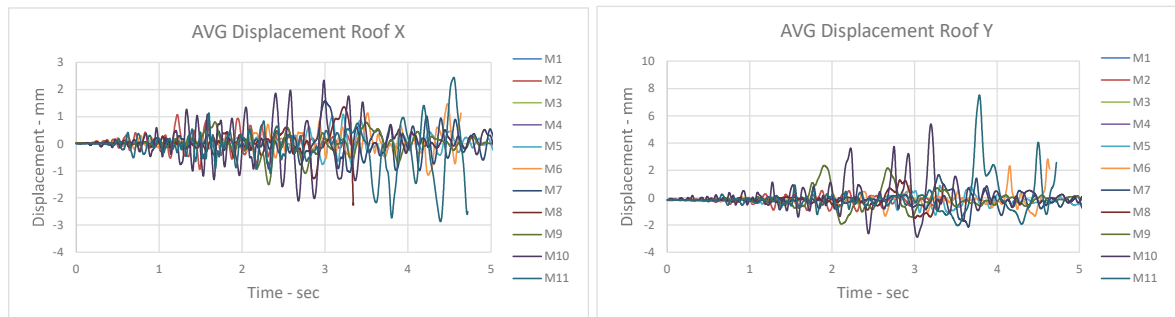


**Figure 27. Average displacement defined at the roof height for the original motion.**

## Appendix C: scaled motions

Appendix C reports the hysteretic curves measured at the effective height for scaled motions applied to the building. In addition, also displacements plots of attic floor and roof are reported. The hysteretic curves are reported for the two different effective masses.

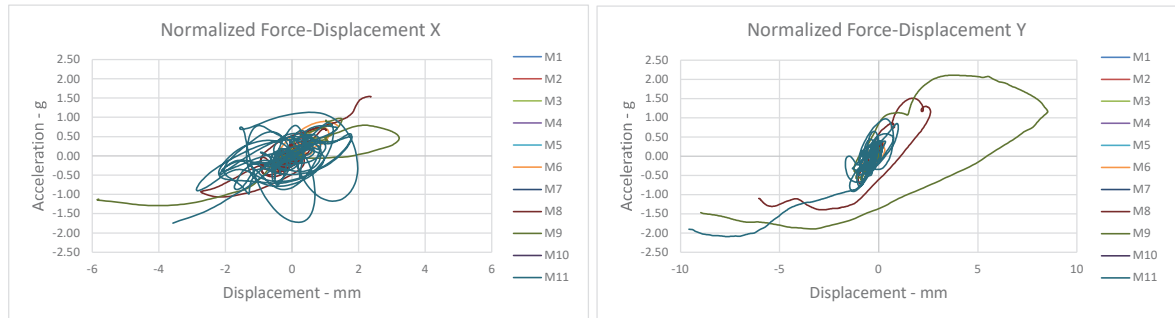


**Figure 28. Hysteretic curves defined at the effective height for the scaled motion. Normalized force computed with Mass A.**

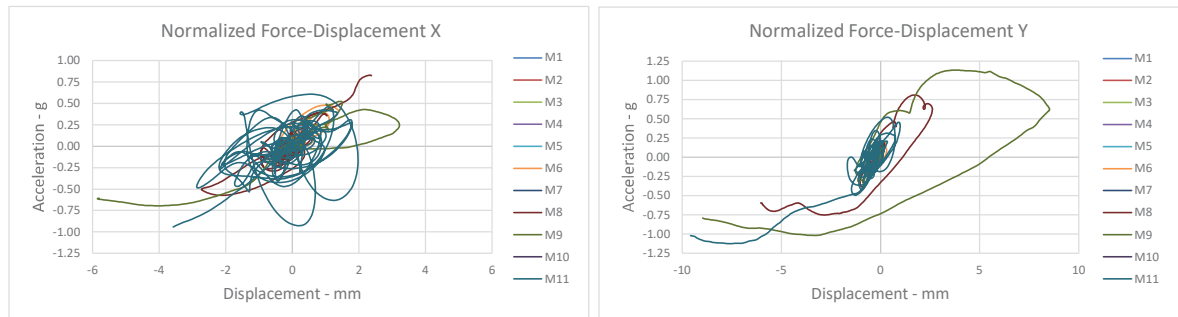


**Figure 29. Hysteretic curves defined at the effective height for the scaled motion. Normalized force computed with Mass B.**

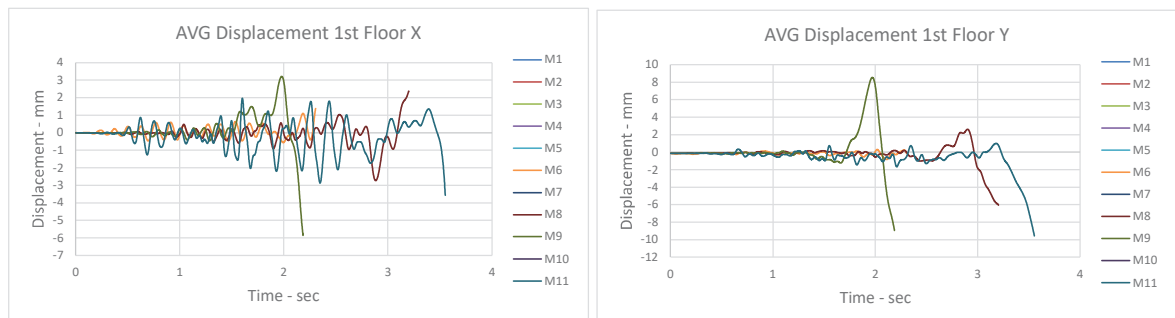


**Figure 30. Average displacement defined at the effective height for the scaled motion.**

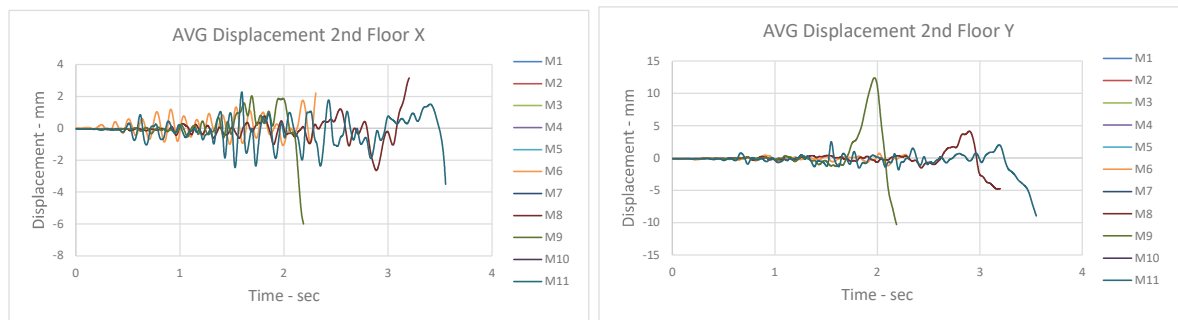


**Figure 31. Average displacement defined at the attic floor height for the scaled motion.**

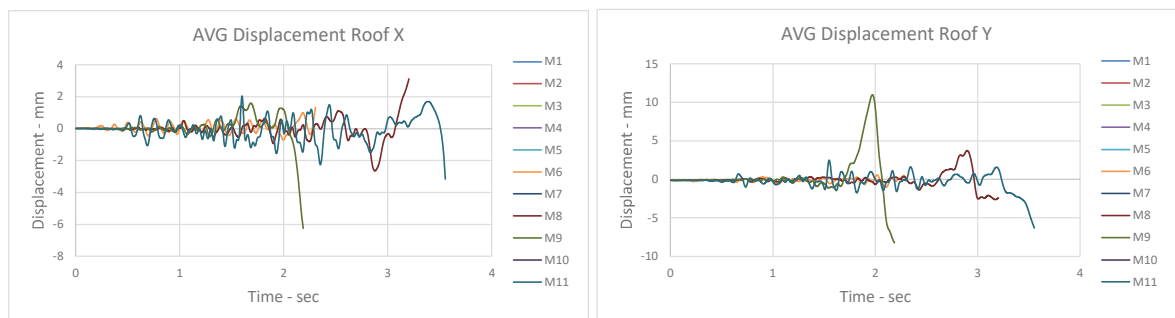


**Figure 32. Average displacement defined at the roof height for the scaled motion.**

## Appendix D: comparison timber beam variation

Due to numerical instability at roof/floor level, the original elastic modulus of the timber beams was increased from 7 GPa to 9 GPa. The results for a specific ground motion (original motions, M11) are compared and an overview of such comparison is provided in this appendix. From the displacement contour plots and the force-displacement curves, it can be observed that the pattern and the amplitude of the displacement is similar for the two simulations. The higher elastic modulus allows the analysis to run for a larger number of steps and avoid numerical problem. With the 9 GPa configuration, the interface relative displacement are more in phase with the gable displacement and thus their relative displacement reduces. This would anyhow not influence the final outcome since the connection failure at that specific location is not leading to the global collapse of the building.

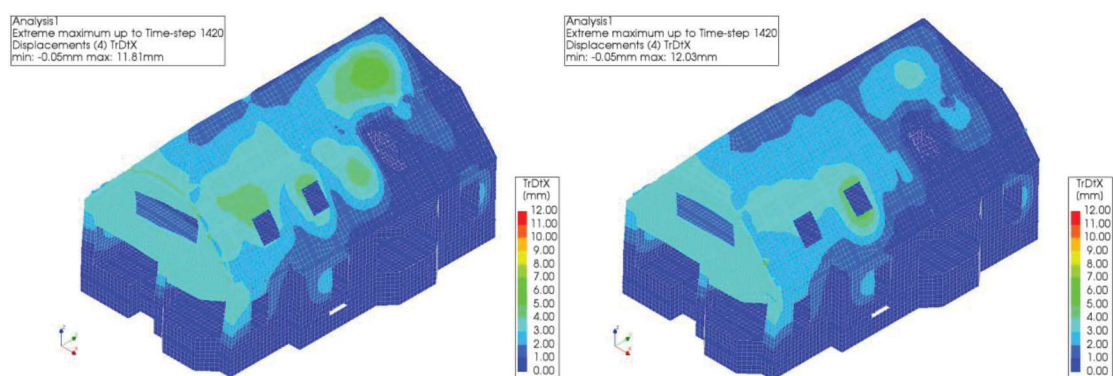


Figure 33. Maximum displacement X-direction of original PGA motion 11 for model with timber elastic modulus of 7 GPa (left) and 9 GPa (right).

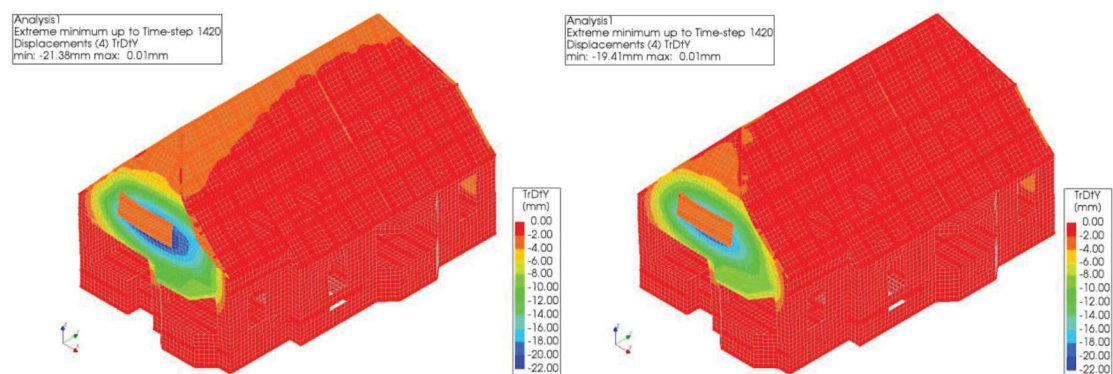
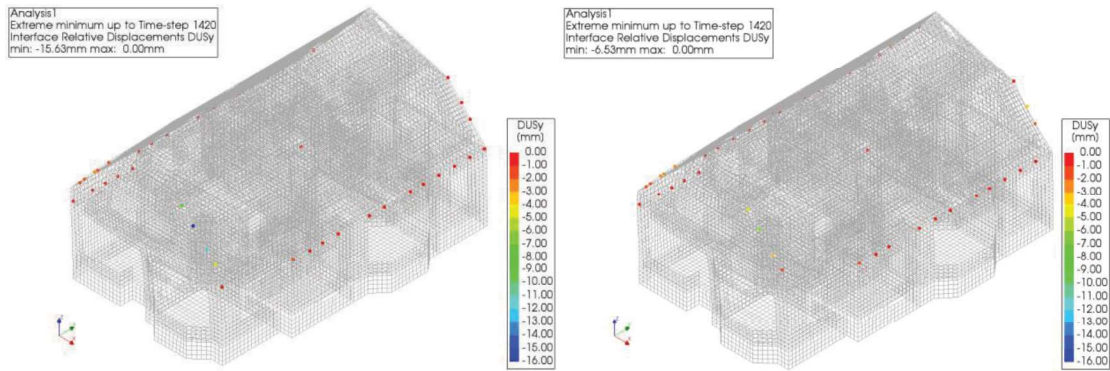
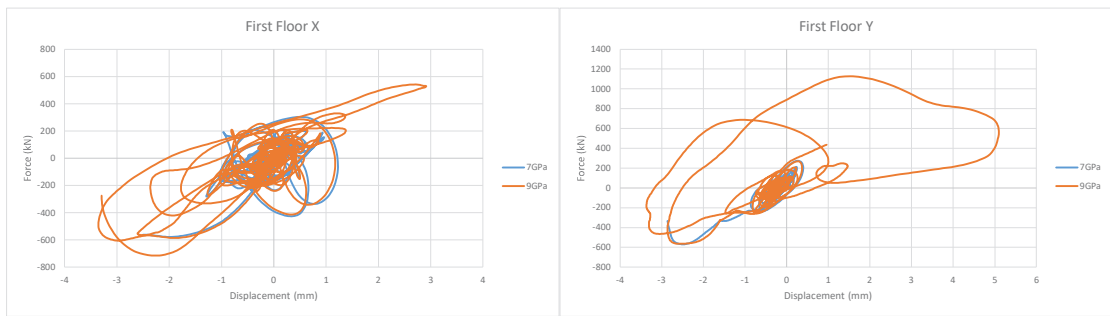


Figure 34. Minimum displacement Y-direction of original PGA motion 11 for model with timber elastic modulus of 7 GPa (left) and 9 GPa (right).



**Figure 35. Minimum relative interface displacement in Y-direction of original PGA motion 11 for model with timber elastic modulus of 7 GPa (left) and 9 GPa (right).**



**Figure 36. Force-displacement curve comparison between models with timber elastic modulus of 7 GPa and 9 GPa at first floor/effective height. Displacements in the X-direction (left) and Y-direction (right).**

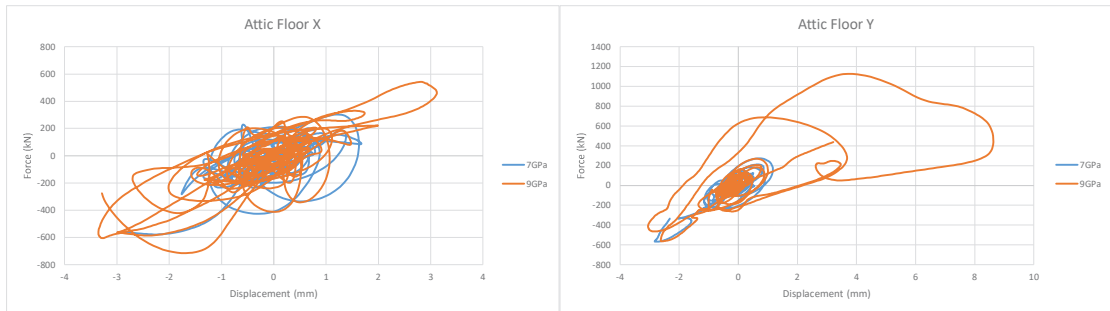


**Figure 37. Force-displacement curve comparison between models with timber elastic modulus of 7 GPa and 9 GPa at attic floor level. Displacements in the X-direction (left) and Y-direction (right).**

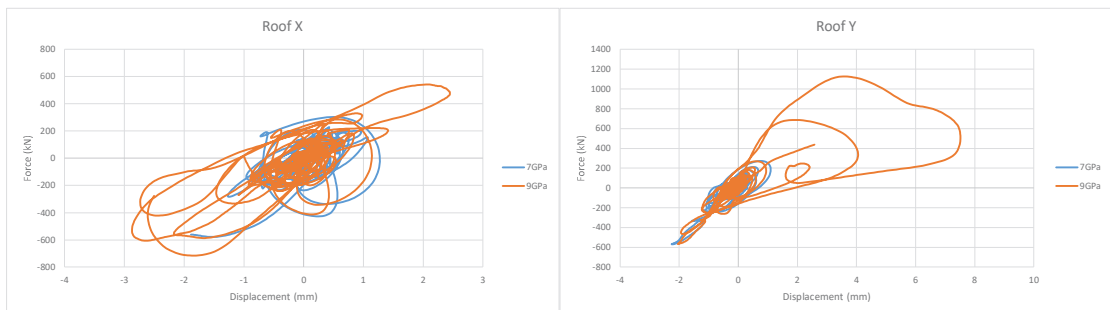


**Figure 38. Force-displacement curve comparison between models with timber elastic modulus of 7 GPa and 9 GPa at roof level. Displacements in the X-direction (left) and Y-direction (right).**